AN ABSTRACT OF THE THESIS OF

KENNETH CHEUNG-PING SUN for the degree of Master of Science in CHEMISTRY presented on DECEMBER 12, 1985.

Title: SYNTHESIS AND LOW-TEMPERATURE MOSSBAUER EFFECT INVESTIGATION OF INTERMEDIATE-SPIN HALOBIS (N,N'-DIALKYLDITHOCARBAMATO) IRON (III) COMPLEXES

Redacted for Privacy

Abstract approved: H. H. Wickman

Ten new halobis(N,N'-dialkyldithiocarbamato) iron (III) X complexes [denoted by $Fe(dtc)_2X$, where X = Cl^-, Br^-, I^-, and SCN^-] are described in this thesis. In these new materials, (i) the length of the alkyl groups attached to the nitrogen of the dithiocarbamates is increased with respect to the reference ethyl group or (ii) the N-alkyl groups are not identical. Their electronic and magnetic properties were studied by Mossbauer Spectroscopy.

The ground state electronic properties of iron (III) are described by the conventional crystal field Hamiltonian,

$$\hat{\mathcal{H}}_{CF} = D[\hat{S}^2_{z'} - S(S+1)/3] + E(\hat{S}^2_{x'} - \hat{S}^2_{y'})$$

with S = 3/2 and $E/D \ll 1$. The Mossbauer hyperfine parameters were obtained by the usual Lorentzian curve fitting with a standard Hamiltonian.

The Mossbauer data taken at 77 K showed that the isomer shift is essentially independent of the variation of the apical ligand or the N-alkyl groups of the complexes. This indicated a constant s-electron density at the Mossbauer nucleus. Qualitative explanations in terms of covalency effects and overlap distortion are provided. Concurrently, it was found that there is a gradual increase in the quadrupole splitting as the iron-halide distance from the Mossbauer nucleus increases. This is consistent with results from molecular orbital calculations reported by Marathe et al.

Three chloro-bis-dtcs were further studied between 1.2 and 4.2 K. It was concluded that the crystal field D parameter was negative for these three complexes. This implies the Kramers' doublet $|m_s=\pm 3/2\rangle$ is lowest in energy. Two samples showed paramagnetic hyperfine structure. Theoretical interpretation of paramagnetic relaxation process was attempted by employing the stochastic model of ionic spin relaxation formulated by Blume et al. A spin-spin coupling constant C and crystal field D parameter were derived. A qualitative conclusion about the nature of C in the paramagnetic materials was made. Finally, the absence of the magnetic pattern in $Fe[S_2CN(n\text{-}pr)_2]_2Cl$ at the lowest temperature of our apparatus indicated that the crystal field D parameter was very small in this complex. It appears that the longer alkyl group at the terminal end of the complex produces a decreased energy separation between the two Kramers' doublets, $|m_s=\pm 3/2\rangle$ and $|m_s=\pm 1/2\rangle$.

Synthesis and Low-temperature Mossbauer Effect Investigation of Intermediate-spin Halobis(N,N'-Dialkyldithiocarbamato) Iron(III) complexes

by

Kenneth Cheung-Ping Sun

A THESIS

submitted to

Oregon State University

in partial fulfillment of
the requirements for the
degree of

Master of Science

Completed December 12, 1985

Commencement June 1986

APPROVED:

Redacted for Privacy

Professor of Chemistry in charge of major

Redacted for Privacy

Chairman of the Department of Chemistry

Redacted for Privacy

Dean of Graduate School

Date thesis is presented DECEMBER 12, 1985

Typed by Katherine Haag for KENNETH CHEUNG-PING SUN

ACKNOWLEDGEMENTS

I would like to thank Prof. H. H. Wickman's critical comments during the preparation of this thesis.

I wish to thank the Chemistry Department at Oregon State University, which has faithfully supported me as a graduate teaching assistant for this long graduate career, the teaching assistant research fund, and partial support from the National Science Foundation Grant DMR-78-08452 to make this work possible.

This thesis is dedicated to my parents and family for their continual encouragement, understanding, monetary support and most of all their faith in me.

TABLE OF CONTENTS

LIST OF FIGURES

LIST OF TABLES

SYNTHESIS AND LOW-TEMPERATURE MOSSBAUER EFFECT INVESTIGATION OF INTERMEDIATE-SPIN HALOBIS(N,N'-DIALKYLDITHIOCARBAMATO) IRON(III) COMPLEXES

CHAPTER I

A. INTRODUCTION

In 1965, Wickman and Trozzolo employed the chloro bis(N,N-dimethyldithiocarbamato) and chloro bis(N,N-diisopropyldithiocarbamato) iron (III) complexes to study magnetic relaxation effects in these materials (a typical complex will be denoted by $Fe(dtc)_2$ X in this thesis) [1]. In 1966, Martin et al. synthesized a similar complex by reacting a benzene solution of tris $Fe[(C_2H_5)_2dtc]_3$ with a stoichiometric amount of concentrated hydrochloric acid [2]. They reported the structure and showed that the unusual orbital singlet, spin quartet ground state (S=3/2) for the iron (III) arose in lower symmetry environments, such as in a distorted five coordinate structure with approximately rectangular pyramidal symmetry at the iron site (Fig. 1) [3]. Since then, a range of halo-bis-dtcs have been prepared and studied by a variety of methods [4-12].

This novel class of iron complexes has been given so much attention in the last two decades in magnestism research because of the varied magnetic properties they display; to name a few: Ising and XY type cooperative magnetic phenomena, Mossbauer hyperfine structure, relaxation effects and lattice dimer or cluster exchange interaction.

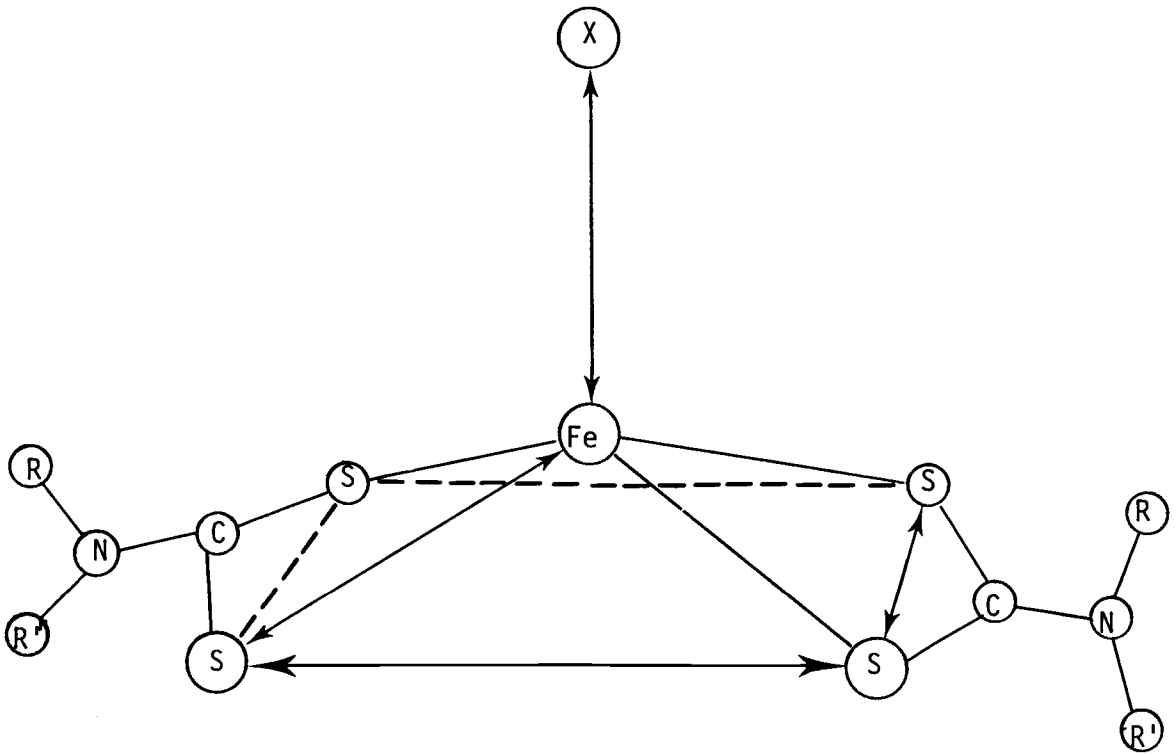

R = CH_3 , C_2H_5 , i-C_3H_7 , n-C_3H_7

R'= CH_3 , C_2H_5 , i-C_3H_7 , n-C_3H_7

Fig.1. General molecular structure diagram of halobis(N,N'-Diakyldithiocarbamato)iron(III), after Ref.[11].

There has been little electron spin resonance (ESR) work on these iron complexes owing to the broad line widths which arise from the strong magnetic exchange interactions [9-10]. In a recent paper, Decurtins [8] et al. added a new perspective on the ESR interest of this class of complexes. They diluted the $Fe(dtc)_2Br$ into the diamagnetic lattice $As(dtc)_2Br$ of similar molecular configuration. Unfortunately, the structure of the host lattice is somewhat complicated and potentially may distort the usual rectangular pyramidal structure of $Fe(dtc)_2Br$. This work also provided a partial analysis of transferred hyperstructure in the pentacoordinate complex.

Recently, Wells and Wickman substituted the sulfur atom in these complexes by the slightly larger selenium atom [13-14]. The implications are simple and direct. The larger covalency should enhance interaction between molecular units, thus leading to a higher critical temperature. Besides the discovery of an unrealized class of magnetic model system, namely, three-dimensional XY ferromagnet(3D-XY-F), they reported a detailed account on structural and magnetic properties.

In principle, much research can still be done by varying the ligands and solvent contents of the crystal lattices. Numerous attempts have been made to increase the length of the alkyl group at the end chain of the complexes but the results have not yet been fruitful. This is due to their enhanced solubility in the mother

organic solvents and difficulty in obtaining highly crystalline materials. Further, possible syntheses of additional pentacoordinate complexes have certainly not been exhausted.

In this thesis, 10 new halobis(N,N'-dialkyldithiocarbamato) Fe(III) complexes are reported. The syntheses are motivated by interest in finding additional magnetically ordered new materials. This possibly can be done by either (i) increasing (with respect to the reference ethyl group) the length of the alkyl groups attached to the nitrogen of the dithiocarbamates or (ii) considering complexes with inequivalent alkyl group. Thus the material preparation of these new iron complexes will be discussed first. Subsequent chapters are devoted to the study of their electronic and magnetic ground state properties using Mossbauer spectroscopy. Specifically, we determine crystal field D and E parameters, the magnetic hyperfine A tensor, dynamic paramagnetic relaxation phenomena and possible magnetic cooperative phenomena in the complexes.

The Mossbauer hyperfine parameters such as isomer shift, quadrupole splitting and nuclear hyperfine parameters are obained by the usual Lorentzian curve fitting with a standard Hamiltonian. In the process of obtaining a theoretical interpretation of paramagnetic relaxation process, the widely accepted stochastic model of ionic spin relaxation developed by Blume and Tjon was adopted to calculate the lineshape [15]. A computer program was written to generate the results at different experimental conditions [14]. More detailed

theories are reviewed by Dattagupta [16] and Bhargave [17] but the available data do not warrant application of these methods.

B. Electronic Properties of Iron (III)

The Fe(III) free ion has a d^5 configuration with a ground state denoted ^6S. An octahedral crystal field removes the five-fold degeneracy of the orbitals yielding two sets of orbitals labelled e_g and t_{2g} as shown in Fig. 2.

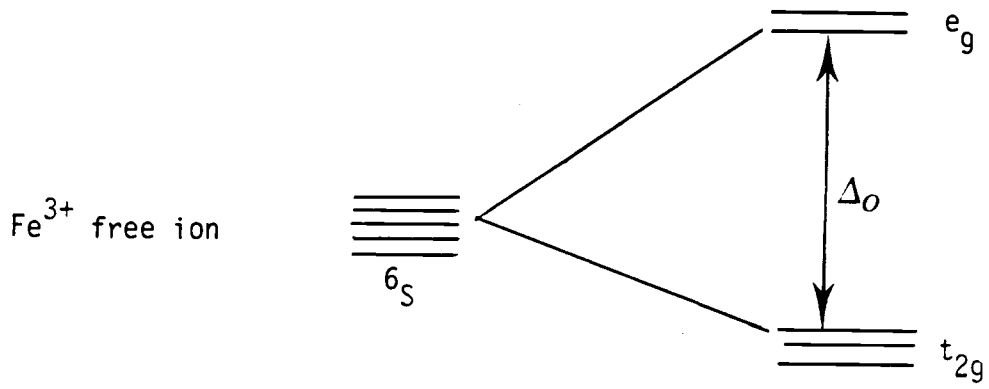

Fig. 2: Diagram showing the relative energies of e_g and t_{2g} orbitals resulting from the splitting of the set of d orbitals by octahedral environment.

According to the Tanabe and Sugano energy level diagram [18], the ground state is either $^6A_1$ or $^2T_2$ depending on the strength of the crystal field splitting, interelectronic repulsion strength and coulombic interaction. In the iron(III) dtc complexes, the interaction along the unique axis is weak, thus the fifth orbital d_{xy} has substantially higher energy than the other four available orbitals, which are subsequently filled by the five electrons (Fig. 3). A $^4A_2$

ground state results. This ground $^4A_2$ state is further split into two Kramers' doublets. The effect of these interactions are described by the conventional spin Hamiltonian

$$\hat{\mathcal{H}}_{CF} = D[\hat{S}_{Z'}^2 - \frac{1}{3} S(S+1)] + E(\hat{S}_{X'}^2 - \hat{S}_{Y'}^2) \qquad (1.1)$$

within the ground quartet manifold with $S = 3/2$ and $D > E$. The primes on the subscripts of the spin operators in equation (1.1) show that the principle axes of the crystal field system need not coincide with the EFG axes [see equation (5.5)]. Which of the doublets is the ground state depends on the sign of the crystal field D parameter [4]. One of these Kramers' doublets is highly anisotropic. This type of ground state occurs in Fe(diethyldtc)$_2$Cl and has been thoroughly studied in previous work [9,11,12]. It was found that this ground state is also characteristic of all the bis-chloro-dtcs reported here. Because of the correspondence in physical properties between the new complexes and previously structurally characterized bis-dtcs, the complexes are assumed to have iron coordination similar to that found in other homologues, such as Fe(diethyldtc)$_2$Cl. Its structure is depicted in Fig. 1.

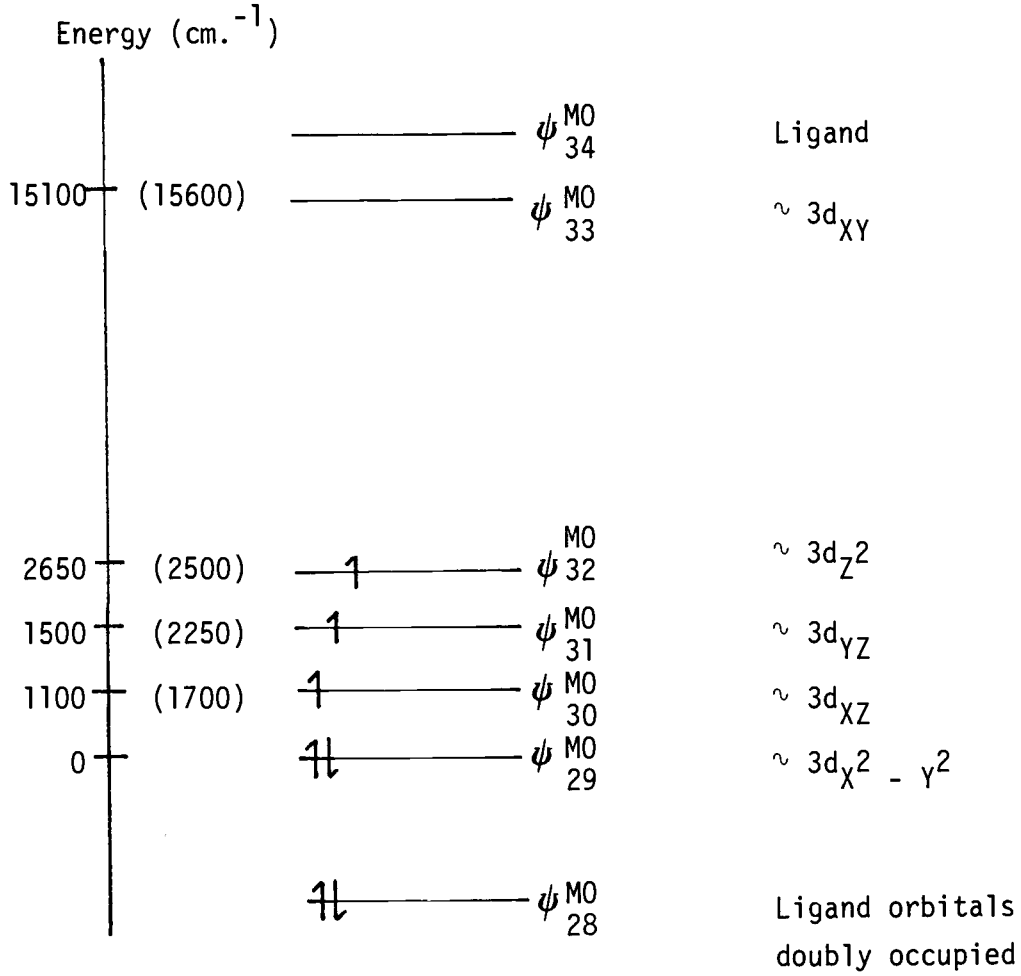

Fig.3. Calculated relative energies of the most important MO's of bis(diethyldithiocarbamate)iron(III)chloride, (values with parentheses correspond to $Fe(dtc)_2I$), after Ref.[19].

CHAPTER II

A. Synthesis

1. $\underline{Fe[S_2CNRR']_2X}$: where X=Cl, Br, or I; R=CH_3, C_2H_5, R'=C_3H_7,C_2H_5

Ethylmethylamine or ethylpropylamine is available commercially. The mixed tris(N,N',dialkyldithiocarbamato)iron(III) compound was prepared and purified as described elsewhere [20]. The resultant precipitate was extracted from benzene. It tended to decompose in polar solvents (e.g. chloroform and dichloromethane).

The bis-dtc derivatives were prepared according to Seki et al. [21]. Tris compound was added in stoichiometric proportion to a solution made from aqueous HX, benzene and sufficient ethanol to maintain the liquid as a single phase during the precipitation. The resulting solution was stirred under dry nitrogen for an hour. The precipitates were recrystallized from different solvents as required. Synthesis of $Fe[S_2CN(Et)(Pr)]_2Cl$ required a slightly different route as shown below.

2. $\underline{Fe[S_2CN(di\text{-}n\text{-}pr)]_2X}$: where X = Cl, Br, or I

The tris (N,N-di-n-propyldithiocarbamato)iron(III) compound was prepared and purified as above.

Sufficient anhydrous ethanol was added to a mixture of ether and minimum amount of hydrohalic acid so that a homogeneous phase was obtained. The tris derivative was added and the reaction solution was carefully reduced to about 10 ml. Filtration immediately followed after the solution was brought to dry ice temperature. The

bis materials came out as fine, black crystalline compounds in high purity. They were washed several times with small amount of cold ether to remove excess acid and possible tris compounds left behind. They were then dried over calcium chloride as rapidly as possible in vacuo and stored in liquid nitrogen for low temperature experiments.

Extra care was taken to avoid hydrolysis by exclusion of moisture from ether used in the preparation.

3. $Fe[S_2CN(Et)(Me)]_2SCN$:

This compound was synthesized by a different method which is similar to that reported by Straub et al. [22]. The following is a typical preparation.

0.504 gm. of sodium thiocyanate (0.00622 mole) was dissolved into a mixture of 1.5 ml. of concentrated sulfuric acid (18M) in 10 ml. of water. This solution was immediately added to a 60 ml. saturated solution of benzene solution with tris compound. The resulting solution was shaken vigorously for 1 minute. Filtration was done immediately. The precipitate was washed three times with 5 ml. of absolute alcohol. It was dried in the desiccator with calcium chloride as drying agent.

No crystals were obtained by recrystallization from different solvents. Only soft dark green solids were obtained.

B. Chemical Reactions

1. Mixed Dtc-X: X = Cl, Br, I

a.

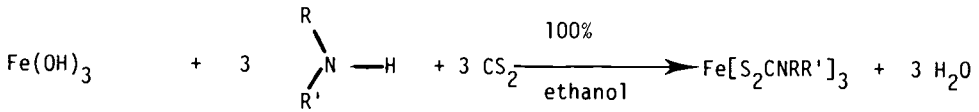

b.

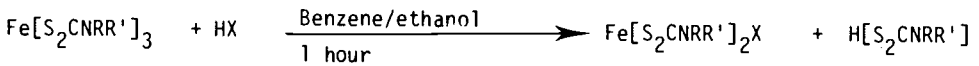

2. Di-n-propyl-dtc-X: X = Cl, Br, I

a.

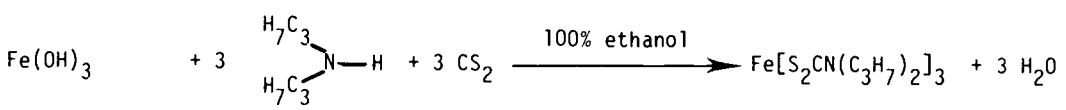

b.

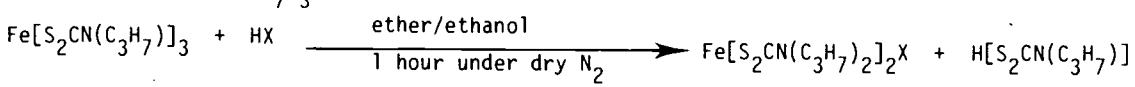

3. Fe[S$_2$CN(Et)(Me)]$_2$SCN:

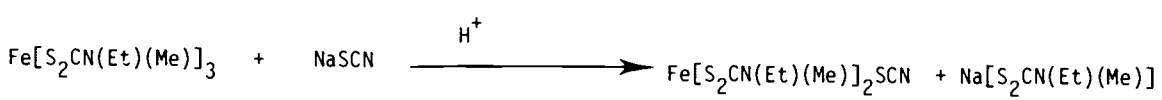

C. Results from Elemental Analysis

One of the materials used for helium experiments was analyzed by Galbraith Laboratories and the following results were obtained:

Sample	%C	%H	%N	%S	%Cl
Et-me-dtc-Cl	26.90	4.63	7.83	35.84	10.01
Theory	26.71	4.48	7.79	35.65	9.85

D. Mossbauer Methodology

A schematic diagram of the Mossbauer spectrometer used in this work is shown in Fig. 4. It was of the conventional constant acceleration type with a ^{57}Co source mounted on a LVsyn-loudspeaker system. The drive system was the standard feedback loop type. A transducer was used to produce an error signal, which was amplified and applied to the drive system to correct the velocity. The variation of the velocity was then synchronized with a multichannel analyzer working in the time mode, so that each channel opening corresponded to a known velocity increment. The velocity function was triangular type, i.e. linear in time. The detection system consisted of: a Reuter Stokes, nitrogen/methane filled proportional counter with a low iron beryllium window, a Tennelec TC914 high voltage bias supply, a Tennelec TC205A linear amplifier and a Nuclear Data ND62 multichannel analyzer. The output from the multichannel analyzer was transferred to a DEC 11/23 microcomputer for subsequent data reduction and plotting on a Hewlett-Packard 7225A plotter.

The sample holder used in the Mossbauer experiments was a two-piece 2.22 cm. diameter lucite disc with a sample thickness of 0.025 cm., sealed with silicon grease.

For measurements in the helium temperature range, sample temperatures were controlled by pumping on liquid helium through a Cartesian Manostat and a needle valve, and monitoring the vapor pressure.

The calibration of the spectrometer was performed by using natural iron foil at 300 K.

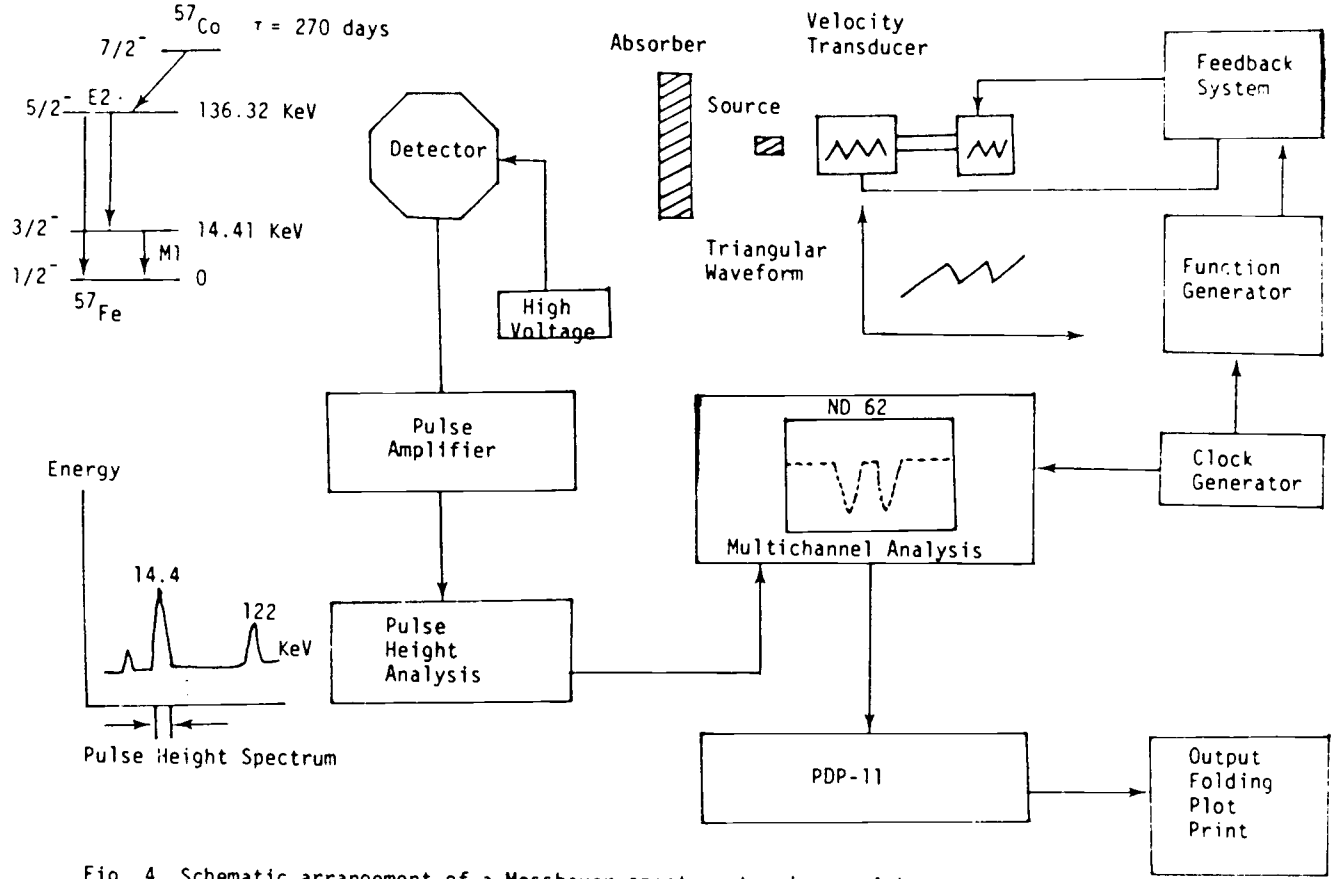

Fig. 4. Schematic arrangement of a Mossbauer spectrometer in our laboratory. See text for details.

CHAPTER III: ELECTRIC MONOPOLE INTERACTION (ISOMER SHIFT)

A. Theory

1. Background

Since the discovery twenty-six years ago of the recoilless emission and absorption of low energy gamma rays by nuclei in solids by R. L. Mossbauer, this technique has been ranked among the most important spectroscopic tools in solid state science. A complete literature survey of the work will find applications in almost all branches of physical and life sciences.

The principles of the Mossbauer Effect can be found in any standard text or review in this field [23-25]. The technique has matured to the point that the experimental parameters can be obtained and fairly well understood. The parameters accessible as a result of this technique will be described and their chemical significance will be pointed out.

A Mossbauer nucleus is penetrated by the surrounding electrical charges, which gives rise to an electrostatic interaction. This energy of interaction can be computed classically with the following assumptions: (a) Non-relativistic effects on the electron densities. This ony faces a challenge when heavy atoms have to be dealt with. A detailed account of the relativistic case is contained in [26]. (b) Constant electron density over the nuclear region. This basically means only s electrons contribute. (c) The size of the

nucleus does not affect the electron wave function. Armed with these assumptions, the first hyperfine interaction in Mossbauer Effect can be derived.

Following Clauser and Mossbauer [27], the Coulomb interaction between a nuclear charge distribution $\rho_n(\underline{r}_n)$ and an electron charge distribution $\rho_e(\underline{r}_e)$ can be written as

$$E = -e^2 \iint \frac{\rho_e(\underline{r}_e)\rho_n(\underline{r}_n)d\tau_e d\ \tau_n}{r} \tag{3.1}$$

where $\rho_e(\underline{r}_e)$ = electronic charge density in the volume element $d\tau_e$ at position $\underline{r}_e$ with the origin at the center of the nucleus under consideration,

$\rho_n(\underline{r}_n)$ = nuclear charge density in the volume element $d\tau_n$ at $\underline{r}_n$,

$r = \left| \underline{r}_e - \underline{r}_n \right|$.

For $\underline{r}_e > \underline{r}_n$, from electrostatics, we can invoke the law of cosines and Binomial Theorem [28] to perform a multipole expansion of the above equation in terms of Legendre polynomial $P(\ell)$'s,

$$E = -e^2 \int_{\tau_n} \int_{\tau_e} \rho_e(\underline{r}_e)\rho_n(\underline{r}_n)\{\frac{1}{r_e} + \frac{r_n \cos\theta}{r_e^2} + \frac{r^2 n}{r^3_e}\frac{1}{2}(3\cos^2\theta - 1) + \cdots\}\, d\tau_e d\tau_n, \tag{3.2}$$

where θ is the angle between $\underline{r}_e$ and $\underline{r}_n$. The first term describes the electric monopole interaction. The second term vanishes due to the absence of an electric dipole moment for a nucleus. The

third term corresponds to the interaction between the nuclear quadrupole moment and the electric field gradient at the nucleus.

The first term can now be written as

$$(E)_{\ell=0} = -e^2 \int_{\tau_n} \int_{\tau_e} \frac{\rho_n(\underline{r}_n)\rho_e(\underline{r}_e)d\tau_e d\tau_n}{r_>} \quad .$$

Integration over angular co-ordinates gives

$$(E)_{\ell=0} = -4\pi e^2 \iint \frac{\rho_n'(\underline{r}_n)\rho_e'(\underline{r}_e)r_e^2 dr_e r_n^2 dr_n}{r_>} \quad , \qquad (3.4)$$

where $\rho'(\underline{r})$ is an average charge density, averaged over a sphere of radius r

$$\rho'(\underline{r}) = \frac{1}{4\pi} \int \rho(r) \sin\theta \, d\theta \, d\phi \quad .$$

Equation (3.4) can be broken up into a sum of two integrals

$$(E)_{\ell=0} = -(4\pi e)^2 \{ \int_{r_n=0}^{\infty} [\int_{r_{\ell=0}}^{r_n} \frac{\rho_e'(\underline{r}_e)}{r_n} r_e^2 \, dr_e + \int_{r_e=r_n}^{\infty} \frac{\rho_e'(\underline{r}_e)}{r_e} r_e^2 dr_e] \rho_n'(\underline{r}_n) r_n^2 dr_n \} \quad .$$

A re-ordering of the limits of the third integral containing dr_e

$$\int_{r_e=r_n}^{\infty} dr_e = \int_{r_\ell=0}^{\infty} dr_e - \int_{r_{\ell=0}}^{r_n} d\, r_e$$

so that

$$(E)_{\ell=0} = -(4\pi e)^2 \{\int_{r_{n=0}}^{\infty} [\int_{r_{\ell=0}}^{r_n} \frac{r'_e(\underline{r}_e)}{r_n} r_e^2 d\gamma_e + \int_{r_{\ell=0}}^{\infty} \frac{\rho'_e(\underline{r}_e)}{r_e} r^2{}_e dr_e$$

$$-\int_{r_{\ell=0}}^{r_n} \frac{\rho'_e(\underline{r}_e)}{r_e} r_e^2 \, dr_e] \times \rho'_n(\underline{r}_n) r^2{}_n dr_n$$

$$= -(4\pi e)^2 \int_0^{\infty} \int_0^{r_n} \rho'_e(\underline{r}_e)\rho'_n(\underline{r}_n) r_e^2 dr_e r_n^2 \, dr_n (\frac{1}{r_n} - \frac{1}{r_e}) + E_o, \quad (3.5)$$

where E_o=monopole shift=$-(4\pi e)^2 \int_{r_{\ell=0}}^{\infty} \int_{r_{n=0}}^{\infty} \frac{\rho'_e(\underline{r}_e) r_e^2}{r_e} dr_e \rho'_n(\underline{r}_n) r^2{}_n dr_n$,

which is just the Coulomb energy for a point nucleus.

In the non-relativistic case, only s electrons have a non-vanishing charge density at the origin. Thus one can set $\rho_e(\underline{r}_e) \approx \rho'_e(0) \left|\psi(0)\right|^2$, where $\psi(0)$ is the non-relativistic wave function at the origin.

If one defined isomer shift = $\delta = (E)_\ell - E_o$, it can be shown by integrating equation (3.5) that

$$\delta = \frac{2}{3} \pi e^2 Z \left|\psi(0)\right|^2 \langle \gamma_n^2 \rangle$$

with

$$Z \langle r_n^2 \rangle = \int r_n^2 \rho_n(\underline{r}_n) d\tau_n \quad .$$

This is universally called the 'isomer shift' because the effect depends on the difference in the nuclear radii of the ground and isomeric, excited states. Consequently a shift of energy is observed as shown in Fig. 5.

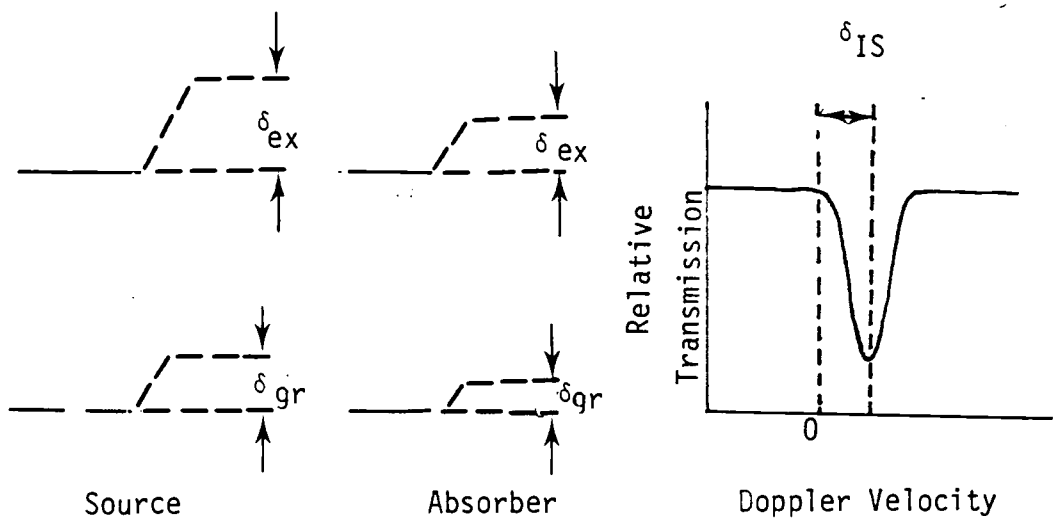

(a) (b)

Fig. 5. (a) Shift of nuclear energy levels due to electric monopole interaction, (b) Typical Mossbauer spectrum in the presence of isomer shift alone.

The shift of the absorption line is just the difference of the shifts of the nuclear ground state δ_{gr}, and the nuclear excited state δ_{ex},

$$\delta_{ex} - \delta_{gr} = \frac{2}{3}\pi e^2 Z\left|\psi(0)\right|^2[\langle r_n^2\rangle_{ex} - \langle r_n^2\rangle_{gr}] \quad .$$

The expression for the source is similar. Thus the difference in shift of the source and the absorber is

$$E_{IS} = (\delta_{ex} - \delta_{gr})_A - (\delta_{ex} - \delta_{gr})_s$$

$$= \frac{2}{3}\pi e^2 Z[\left|\psi_A(0)\right|^2 - \left|\psi_x(0)\right|^2][\langle r_n^2\rangle_{ex} - \langle r_n^2\rangle_{gr}] \quad .$$

In order to observe resonance, this shift of energy is achieved by a relative motion of the source and the absorber with a Doppler

$$\text{velocity } V = \frac{c}{E_\gamma}\frac{2}{3}\pi e^2 Z \Delta|\psi(0)|^2 \Delta\langle r^2 n\rangle \quad , \tag{3.6}$$

where E_γ = gamma ray energy (KeV),

c = velocity of light.

A typical Mossbauer spectrum in the presence of isomer shift alone is shown in Fig. 5b. Equation (3.6) is frequently used in the Mossbauer literature. It is obvious that there are only two important factors in the measurement of isomer shift, namely the electronic density at the nucleus, and the difference in the mean square nuclear radii, which is a nuclear factor. The latter has the advantage of model independence. If a constant density inside a sphere of radius R is assumed and zero outside, then $\Delta\langle r^2_n\rangle = 2/3\ \Delta R^2$. Equation (3.6) becomes $\frac{2\pi c}{5E_\gamma} e^2 Z \Delta|\psi(0)|^2 \Delta R^2$.

Calibration techniques independent of the computation of electron densities have been developed to determine the nuclear parameter $\Delta\langle r^2_n\rangle$. A detailed compilation of $\Delta\langle r^2_n\rangle$ values was done by Kalvius and Shenoy [29].

Once the value of $\Delta\langle r^2_n\rangle$ has been established, eq. (3.6) can be used to measure electronic charge density [30]. For chemical applications the investigation of electron densities is of interest.

It is worth while to pause a moment to briefly examine the qualitative aspects of electron charge density from a chemist's perspective. Some of the general facts which are relevant to latter discussions are summarized as follows:

1. To first order, only the s electrons have a finite density within the nuclear volume. Thus the total electron density $\rho(0)$ is composed of three contributions: $\rho_c(0)+\Delta\rho_c(0)+\rho_v(0)$, where $\rho_c(0)$ is the core contribution due to the inner atomic s orbitals, $\Delta\rho_c(0)$ is the change of the core contribution as a result of modification in outer s or non-s valence orbitals, and $\rho_v(0)$ corresponds to direct contribution from the s valence shell.
2. There is a linear proportionality between experimental isomer shift and its calculated charge density as first shown by Nieuport et al. [31]. A decrease of electron charge density at the nucleus results in a larger, positive isomer shift and vice versa (for the ^{57}Fe resonance, $\Delta\langle r^2_n\rangle$ is negative).
3. The electron charge density at the nucleus is affected by the valence state of the atom, thus the isomer shift provides information on the nature of the chemical bonding.
4. Isomer shift uniquely provides information of the electron densities of different valence states. The Mossbauer technique is sensitive enough to detect the spread of the isomer shift values within a given valence state of an element. In such circumstances, several experimentally observed systematic trends attribute to the consequences of covalency effects and overlap distortion were reported [32-33]. Attempts will be made to incorporate these mechanisms to explain the observed

constancy of the isomer shift of the $Fe(dtc)_2X$ complexes (see the discussion).

2. Molecular Orbital Calculations Methodology:

Semi-empirical molecular orbital methods have been used extensively to calculate electron densities and various contributions to the internal magnetic field at the Mossbauer nucleus and the electric field gradient tensors [31,34-36]. A good review on theoretical aspects of molecular orbital calculations has been given by Marathe et al. [35]. Basic principles are outlined here.

For molecular systems of any size, we can approximate each molecular orbital by a linear combination of atomic orbitals,

$$\psi_i^{MO} = \sum_u C_{ui}\, \phi_u^{At} \quad . \tag{3.7}$$

The total n-electron wavefunction Ψ_{el} is a product of the individual molecular orbital wave functions, which can satisfy the antisymmetry principle by being written in the form of Slater determinant. Using the Schrodinger equation to determine the energy, we get

$$E_{el} = \int \Psi_{el}^{*} \hat{\mathcal{H}}_{el}\, \Psi_{el}\, d\tau$$

$$= \sum_{i=1}^{n} H_i + \frac{1}{2} \sum_{i,j}^{n} J_{ij} - \frac{1}{2} \sum_{i,j=1}^{n} K_{ij} \quad ,$$

where H_i = Orbital energies = $\int \psi_i^{*}(\underline{r})\, h\, \psi_i(\underline{r})\, d\tau$,

$$h = -\frac{1}{2}\nabla^2 - \sum_{k=1}^{n} \frac{1}{|\underline{R}_K - \underline{r}|} \quad \text{in atomic units,}$$

$\underline{R}_k$ = Position vector of nucleus K,

$\underline{r}$ = Position vector of electron i ,

$$J_{ij} = \text{Coulomb integrals} = \int \frac{\psi_i^*(\underline{r}_1)\psi_i(\underline{r}_1)\psi_j^*(\underline{r}_2)d\underline{r}_1 d\underline{r}_2}{|\underline{r}_1 - \underline{r}_2|} \quad ,$$

and K_{ij} = Exchange integrals

$$= \delta(m_{s_i}, m_{s_j}) \frac{\int \psi_i^*(\underline{r}_1)\psi_j(\underline{r}_1)\psi_j^*(\underline{r}_2)\psi_i(\underline{r}_2)d\underline{r}_1 d\underline{r}_2}{|\underline{r}_1 - \underline{r}_2|} \quad .$$

Substituting equation (3.7) into the molecular integrals H_i, J_{ij} and K_{ij}, the total electronic energy of the system can be written as

$$E_{el} = \sum_{uv} P_{uv}H_{uv} + \frac{1}{2} \sum_{\substack{u,v \\ \lambda,\sigma}} P_{uv}P_{\lambda\sigma}\left[(uv|\lambda\sigma) - \frac{1}{2}(u\lambda|v\sigma)\right. \quad ,$$

where $P_{uv} = \sum_{i=1}^{n} n_i C_{ui}^* C_{vi}$, known as bond order or density matrix, (3.8)

$$H_{uv} = \int \phi_u^*(\underline{r})dr \quad ,$$

and $(uv|\lambda\sigma) = \dfrac{\int\int \phi_u^*(\underline{r}_1)\phi_v(\underline{r}_1)\phi_\lambda^*(\underline{r}_2)\phi_\sigma(\underline{r}_2)dr_1 dr_2}{|\underline{r}_1 - \underline{r}_2|}$.

According to variational principle, one can optimize the coefficients C_{ui}^* and C_{vi} so as to minimize the electronic energy

E_{el}. This leads to a set of linear homogeneous Roothaan equations

$$\sum_u (F_{uv} - \varepsilon_i S_{uv}) C_{vi} = 0 \quad , \tag{3.9}$$

where F_{uv}=Fock Matrix=$H_{uv} + \sum_{\lambda\sigma} P_{\lambda\sigma}[(uv|\lambda\sigma) - \frac{1}{2}(u\lambda|v\sigma)]$,

S_{uv} = overlap integral between ϕ_u and ϕ_v ,

and ε_i = orbital energies.

By rewriting equation (3.9) into matrix form, i.e.

$$FC = SCE, \tag{3.10}$$

and defining a set of new relations: $F' = S^{-1/2} F S^{-1/2}$ and $C' = S^{1/2} C$, one can transform equation (3.10) into $F' C' = E C'$. This is a standard eigenvalue problem and the coefficients C can be found from the linear equations $\sum_v (F'_{uv} - E_i \delta_{uv}) C'_{vi} = 0$. and the coefficients C_{vi} are determined by using $C = S^{-1/2} C'$.

The following steps are the routine procedures to solve the Roothaan equations:

a. An initial guess of the LCAO coefficients C_{vi} is made in equation (3.7).

b. The density matrix P_{uv} is calculated and used to form the Fock matrix F_{uv}.

c. A diagonalization process is performed as described in the previous paragraph, thus a new set of coefficients C_{vi} is obtained.

d. Steps b and c are repeated until the coefficients C_{vi} are constant within a given iteration.

In reality, the computation time is large for large systems using the above procedures. A number of approximate MO theories have been developed within the mathematical framework of molecular orbital theory. One of them is the iterative extended Huckel theory (IEHT). In this method, the diagonal elements of the Fock matrix take the form

$$F_{uu} = (\alpha_u + \delta\alpha_u Q_A),$$

where α_u and $\delta\alpha_u$ are adjustable parameters which are related to atomic ionization potentials of AO ϕ_u, and Q_A is the net charge of the atom at which orbital ϕ_u is centered. The off-diagonal matrix elements F_{uv} are determined by the Wolfsberg-Helmholz approximation,

$$F_{uv} = S_{uv}K_{uv}(F_{uu} + F_{vv}),$$

where K_{uv} is a fixed parameter, which has a value between 0.8 and 1.0.

In Cusachs approximation, the parameter K_{uv} is written as

$$K_{uv} = 1 - b|S_{uv}| \quad ,$$

where a and b are 1.0 and 0.5 respectively.

The Huckel-method output includes orbital energies and corresponding MO's, the bond-order matrix, net atomic and orbital charges, and the molecular dipole moment.

Equipped with these concepts, Marathe [19] proceeded to compute the electron density at the iron nucleus. As stated in chapter III A.1, only s electrons contribute to the total electron density, thus

the Fe 3d and 4p orbitals are neglected. The 1s and 2s contributions are also omitted because they can be assumed to be constant [32]. The Fe 4s density at the nucleus is obtained by multiplying $|\psi_{4s}(0)|^2$ by the bond density $P_{4s,4s}$. With non-orthogonality correction, the Fe 3s orbital wavefunction can be written as

$$\phi_{3s} = N[\psi_{3s} - \sum_{i\neq 3s} \langle\phi_i|\psi_{3s}\rangle\ \phi_i]$$

where

$$N = (1 - \sum_{i\neq 3s} |\langle\phi_i|\psi_{3s}\rangle|^2)^{-1/2} \quad ,$$

the ϕ_i are occupied MO's and ψ_{3s} is the 3s Hartree-Fock atomic orbital. Finally, the density at the Fe nucleus may be written as

$$\rho(0) = |\psi_{4s}(0)|^2 P_{4s,4s} + 2N^2|\phi_{3s}(0)|^2$$

$$= |\psi_{4s}(0)|^2 P_{4s,4s} + \frac{2}{1-A}|\psi_{3s}(0) - B\psi_{4s}(0)|^2 \qquad (3.11)$$

where

$$A = \frac{1}{4}\sum_{uv} P_{uv} S_{u,3s} \quad \text{and}$$

$$B = \frac{1}{2}\sum_{u} P_{4s,u} S_{u,3s} \quad .$$

B. Experimental Results

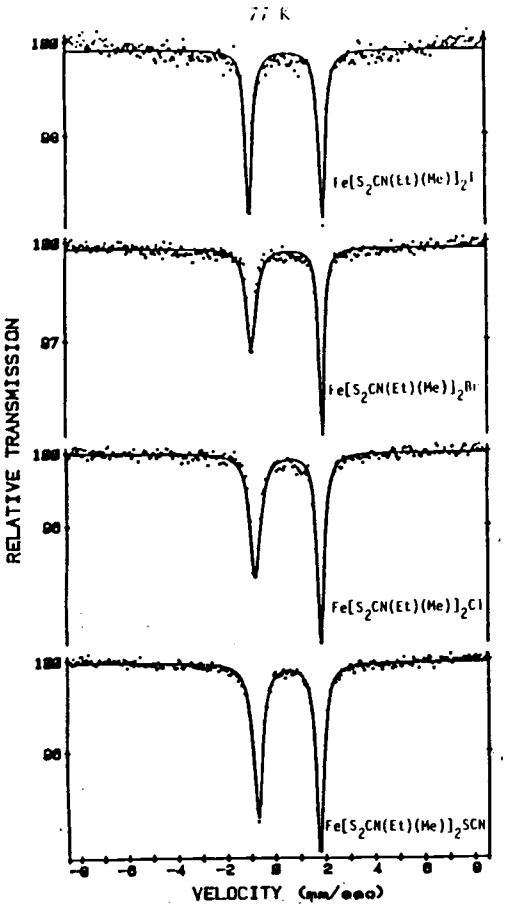

Fig. 6. Mossbauer spectra for halobis(N,N'-ethylmethyl-dithiocarbamato)iron(III) with computer fits.

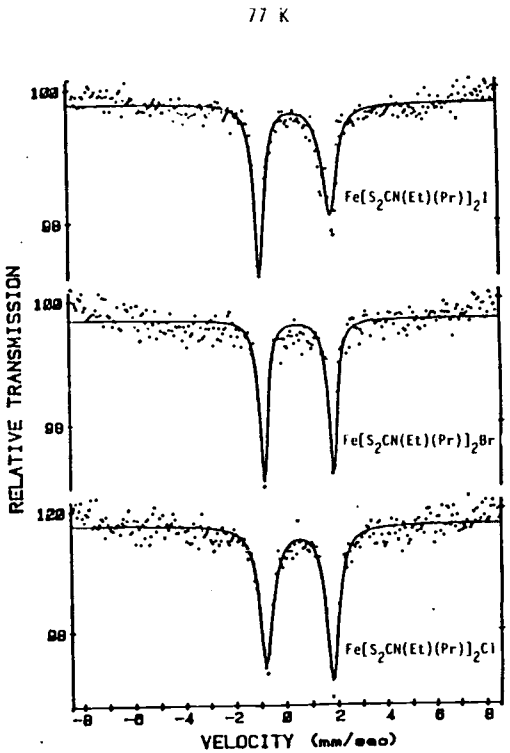

Fig. 7. Mossbauer spectra for halobis(N,N'-ethylpropyl-dithiocarbamato)iron(III) with computer fits.

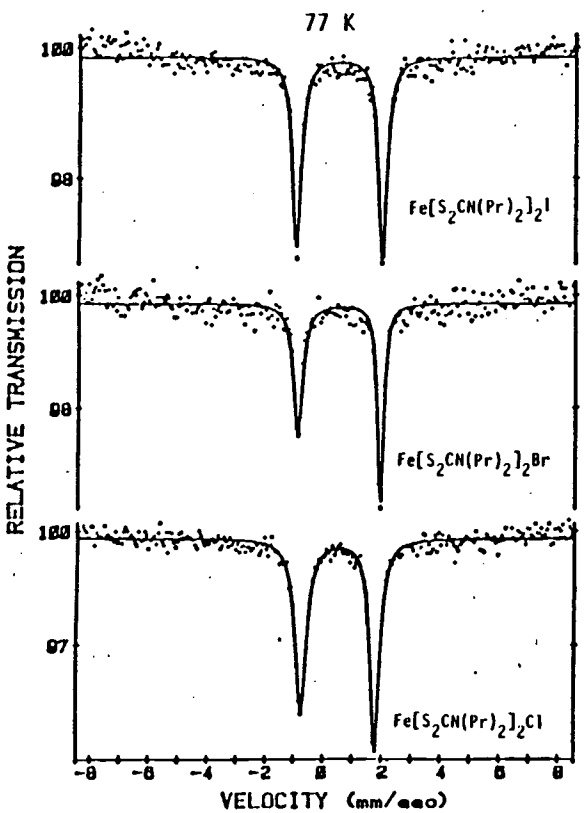

Fig. 8. Mossbauer spectra for halobis(N,N'-di-n-propyl-dithiocarbamato)iron(III) with computer fits.

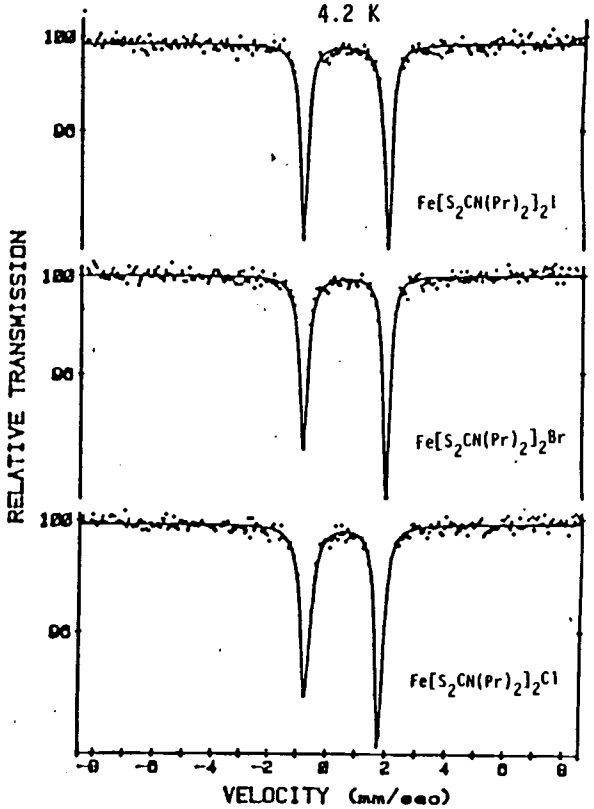

Fig. 9. Mossbauer spectra for halobis(N,N'-di-n-propyl-dithiocarbamate)iron(III) with computer fits.

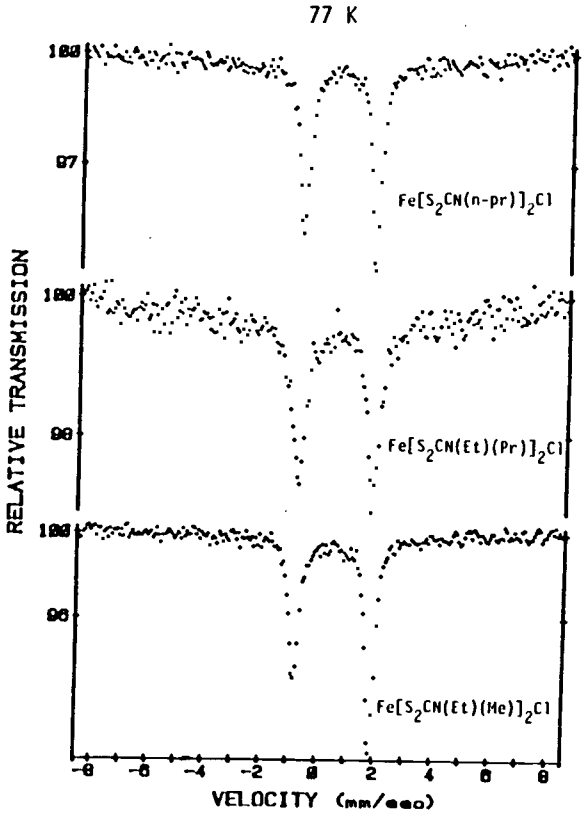

Fig. 10. Mossbauer spectra for a given chloro ligand and varying alkyl groups.

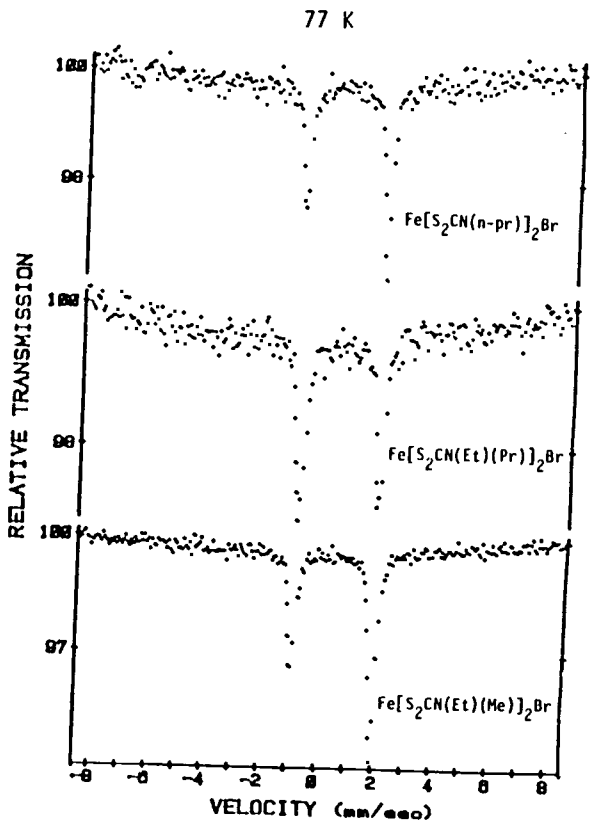

Fig. 11. Mossbauer spectra for a given bromo ligand and varying alkyl groups.

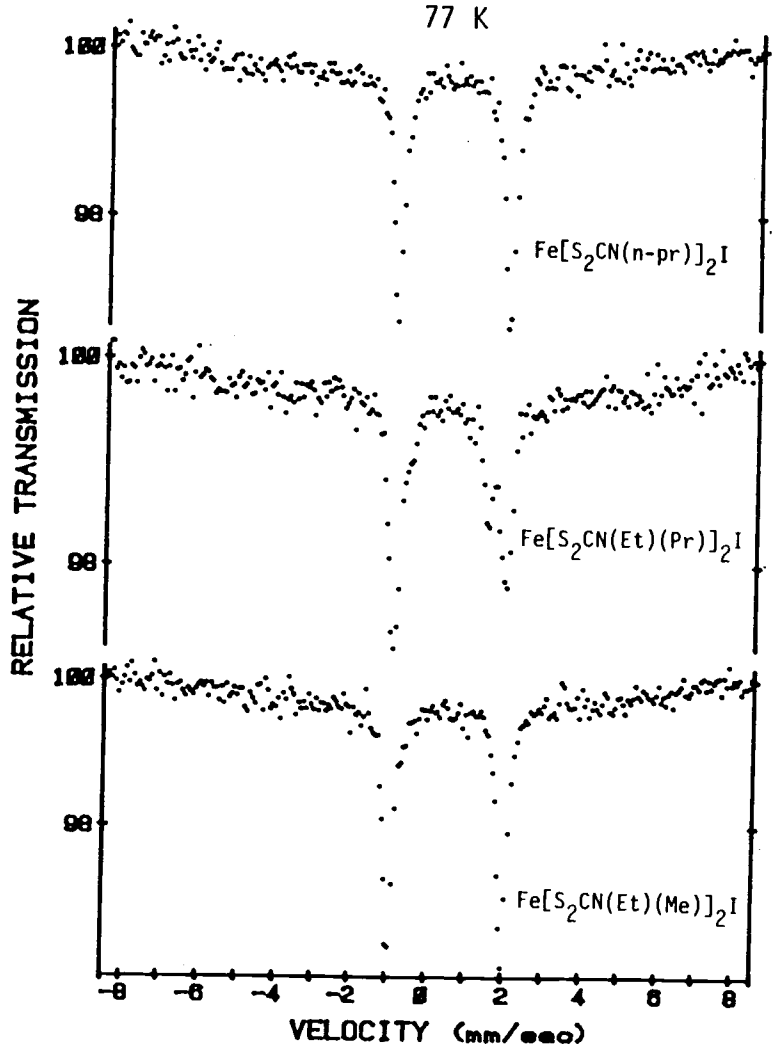

Fig. 12. Mossbauer spectra for a given iodo ligand and varying alkyl groups.

Table 1: Isomer shift of $Fe(dtc)_2X$ at 77 K

		Isomer shift (mm/s.)	Comments
1. R = Me	X = Cl	-------	-------
R'= Me			
2. R = Me	X = SCN	0.515	This work
R'= Et	= Cl	0.517	This work
	= Br	0.517	This work
	= I	0.510	This work
3. R = Et	X = SCN	-------	-------
R'= Et	= Cl	0.518	This work
	= Br	0.522	This work
	= I	0.521(4.2 K)	Ref. [6]
4. R = Et	X = Cl	0.522[d]	This work
	= Br	0.520	This work
	= I	0.479[e]	This work
5. R = Pr	X = Cl	0.526	This work
R'= Pr	= Br	0.517[f]	This work
	= I	0.506[g]	This work
6. R = i-pr	X = Cl	-------	-------
R'= i-pr			

Notes: a. The average isomer shift for twelve measurements is 0.515 mm/s.

b. The standard deviation is $\pm$ 0.008 mm/s. for twelve measurements.

c. For any given R, the average deviation is $\pm$ 0.01 mm/s.

d,f,g. Average of three runs.

h. Isomer shift is the displacement of the centroid of the doublet from the zero velocity.

Table 2: Isomer shift of $Fe(dtc)_2X$ at 4.2 K

			Isomer shift (mm/s.)	Comments
1.	R = Me R'= Et	X = Cl	0.522	This work
2.	R = Et R'= Et	X = Cl	0.490	Ref.[10]
3.	R = Et R'= Pr	X = Cl = Br	0.498 0.520	This work This work
4.	R = Pr R'= Pr	X = Cl = Br = I	0.520 0.517 0.506	This work This work This work

Notes: a. The average for the six measurements is 0.514 mm/s.

b. The standard deviation is $\pm$ 0.008 mm/s.

C. Discussion

Mossbauer spectra data are given in Figs. 6 to 12. Isomer shift data at 77 K and 4.2 K are summarized in Tables 1 and 2 respectively.

The isomer shift values did not show any systematic variation with respect to either the alkyl group R at the terminal end or apical ligand X. The average of twelve measurements is 0.515 mm/sec. ± 0.008 mm/sec. at 77 K (relative to natural iron foil at 300 K). For any given R, the average deviation is ± 0.01 mm/sec., which can be considered as experimental error. The narrow range of observed isomer shifts suggests the differences in electron density of these complexes are very small.

Marathe [19,35] applied equations (3.8) and (3.11) to compute the electron density at the Fe nucleus for two of the halo-bis-dtc complexes. By also varying the terminal alkyl groups H, CH_3, and C_2H_5, they had reported an almost constant electron density in both complexes.

To provide a qualitative interpretation of isomer shift data together with the above inference require the incorporation of two mechanisms in this discussion.

A number of papers have demonstrated the determinant influence of the 'covalency effects' [35-39], which correlate the isomer shift at a metal nucleus and the electronegativity of the ligand for a constant geometry and co-ordination. This correlation predicts a monotonic dependence of the electron density at the nucleus on the

ligand electronegativity. The second mechanism is the 'overlap distortion', which is relevant as soon as the bond distance changes, since this affects the overlap integrals.

Combining these two mechanisms, Axtmann et al. [33] successfully showed a decreasing isomer shift as the electronegativity of the ligand decreases for a class of distorted octahedral Fe(II) halides ($\delta_{Cl} > \delta_{Br} > \delta_{I}$). The reverse trends were observed for the tetrahedral Fe(III) halides ($\delta_{Cl} < \delta_{Br} < \delta_{I}$) [32]. These results arose from different balances of the several contributions to $\rho(0)$ due to the relative strength of the covalency effects and overlap distortion, and were well accounted for by their calculations.

The five-coordinated dtcs compounds may not be too appropriate to discuss along with the octahedral Fe(II) and the tetrahedral Fe(III) halides systems because the dtcs don't have five equivalent ligands surrounding the central metal nucleus. However, the covalency effects and overlap distortion, in principle, could give a qualitative explanation for the constancy of the isomer shift.

Isomer shift is dependent on the charge density at the iron nucleus so that it is very sensitive even to a small change in the core electron orbitals, which themselves are not directly involved in the chemical bonding. The contributions from these core orbitals are modified due to the overlap distortion, which requires all the occupied metal orbitals be mutually orthogonal to each other and also orthogonal to those of the ligands. This requirement is needed

in order to calculate the expectation value of $\rho(0)$. Sawatzky et al. [37] showed that the electron density at the metal nucleus is given by

$$\rho(0) = 2\sum_n \left| \varphi_{ns}(0) \right|^2 + \sum_i \left(\frac{1}{1-\sum_n S_{in}^2}\right) \{\sum_n [S_{in} \varphi_{ns}(0)]^2 - 2\sum_n S_{in} \varphi_{ns}(0)\psi_i(0) + \left|\psi_i(0)\right|^2\}$$

where φ_i designates the one-electron orbital of metal,

ψ_i designates the one-electron orbital of ligands,

and the summation is over the n s orbitals of the metal.

The first term represents the free ion contribution. The second one is the most important one because it involves only wave functions centered on the metal nucleus. As the metal-ligand distance increases, the overlap integrals (S_{in}) become smaller. Thus the charge density at the metal nucleus decreases. Consequently, a larger isomer shift is expected. In short, $\delta_I > \delta_{Br} > \delta_{Cl}$ as Fe-I > Fe-Br > Fe-Cl.

The overlap correction alone is not the whole story to explain the constancy of the isomer shift of $Fe(dtc)_2X$. The first aspect of covalency effects deals with the isomer shift dependency on the ligand electronegativity. Higher electronegativity restricts the delocalization of the 3d electrons, which contribute negatively to the electron density via the screening of the 3s electrons. An increase in isomer shift was observed as the ligand electronegativity increases for iron halides [33].

An alternative point of view has been considered concerning covalency effects on the isomer shift involving the exchange of electron between the metal and the ligand ions through the chemical bonding. The charge transfer is usually referred to as covalency. Backbonding can occur from the filled metal orbitals to the ligand orbitals with low energy and empty $*\pi$ orbitals (e.g. cyanide, nitrosyl or carbonyl ligands) as pointed out by Danon [39]. Alternatively, it is possible for electron transfer to occur from the ligand orbitals into the non-filled orbitals of the metal. A simplified MO diagram for $Fe(dtc)_2X$ is shown in Fig 3. The empty $3d_{XY}$, which substantially has higher energy than the other four available orbitals illustrates that charge transfer is a distinct possibility. Electron can either come from the apical halide or due to the σ-bonding with the four sulphur in the plane [40]. The s electron density will decrease due to the additional shielding effect of the $3d_{XY}$ electron. This results in a larger isomer shift. Molecular orbital calculation showed that the $3d_{XY}$ has 0.93 orbital charges [35] or populated with 0.7 electrons [40].

It is difficult to assess the relative importance of the various mechanisms. A detailed account was given by Sawatzky [37]. Their result is quoted to corroborate the postulates here. They first calculated the 'charge transfer coefficients λ_{ij}' from the first order perturbation theory. The molecular orbital ψ_i^M is a linear combination of the filled ligand orbitals ψ_i and of the non-filled metal orbitals φ_g^e. The final wave function $\psi_i'^M$ which are

orthogonal to all occupied orbitals ψ_i can be written as

$$\psi_i'^{M} = (1+2S_{ij}\lambda_{ij} + \lambda_{ij}^2 - \sum_k S_{ik}^2)^{-1/2}[\psi_i+\lambda_{ij}\ \varphi_g^e - \sum_k S_{ij}\ \varphi_k] \ ,$$

$$\varphi_k' = \varphi_k \ .$$

The charge transfer parameter is taken as an empirical parameter and is calculated from

$$\lambda_{ij} = \frac{\langle \psi_i | \hat{\mathcal{H}} | \varphi_j^e \rangle}{(E_{A_i}^{G-1} + E_{C_j}^{H+1}) - (E_A^G + E_C^H)}$$

where E_A^G and E_C^H are the ligand anion and metal cation ground state binding energies respectively with G and H electrons and $E_{A_i}^{G-1} + E_{C_j}^{H+1}$ is the total energy of a state where one electron has been transferred from the ith orbital of the anion to the jth orbital of the cation. This denominator clearly shows how the electronegativity comes into this discussion.

The direct contribution to the electron density at the Mossbauer nucleus is obtained by considering only the s orbitals of the metal ion. One can write

$$\rho(0) = 2\sum_n |\varphi_{ns}(0)|^2 + \sum_i N_i^2\{\sum_n[S_{in}\ \varphi_{ns}(0)]^2 - 2\sum_n S_{in}\ \varphi_{ns}(0)\ \psi_i(0)$$
$$- 2\sum_n \lambda_{ij}\ S_{in}\ \varphi_{js}^2(0) + |\lambda_{ij}\ \varphi_{js}^e(0)|^2$$
$$+ 2\ \lambda_{ij}\ \varphi_{js}^2(0)\ \psi_i(0) + |\psi_i(0)|^2\} \ ,$$

$$\text{with } N_i^2 = (1 + 2\ S_{ij}\ \lambda_{ij} + \lambda_{ij}^2 - \sum_n S_{ij}^2) \ . \qquad (3.12)$$

Several comments can be made about equation (3.12). The first term indicates the free ion charge density. The additional terms represent the effects of covalency and overlap. The appearance of λ_{ij} in N_i makes it impossible to separate completely the two mechanisms. Further, to apply equation (3.12) to an actual solid requires the consideration of various symmetry representations of orbitals. This is necessary because only ligands orbitals will have non zero overlap with the metal orbitals of corresponding symmetry. For simplicity, this problem is omitted here.

For iron compounds the terms involving the ligand orbitals are usually less than 10% of the first correction and can be neglected. The first term $2 \sum_{n}^{3} \left| \varphi_{ms}(0) \right|^2$ becomes dominant and depends on the pure 3d character. From the Hartree Fock calculations, one obtains

$$2 \sum_{n=1}^{3} \left| \varphi_{ns}(0) \right|^2 = C + 1.8(\delta n_{3d}) \tag{3.13}$$

where δM_{3d} is the change in the occupation of the 3d orbitals and C is the free ions electrons due to overlap and covalency which can be parameterized using Linear Combination of Atomic and Molecular Orbitals (L.C.O.A.M.O.) theory. The charge density of pure 3d character is then given by [38]

$$\delta n_{3d} = \sum_{\ell} [1 - S_{\ell d}^2 m_d + (B_{\ell d}^2 + 2B_{\ell d} S_{\ell d})(1-m_d)]^{-1} [B_{\ell d}(1-m_d) - S_{\ell d} m_d]^2 \tag{3.14}$$

where the sum is over the five different d type orbitals, $B_{\ell d}$ is the group transfer integral and $S_{\ell d}$ is the group overlap integral, m_d is the occupation number of the d orbital in question and it is 0 or 1 to ensure that charge transfer can occur only into the unoccupied orbitals. This has to be modified in $Fe(dtc)_2X$, because it was calculated by Ganguli et al. [40] that the d_{XY} is populated with 0.7 electron. Obviously both overlap distortion and covalency effects would increase the 3d electrons due to the square term in equation (3.14). The final problem is to estimate the various $B_{\ell d}$ and $S_{\ell d}$. In literature, a detailed calculation was done on iron in octahedral coordination only ([38] and references therein).

Ingalls et al. [38] argued that this description involving the 3d orbitals predicts an increase in the isomer shift with decrease in Fe-ligand distances as well as a decrease with increasing electronegativity of the halides. Both of these are opposite to those experimental trends discussed earlier here. They concluded that either (i) the s electrons are dominant and wash out the small effect due to the 3d electrons or (ii) this L.C.A.O. treatment of 3d orbital covalency is not valid.

Ingalls et al. were doubtful about L.C.A.O. approach of 3d orbitals because there are no experimental data to support the theory. This may not be true any more because in $Fe(dtc)_2X$ complexes, the quartet state exists such that covalency effects and overlap distortion result in an experimentally observed constant

isomer shift. This leads to a prediction of a constant δn_{3d}, which is a function of $B_{\ell d}$ and $S_{\ell d}$ for all these complexes. This qualitative conclusion is all that can be said at this stage.

CHAPTER IV: ELECTRIC QUADRUPOLE INTERACTION (QUADRUPOLE SPLITTING)

A. Theory

1. Background

As mentioned in the previous chapter, the quadrupole splitting is given by the third term in equation (3.2). In Cartesian co-ordinates, it can be written in a compact manner as follows [25]:

$$\mathcal{H}_Q = -\frac{1}{6}\sum_{ij} Q_{ij}\,(\nabla E)_{ij}$$

where $Q_{ij} = \int_{\tau_n} \rho_n(\underline{r}_n)(3X_{ni}X_{nj} - \delta_{ij}r_n^2)d\tau_n$,

$$\nabla E_{ij} = -\int_{\tau_n} \frac{\rho_e(\underline{r}_e)}{r_e^5}\,(3X_{ei}\,X_{ej} - \delta_{ij}r_n^2)d\tau_e \quad .$$

Q_{ij} and ∇E_{ij} are symmetric second rank tensor and have vanishing traces. The angular dependence of the integral in Q_{ij} along the Z-axis is identical to the quadrupole moment (eQ). By using the Wigner-Echart theorem, the mean value of the spin operator taken over a given nuclear level equals to eQ also. Thus

$$\int_{\tau_n} \rho_n(\underline{r}_n)(3Z_n^2 - r_n^2)d\tau_n = C\langle\frac{3}{2}\,(\hat{I}_i\hat{I}_j+\hat{I}_j\hat{I}_i-I^2)\rangle = eQ \quad .$$

It follows that $C = eQ/I(2I-1)$. Denoting the electric field gradient at the origin as $V_{ij} = -(\nabla E)_{ij}$, .

$$\hat{\mathcal{H}}_Q = \frac{eQ}{6I(2I-1)}\sum_{i,j} V_{ij}[\frac{3}{2}(\hat{I}_i\hat{I}_j + \hat{I}_j\hat{I}_i) - \delta_{ij}I^2] \quad ,$$

$$= \frac{e^2q\,Q}{4I(2I-1)} [3\hat{I}_Z^2 - I^2 + \frac{n}{2}(\hat{I}_+^2 - \hat{I}_-^2)] \quad . \qquad (4.1)$$

All the notations have their standard meanings.

The ground nuclear state of ^{57}Fe has I = 1/2, thus is not split by $\hat{\mathcal{H}}_Q$. Upon diagonalization for the different I levels of the first excited state I = 3/2, two, two-fold degenerate energy levels separated in energy $\Delta E_Q = \frac{1}{2} e^2qQ\,(1+\frac{n^2}{3})^{1/2}$ are obtained.

A typical Mossbauer spectrum is shown as below:

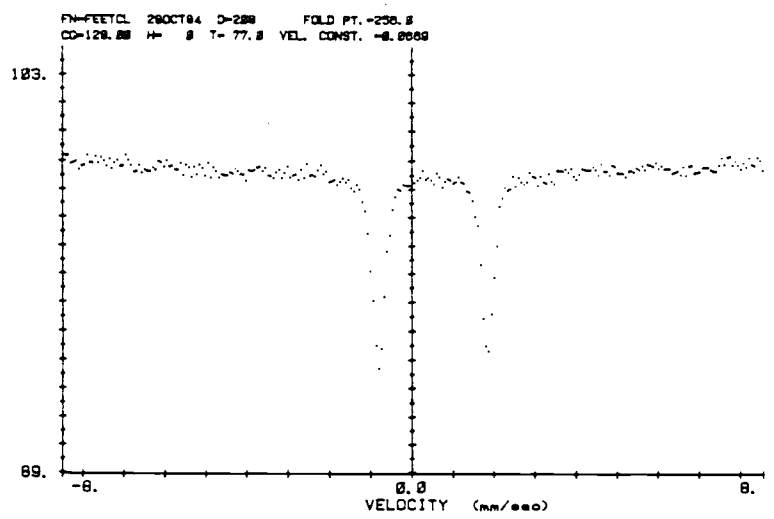

Fig. 13. Mossbauer spectrum of ^{57}Fe in presence of quadrupole interaction.

The origin of the electric field gradient (EFG) in pentacoordinated Fe(III)-dithiocarbamates has stimulated several theoretical calculations. The relatively high quadrupole splitting in these

complexes which is about 2.7 mm/s. could not be explained by the crystal field model, since the EFG arising from the 3d valence electrons in a quartet state is zero. Ake et al. [41] therefore proposed the lattice contributions as its origin. De Vries [42] pointed out that due to the low symmetry of the complexes, the covalency differences in the various iron atomic orbitals give rise to the large EFG. The latter view was substantiated by a molecular orbital calculation on $Fe(dtc)_2Cl$. Additional supports for this view were than supplied by other authors who used slightly different approaches [19,40].

2. Molecular Orbital Methodology

De Vries [42] calculated the EFG with the aid of the extended Huckel LCAO-MO method on $Fe(dtc)_2Cl$. Their method will not be described here because only one calculation was done. Marathe et al. [19] extended the calculations by using the semi-empirical Iterative Extended Huckel Theory (IEHT)(Chapter IIIA), which included various choices of the dithiocarbamate ligand and groups. Hasselback et al. [40] completed the picture by using the Self-Consistent Charge Extended Huckel Molecular Orbital (SCCEHMO). The method involved a selection of ligands at the apical position.

Excluding metals in our discussion, in solids the EFG at the Mossbauer nucleus arises from the ligand cores and the valence electrons of the molecules, i.e.

$$V_{ab} = V_{ab}^{\text{ligand cores}} + V_{ab}^{\text{valence electrons}} \quad . \qquad (4.2)$$

The first term in equation (4.2) is given by

$$V_{ab}^{\text{ligand cores}} = \frac{\sum_{k=H} Z_k[1-\gamma(|\underline{R}_k-\underline{R}_M|)]3(a_k-b_k)(b_k-b_M)-\delta_{a_k}\delta_{b_k}|\underline{R}_k-\underline{R}_M|^2}{|\underline{R}_k-\underline{R}_M|^5}$$

where $\underline{R}_M$ is the position vector of the Mossbauer atom,

$\underline{R}_k$ is the position vector of the other atoms in the molecule,

Z_k is the core charges of the other atoms in the molecule,

and $\gamma(\underline{r})$ is the Sterheimer shielding function, which arises from the polarization of the core electrons of the Mossbauer atom. It is an important parameter in the numerical method, thus the evaluation of this factor has been discussed in detail by Trautwein [35]. The second term can be written in a compact tensor form

$$\hat{V}_{ab}^{(i)} = \frac{[1-\gamma(\underline{r}_i)](3\hat{a}_i\hat{b}_i - \hat{r}_i^2\,\delta_{a_ib_i})}{\hat{r}_i^5}\,,\quad (a_ib_i = X_i,Y_i,Z_i) \quad .$$

$V_{ab}^{\text{valence electrons}}$ then is calculated from $-e\sum_i^n \langle\psi_i|\hat{V}_{ab}(i)|\psi_i\rangle$,

where ψ_i is the molecular orbital defined in equation (3.7). By using equations (3.7) and (3.8), the final form of the contribution due to the valence electrons of the molecule can be molded as

$$V^{\text{valence electrons}} = -e\sum_{uv} P_{uv}\langle\phi_u|\hat{V}_{ab}|\phi_v\rangle \quad . \qquad (4.3)$$

To be more explicit, $V_{ab}^{\text{valence electrons}}$ is composed of the following four contributions: (a) Valence contribution by the valence electrons of Mossbauer nucleus, (b) contribution by the valence electrons of ligands, (c) contribution by the bonding electrons

between the Mossbauer nucleus and the surrounding ligands, and (d) contribution due to the overlap charges between two ligands. Each of these can be represented by integrals in which the wave functions are written in radial and angular parts. Reschke [43] solved all these integrals by a three-dimensional numerical integration method.

Ganguli [40] carried out the SCCEHMO calculation, which is similar to the above method to study the origin of the EFG. However, a slightly different tensor operator $\hat{V}_{ab}$ was employed,

$$V_{ab} = \frac{[1 - \gamma(\underline{r}_i)]q(3\,\hat{r}_{a_i}\,\hat{r}_{b_i} - \hat{r}^2\,\delta_{a_i\,b_i})}{\hat{r}_i^5} \quad , \tag{4.4}$$

where q is the charge at position $\underline{r}$. This operator is made up of the contributions (a) to (d) that we just mentioned.

The valence shell contribution was calculated using the operator equivalence

$$V^i_{ab} = e\langle\|V_{a_i\,b_i}\|\rangle(1-R_{nb_i})\langle r^{-3}\rangle_{nb_i}[\tfrac{1}{2}(\hat{\ell}_{a_i}\ell_{b_i}+\ell_{b_i}\ell_{a_i}-\frac{\ell(\ell+1)}{3}\delta_{a_i\,b_i}] \ .$$

The following parameters were used: (a) The reduced element $\langle\|V_{a_i b_i}\|\rangle$ is 2/7 for d, 6/5 for p$^-$ and zero for s-electrons. (b) $R_{3d} = R_{4p} = 0.32$. (c) $\langle r^{-3}\rangle_{3d} = 5.1\ a_o^{-3}$, and $\langle r^{-3}\rangle_{4p} = 1.7\ a^{-3}$.

All other contributions were calculated using equation (4.4) in a point charge approximation. Results were given in Table 3 of Ref. [40].

B. Experimental Results

Table 3: Quadrupole splitting of $Fe(dtc)_2X$ at 77 K

		Quadrupole splitting (mm/s.)	Comments
1. R = Me	X = SCN	2.56	Ref.[22][a]
R'= Me	= Cl	2.67	Ref.[22]
	= Br	2.86	Ref.[22]
	= I	2.96	Ref.[22]
2. R = Me	X = SCN	2.53	This work
R'= Et	= Cl	2.67[b]	This work
	= Br	2.84	This work
	= I	2.96	This work
3. R = Et	X = SCN	2.55	Ref.[22]
R'= Et	= Cl	2.65(2.63)	This work(Ref.[22])
		2.71	Cal'd(Ref.[40])
	= Br	2.84(2.78)	This work(Ref.[22])
		2.84	Cal'd(Ref.[40])
	= I	2.87	Ref.[22]
		2.90	Cal'd(Ref.[40])
4. R = Et	X = Cl	2.62[c]	This work
R'= Pr	= Br	2.75[d]	This work
	= I	2.81[e]	This work
5. R = Pr	X = Cl	2.51[f]	This work
R'= Pr	= Br	2.81[g]	This work
	= I	2.91[h]	This work
6. R = i-pr	X = Cl	2.68	Ref.[11]
R'= i-pr			

Notes: a. All measurements quoted from Ref.[22] were done at room temperature and relative to sodium nitroprusside.

b,c,d,f,g and h are average of two measurements.

e. Average of three runs.

i. For X = Cl, the average is 2.61 mm/s., $\pm$ 0.05 mm/s. taken over the Rs.

j. For X = Br, the average is 2.81 mm/s., $\pm$ 0.03 mm/s. taken over the Rs.

k. For X = I, the average is 2.89 mm/s., $\pm$ 0.06 mm/s. taken over the Rs.

Table 4. Quadrupole splitting of $Fe(dtc)_2X$ at 4.2 K

		Quadrupole splitting (mm/s.)	Comments
1. R = Me, R'= Et	X = Cl	2.67	This work
2. R = Et, R'= Et	X = Cl	2.70	Ref.[48]
	= Br	2.87	Ref.[48]
3. R = Et, R'= Pr	X = Cl	2.65	This work
	= Br	2.74	This work
4. R = Pr, R'= Pr	X = Cl	2.50	This work
	= Br	2.81	This work
	= I	2.90	This work

Notes: a. For X = Cl, the average is 2.61 mm/s. $\pm$ 0.05 mm/s. taken over the Rs.
b. For X = Br, the average is 2.81 mm/s. $\pm$ 0.03 mm/s. taken over the Rs.

C. Discussion

Mossbauer spectra data are given in Figs. 6 to 12. The results for the quadrupole splitting at 77 K and 4.2 K are summarized in Tables 3 and 4 respectively.

Even though the samples are polycrystals, the two quadrupolar lines are not of equal intensity in some of the figures. There are two possible explanations for this. The first explanation is based on the anisotropy of the recoil-free fraction of the absorber iron nucleus. A possible cause was discussed by Karyagin [44]. Blume [45] pointed out that such asymmetries can also arise as a result of the fluctuations of the paramagnetic iron nucleus, which have a different effect on the two components of the quadrupole-split line. A more detailed discussion is given in the chapter of paramagnetic relaxation. Experimentally, these two mechanisms can be distinguished by observing the quadrupole pattern in a single crystal. The relaxation effects will give a broadening which affects the same line regardless of the direction of observation. On the other hand, the recoil free fraction depends on a specific direction in which the ion can most easily recoil.

Generally for any given alkyl group R, the splitting increases as the apical ligand distance increases.

A simple model which was postulated by Epstein et al. [22], proposed a large, positive and constant valence contribution directed along the Fe-halide (Fe-X) major axis. The contribution due to X along the major axis was assumed to be negative and subtracted

directly from the valence contribution. As a result, when X is farther away from the iron nucleus, its contribution decreased, and so the splitting increased from Cl to I. This description looks compatible to our observed data.

No doubt, this over-simplified picture could face serious challenges. The MO calculation [40] showed that there are only small charges on the atoms (Table 3 of Ref. [40]), thus the lattice contribution was indeed very small. This proved the crystal field model calculation by Ake [41] was wrong. The $^4A_2$ quartet is expected to have the electronic configuration $3d^2_{X^2-Y^2}\ 3d^1_{XZ}\ 3d^1_{YZ}\ 3d^1_{Z^2}\ 3d^0_{XY}$ [19]. A simplified MO diagram is shown in Fig. 3. The high energy of '$3d_{XY}$' accounts for the spin pairing of the fifth electron. It was shown by the population analysis that the $3d_{XY}$ atomic orbital, which points to the sulphur atoms in the plane, is not empty but is populated by about 0.7 electronic charge [40]. This gives rise to a 'positive' EFG, as the contributions from the other 3d atomic orbitals nearly cancel each other. This result is not surprising because it is possible electron transport can occur from the negative dtc$^-$ ligands to the Fe^{3+} ion through the initially empty $3d_{XY}$ orbital. This accounts for the measured large quadrupole splittings. By using equation (4.4) to calculate the contribution due to the valence electrons of the ligand atoms, it was shown that as the Fe-halide distance increases, the negative valence contribution becomes smaller ($-0.87 < -0.82 < -0.78$). This results in a larger quadrupole splitting as postulated by Epstein [22] and supported by this work.

Spin-orbital coupling tends to mix electron states which are energetically close to each other. Thermal energy affects the population of these electron states according to Boltzmann statistics. From our experimental data at 4.2 K and 77 K, the nuclear quadrupole splitting is unchanged over a wide range of temperature. These data show that the splittings between the adjacent energy levels shown in Fig. 3 are indeed large (> 1000 cm^{-1}) compared to the spin-orbital coupling constant λ(λ is 104 cm^{-1} for Fe^{3+}).

CHAPTER V: MAGNETIC DIPOLAR INTERACTION (MAGNETIC SPLITTING)

A. Theory

The interaction of the nuclear magnetic moment $\underline{u}_I$ with a magnetic field $\underline{H}$, due to the atom's own electrons, is known as the Zeeman effect,

$$\hat{\mathcal{H}}_M = - \hat{\underline{u}}_I \cdot \underline{H} = - \gamma h \hat{\underline{I}} \cdot \underline{H} = - g_I u_N \hat{\underline{I}} \cdot \underline{H} , \qquad (5.1)$$

where γ is the gyromagnetic ratio, g_I is the nuclear g factor and μ_N is the nuclear magneton. The energy levels are given by

$$E = - g_I \mu_N H m_I \qquad , \quad m_I = - I, - I + 1 \ldots I - 1, I.$$

As a classic example, the interaction of the ^{57}Fe nucleus with $\underline{H}$ gives rise to six magnetic dipole transitions between the excited and the ground states as governed by the selection rule $\Delta m = 0, \pm 1$. The resulting Mossbauer spectrum is shown in Fig. 14b.

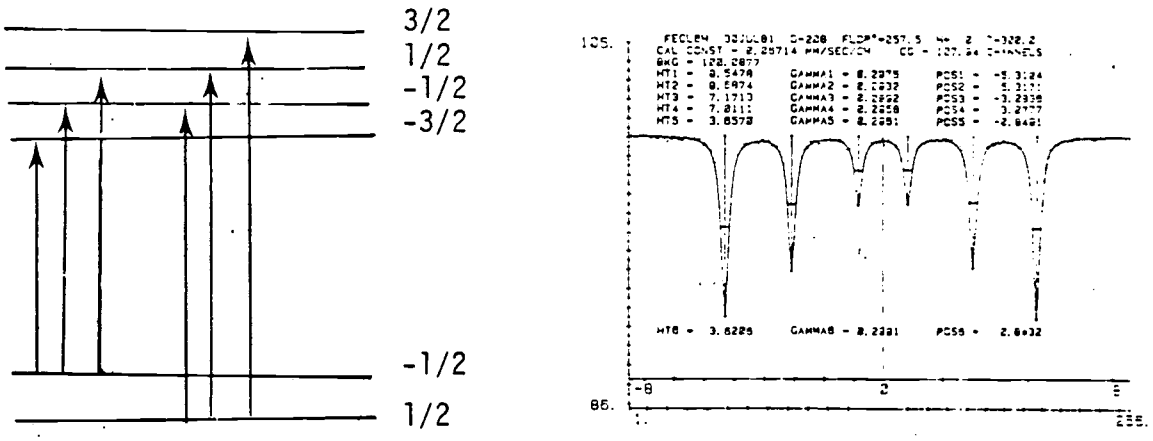

(a) (b)

Fig. 14(a) Zeeman splittings of nuclear levels of ^{57}Fe and (b) the resulting Mossbauer spectrum.

In equation (5.1), the magnetic field acting on the nuclear moment $\underline{u}_I$ may be an external applied field or the internal field due to the presence of the unpaired electrons in the vicinity of the nucleus. Here, only the latter situation will be discussed.

In general, the internal field consists of three parts, the contact field $\underline{H}_C$, the orbital field $\underline{H}_L$, and the spin dipolar field $\underline{H}_{SD}$,

$$\underline{H}_{int} = \underline{H}_C + \underline{H}_L + \underline{H}_{SD} \quad .$$

These various contributions can be estimated from MO calculations [19,35].

The contact interaction is the direct interaction of the nuclear magnetic moment with the spherically symmetric spin density at the nucleus. Only s electrons possess non-zero density at the nucleus and are involved in this interaction. This direct interaction sometimes is termed the 'Fermi Contact Interaction', which is isotropic.

The Mossbauer nucleus can be considered as a small sphere of volume $V = (4\pi\, r^3/3)$ with uniform magnetization $\underline{M} = \underline{u}_N/V$. This provides a flux density $\underline{B}_N = (8\pi/3)\underline{\mu}_N/V$ inside this nuclear volume [25]. The interaction Hamiltonian for the Fermi Contact interaction can be written as

$$\hat{\underline{\mathcal{H}}}_C = - \underline{B}_N\, (-2\mu_B \hat{\underline{S}})\rho(0) = \frac{16\pi}{3}\, g_I\, \mu_N\, \mu_B\, \hat{\underline{I}} \cdot \hat{\underline{S}}\, \rho(0) \quad , \qquad (5.2)$$

where $\rho(0)$ is the electron density at the origin. Considering all the effects from s electrons, with spin up and down, the net field is

$$B(0) = \frac{8\pi}{3} g\mu_B S \sum_n \{\rho_\uparrow(0) - \rho_\downarrow(0)\}$$

Usually, there are two distinct contributions to the Fermi interaction: (a) electrons of neighboring ions covalently mixed into valence s shell of the parent atom, and (b) a spin polarization is induced in the filled s core orbitals by the unpaired non s electrons due to the exchange interaction. In this case, the contact field is proportional to an effective spin $\langle S_Z \rangle$.

The core-polarization contributions ave been calculated by the unrestricted Hartree-Fock technique. Both theoretical and experimental arguments have determined that the core-polarization is directly proportional to the effective spin $\langle S_Z \rangle$ of the open non-s valence shell [46]. The constant of proportionality is roughly $-125/\langle s_Z \rangle$ KOe for the 3d series.

The orbital hyperfine interaction arises from the unquenched orbital angular moment ℓ of the valence electron:

$$\underline{H}_L = \frac{-e\underline{v} \times \underline{r}}{r_e^3} = -2\mu_B \underline{\ell} \left\langle \frac{1}{r_e^3} \right\rangle ,$$

where $\mu_B = \frac{e\hbar}{2mc}$ is the Bohr magneton. The interaction with the nuclear moment is thus described by

$$\hat{\mathcal{H}}_L = 2 \mu_N \mu_B g_I \left\langle \frac{1}{r_e^3} \right\rangle \hat{\underline{I}} \cdot \hat{\underline{\ell}} \qquad (5.3)$$

In bis(dtc) complexes, the ground state satisfies $\langle L \rangle = 0$, so $\hat{\mathcal{H}}_L$ may be neglected [4].

The spin-dipolar interaction $\hat{\mathcal{H}}_{SD}$ is the contribution to $\underline{H}_{int}$ from the spin magnetic moment of the electrons outside the nucleus. The appropriate Hamiltonian is

$$\hat{\mathcal{H}}_{SD} = 2\, g_N\, \mu_N\, \mu_B \left\{ \sum \left(\frac{\hat{S}_i}{r_e^3} \right) + \left[3(\underline{S}_i \cdot \underline{r}_i)\underline{r}_i / r_i^5 \right] \right\} \cdot \hat{\underline{I}} \quad , \qquad (5.4)$$

where $\underline{r}$ is the unit vector from the nucleus to the electron.

In summary, equation (5.1) is equivalent to the sum of equations (5.2), (5.3), and (5.4). However, the interaction between the unpaired electrons and the nuclear moment has a tensor character. In the paramagnetic system as described here, it's more appropriate to apply the spin Hamiltonian formalism. Thus, equation (5.1) is replaced by $\hat{I} \cdot \bar{\bar{A}} \cdot S'$ where the fictitious spin operator S' acts within a manifold of (2S' + 1) electronic states.

Earlier measurements on $Fe(dtc)_2X$ complexes had shown that $\underline{H}_c + \underline{H}_{SD} \approx 221$ KOe $\langle S_Z \rangle$, where $\langle S_Z \rangle$ is the expectation value of the total spin [4].

In paramagnets, the hyperfine structure will show up if the electronic fluctuations are slow enough with respect to the Larmor precession time of nuclear spin ($\tau_e \gg \tau_L$) and the nuclear lifetime, $\tau_N \leq \tau_e$ [47]. One observes a quasi-static situation which is measured as a superposition of several spectra corresponding to the magnetic fields B_i from individual electronic states thermally populated at the temperature of the measurement. A conventional Hamiltonian for the excited state I = 3/2 is given by [48]

$$\hat{\mathcal{H}} = g_N \mu_N \underline{B}_i(\theta,\phi)\cdot\underline{\hat{I}} + \frac{e^2qQ}{12}\left[3\hat{I}_Z^2 - I(I+1) + n(\hat{I}_X^2-\hat{I}_Y^2)\right] , \quad (5.5)$$

which is employed to fit experimental data. This includes a polycrystal averaging procedure. The resulting process gives valuable information on the electronic wave-functions and the internal field at the nucleus.

In the intermediate regime ($\tau_L \approx \tau_e$), the spectra will no longer be the superposition spectra, then a more complete theory must be invoked. The next chapter is devoted to the required relaxation formalism.

Finally, in the fast relaxation limit, the nucleus 'sees' a zero time-average magnetic field. The magnetic splitting then collapses with the emergence of a familiar quadrupole doublet.

B. Discussion

In the past, a programme called 'P1' was employed, whose outputs are polycrystalline absorption patterns for the Hamiltonian of equation (5.5). From a spectral fit, one obtained the effective magnetic field around the Mossbauer nucleus and the asymmetry parameter η. We then used these results to fit other data at all other temperatures. Unfortunately, the same procedures could not produce reasonable fits to the experimental data shown in Figs. 17a and 22a. Thus only a rough estimation of the effective magnetic field can be made.

The outer two peaks arise from the transition $|\, I_g \pm 1/2\rangle$ to $|\, I_{ex} \pm 3/2\rangle$. The splitting between these peaks can be measured from the plots. The distances were then compared with the ones that obtained from other chloro-dtcs with known effective magnetic fields. The results are summarized in Table 5.

Table 5. Nuclear hyperfine data

Complex	E (4.2 K) (mm/s.)	H_{eff} (KG)
(a) $Fe[S_2CN(Et)(Me)]_2Cl$	2.67	334 ± 5
(b) $Fe[S_2CN(Et)(Pr)]_2Cl$	2.65	337 ± 5
(c) $Fe[S_2CN(n\text{-}pr)_2]_2$ Cl	2.50	-------

CHAPTER VI: PARAMAGNETIC RELAXATION THEORY

A. Theory

1. Introduction

The philosophy is direct and simple to analyze paramagnetic hyperfine structure. A Mossbauer spectral simulation model with a given set of parameters (e.g. relaxation constant C. and the crystal field D parameter) is searched to simulate theoretical spectra that can match our experimental data successfully under a variety of experimental conditions (e.g. temperature). Theoretical study of Mossbauer lineshape is a complicated one in condensed matter physics but has been investigated by a number of authors in recent years [15-16, 49-52]. No attempt will be made here to repeat the derivation of the lineshape. However, the underlying physical principles will be described with justification from the experimental data.

The theoretical treatment can be divided into two categories. The first one is termed as perturbation treatment which considers some of hyperfine interactions as perturbations. In depth attack to this problem by using the relaxation equation for the density matrix was done by Hartmann-Boutron and coworkers [53,54]. Blume utilized the ideas developed by Anderson and Kubo [15,49] in magnetic resonance studies, called the Anderson-Weiss stochastic model by recognizing the fluctuations in the surroundings of nucleus produce a time-dependent interaction for the latter. The effect of the envi-

ronment is thus replaced by a classical randomly varying magnetic field, which can be either parallel. oriented at an angle or perpendicular with respect to the 'stationary' EFG. The last case appears in the Fe(III) penta-co-ordinate dithiocarbamate complexes [55].

2. Origin of the paramagnetic relaxation:

$Fe(dtc)_2X$ is typical of an intermediate state (S=3/2) whose ionic levels are split into two doublets $| m_s = \pm 3/2 \rangle$ and $| m_s = \pm 1/2 \rangle$ by the crystalline field. Relaxation occurs due to the transitions between different ionic levels. There are different electronic mechanisms that account for these transitions, namely 'spin-spin relaxation', 'spin-lattice relaxation', 'cross-relaxation' and 'dynamic Jahn-Teller Effect' [15,25]. The dipole-dipole interaction is believed to be the sole factor to induce transitions. The time dependence of the magnetic field at the Mossbauer nucleus arises due to the spin fluctuations among the spin states. The Mossbauer nucleus feels this effect through the magnetic hyperfine interaction coupled to the ionic spin. The relaxation processes are schematically shown in Fig. 15. Notice that in the paramagnetic case, there is no splitting of the electronic levels due to the absence of an exchange field, which is a characteristic of an ordered magnetic system. the transition rates are given by the relations [4].

$$P_1 (\mp 1/2 \rightarrow \pm 1/2) = 16\ C\ \bar{n}\ (\pm 1/2)$$

$$P_2 (\pm 3/2 \rightarrow \pm 1/2) = 9\ C\ \bar{n}\ (\pm 1/2)$$

$$P_3 (\pm 1/2 \rightarrow \pm 3/2) = 9\ C\ \bar{n}\ (\pm 3/2) \qquad (6.1)$$

In the simplest approximation, $P_4(\pm 3/2 \rightarrow \pm 3/2)$ is neglected owing to the selection rules on the relaxation operators. More will be said about these relations in section 4 of this chapter. When electronic relaxation times are long, the nucleus will experience a hyperfine field (Chapter VA). In a magnetic system such as iron, the effective field felt by the nucleus is about 110 <s> kG.

The accountable relaxation process affects the correlation function of the nuclear emission or absorption operator. The lineshape is obtained from the Fourier transform of the correlation function discussed in the next section.

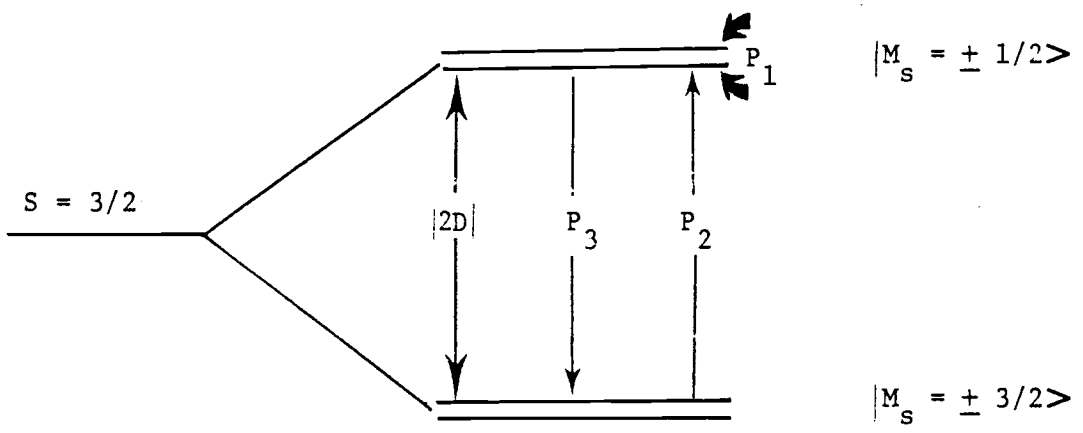

Fig. 15. Schematic illustration of electronic energy levels and relaxation processes for S = 3/2.

3. Expression for the line shape:

Beginning with a two-level system with states $|\lambda'\rangle$ and $|\lambda\rangle$. A direct process involves a transition of the system between these two states with the simultaneous emission or absorption of a phonon of energy $|E_\lambda - E_{\lambda'}|$, conserving the energy. From Carrington [56], the probability for transition can be written as

$$W_{\lambda' \to \lambda} = \left|\langle\lambda| \hat{\mathcal{H}}_{\text{int}}^{(+)} |\lambda'\rangle\right|^2 \delta(\lambda + E_\lambda - E_{\lambda'}) \quad , \tag{6.2}$$

where $\hat{\mathcal{H}}_{\text{int}}^{(+)}$ is the coupling between the photon of the electromagnetic field and the spin, and $\delta(\omega + E_\lambda - E_{\lambda'})$ is the Dirac delta function. If the density of the final state is not a delta function but is given by $[(\omega + E_\lambda - E_{\lambda'})^2 + \frac{\Gamma^2}{4}]^{-1}$, then we obtain the so-called Wigner-Weisskopf expression:

$$W_{\lambda' \to \lambda} = \frac{\left|\langle\lambda| \hat{\mathcal{H}}_{\text{int}}^{(+)} |\lambda'\rangle\right|^2}{(\lambda + E_\lambda - E_{\lambda'})^2 + \frac{\Gamma^2}{4}} \quad . \tag{6.3}$$

Equation (6.3) can be generalized to give the following expression for the line shape

$$I(\omega) = \sum_{\lambda\lambda'} p W_{\lambda\lambda'} = \sum_{\lambda\lambda'} p \, \frac{\left|\langle\lambda| \hat{\mathcal{H}}_{\text{int}}^{(+)} |\lambda'\rangle\right|^2}{(\omega + E_\lambda - E_{\lambda'})^2 + \frac{\Gamma^2}{4}} \quad ,$$

where p is the probability that the initial state $|\lambda'\rangle$ occurs.

In the lineshape problem, it is natural to deal with the time-development in the Heisenberg picture and assuming $\hat{\mathcal{H}}_{int}^{(+)}$ is an Hermitian operator, i.e. $\hat{\mathcal{H}}_{int}^{(-)} = (\hat{\mathcal{H}}_{int}^{(+)})^*$. By carrying out the Laplace transform, one finds

$$I(\omega) = (\frac{2}{\Gamma})\mathrm{Re} \int_{-\infty}^{\infty} dt \exp(-i\omega t - \frac{1}{2}\Gamma t) < \hat{\mathcal{H}}_{int}^{(-)} \hat{\mathcal{H}}_{int}^{(+)}(t) >_{average} , \tag{6.4}$$

where the symbol "Re" indicates that only the real part of the expression is to be considered. Equation (6.4) is traditionally considered as the starting piont for stochastic lineshape calculations.

One of our aims is to test the validity of this theoretically derived lineshape by a detailed analysis of the relaxation phenomena from the $Fe(dtc)_2X$ complexes.

4. Markov process:

In the long relaxation time limit, all the magnetic interactions can be approximated by the classical field $\hat{\underline{H}}m = (A/g_N u_N)M_S(t)$, where M_S = -S, -S+1, ... S-1, S. Since it is assumed to be perpendicular to the EFG principal axis, $\hat{\underline{H}}m$ does not commute with the quadrupolar term, i.e. $[\hat{\underline{H}}_m(t), \hat{H}_Q] \neq 0$. This situation has been termed "nonadiabatic" relaxation. An appropriate Hamiltonian for this regime will be

$$\hat{\mathcal{H}} = g_N \mu_N \underline{B}_m(\theta,\phi)\cdot\hat{\underline{I}} + \frac{e^2qQ}{12}[3\hat{I}_Z^2 - I(I+1) + \eta(\hat{I}_X^2 - \hat{I}_Y^2)] . \tag{6.5}$$

With this Hamiltonian in mind, Blume and Tjon [15] evaluated the stochastic average $\langle \hat{\mathcal{H}}_{int}^{(-)} \hat{\mathcal{H}}_{int}^{(+)} \rangle$ from equation (6.4). The idea is to give an expression for the lineshape in terms of the matrix of transition probabilities per unit time, W_{ij}. The procedure utilizes the concept of Markov process, which is well-known in the adiabatic theory of motion narrowing [57].

To continue with the Heisenberg approach, the time dependent radiation interaction Hamiltonian becomes

$$\hat{\mathcal{H}}_{int}^{(+)}(t) = \exp\left(i \int_0^\tau \hat{\mathcal{H}}(t')\, dt'\right) \hat{\mathcal{H}}_{int}^{(+)} \exp\left(-i \int_0^\tau \hat{\mathcal{H}}(t')\, dt'\right) .$$

Replacing $\hat{\mathcal{H}}(t')$ by the electron-nuclear interaction $A_{zz} I_z S(t')$. the stochastic average is

$$\left| \langle \hat{\mathcal{H}}_{int}^{(+)} \rangle \right|^2 \exp\left[i A_{zz}(m_I - m_{I'}) \int_0^\tau S(t')\, dt'\right] ,$$

where m_I is the eigenvalue of I_Z.

The main problem is to show how the integral $\exp[i\int^\tau S(t')dt']$ is evaluated. Details can be found in Abragram's book [57]. To begin with, the Markovian behavior is assumed, which means the probability depends only through the time interval and not on the time itself. The probability function $W(S_1|S_2, \Delta t)$ means that $S(t)$ has a value S_2 if the value is S_1 at Δt seconds earlier. For a physically reasonable system and small Δt, W may be written as

$$W(S_1|S_2, \Delta t) = \delta_{S_1,S_2} + P(S_1,S_2)\Delta t \quad , \qquad (6.6)$$

where $P(S_1,S_2)$ is the probability per unit time of a transition from S_1 to S_2. δ is Kronecker if the S's form a discrete set.

By dividing the time interval into n equal parts, the integral $\exp[i \int_0^\tau S(t')dt']$ can be approximated as

$$\sum_{S_1 \ldots S_n} [B(S_1,t_1 \ldots . S_n,t_n)] x \exp\left[i(S_1 + \ldots . S_n)\frac{\tau}{n}\right] , \qquad (6.7)$$

where $B(S_1,t_1;S_2,t_2 \ldots .)$ is the probability that $S(t)$ is at S_1 at t_1 and S_2 at t_2, etc. For a Markov process, this is equivalent to write

$$B(S_1, t_1; S_2, t_2 \ldots) = W_1 W(S_1 \mid S_2, \tau/n) \ldots \ldots . W(S_{n-1}) \mid S, \frac{\tau}{n}).$$

W is defined at (6.6) while W_1 is the probability that $S(t)$ has the value S at time zero. Equation (6.7) can be rewritten as

$$\sum_{S_1 \ldots S_n} [W_1 \prod_{m=2}^{n} W(S_{m-1} \mid S_m, \frac{\tau}{n})] \times \exp(i\frac{\tau}{n} \sum_{m=1}^{n} S_m)$$

$$= \sum_{S_1 \ldots S_n} \ldots . \prod_{n=1}^{n-1} [\exp(i\frac{\tau}{n} S_m) \times W(S_m \mid S_{m+1}, \frac{\tau}{n})] \exp(iS_n\frac{\tau}{n}) \times W_1 . \qquad (6.9)$$

Neglecting $S_n(\frac{\tau}{n})$, and introduce $\tilde{W}$ as a row vector in S space and $\bar{1}$ as a column vector. Equation (6.7) can be molded into matrix form

$$\tilde{W} [\exp(i \frac{\tau}{n} \bar{S}) \bar{W}]^{n-1} \cdot \bar{1}$$

$$= \tilde{W} [\exp(i(i\bar{S} + \bar{P}))] \cdot \bar{1}$$

by using equation (6.6) and letting n go to infinity.

To be more specific in the problem, the function S(t) has four allowed electronic states (±3/2, ±1/2). Wickman and Wagner [4] called this the "four-state model". The electronic fluctuations are limited to these four states, in which the dipole-dipole interaction randomly modulates the electronic states [Fig. 15].

The Hamiltonian for the electronic dipole-dipole interaction can be written as [58]:

$$\hat{\mathcal{H}}_{d\text{-}d} = \gamma^2 \sum_j \frac{1}{r_j^3} [(\hat{\underline{S}}_i \cdot \hat{\underline{S}}_j) - 3(\hat{\underline{S}}_i \cdot \underline{r}_{ij})(\hat{\underline{S}}_j \cdot \underline{r}_{ij})] \quad . \quad (6.10)$$

This can be conveniently represented by

$$\hat{\mathcal{H}}_{d\text{-}d} = \text{Constant } (\frac{1}{r^3}) [A + B + C + D + E + F]$$

where $A = \hat{S}_{1Z} \hat{S}_{2Z} (1-3 \cos^2 \theta)$

$$B = -\frac{1}{4} (1-3 \cos^2\theta)(\hat{S}_{1+} \hat{S}_{2-} + \hat{S}_{1-} \hat{S}_{2+})$$

$$C = -\frac{3}{2} \sin\theta \cos \theta \exp(-i\phi) (\hat{S}_{1Z} \hat{S}_{2Z} + \hat{S}_{2Z} \hat{S}_{1-})$$

$$C^* = D = -\frac{3}{2} \sin\theta \cos \theta \exp (i\phi)(\hat{S}_{1Z} \hat{S}_{2-} + \hat{S}_{2Z} \hat{S}_{1-})$$

$$E = -\frac{3}{4} \sin^2 \theta \exp (-2i\phi)\hat{S}_{1+} \hat{S}_{2+}$$

$$E^* = F = -\frac{3}{4} \sin^2\theta \exp(2i\phi) \hat{S}_{1-} \hat{S}_{2-}$$

Grow [58] has calculated all the elements of the dipole-dipole relaxation matrix. Transitions between the field states are computed by the expression

$$P_{ij} = \left|\langle i|\langle j|\hat{\mathcal{H}}_{d-d}|i\rangle|j\rangle\right|^2 \bar{n}(j) \quad .$$

The wavefunctions $|i\rangle$ ad $|j\rangle$ are eigenstates of equation (1.1). The most probable transitions are those which conserve crystal field energy.

In this work, the Hamiltonian is truncated into a simpler form

$$\hat{\mathcal{H}}'_{d-d} = \text{Constant } (\frac{1}{r_{ij}^3})[(1-3\cos^2\theta_{ij})(\hat{S}_{1+}\hat{S}_{2-} + \hat{S}_{1-}\hat{S}_{2+})] \quad . \quad (6.11)$$

The constant in equation (6.11) represents both dipolar and isotropic exchange coupling spins i and j. $\hat{\mathcal{H}}'_{d-d}$ induces a transiion tion rate which is given by

$$P_{ij}(M_s \rightarrow M_{s'}) = c\left|\langle M_s|S_{\pm}|M_{s'}\rangle\right|^2 \bar{n}(M_s) \quad , \quad (6.12)$$

where $\bar{n}(M_s)$ is the normalized population of the M_s state and were explicitly written in equation (6.1). The strength of the spin-spin interaction depends on the varied parameter 'C'.

In summary, the matrices $\tilde{\tilde{W}}$, $\bar{P}$ and $\bar{S}$ are written as follows:

$$\tilde{\tilde{W}} = \begin{vmatrix} \tilde{W}_1 \text{ or } \bar{n}_1 & \exp[E(-\frac{3}{2})/kT] \\ \tilde{W}_2 \text{ or } \bar{n}_2 & = \exp[E(-\frac{1}{2})/kT] \\ \tilde{W}_3 \text{ or } \bar{n}_3 & \exp[E(+\frac{1}{2})/kT] \\ \tilde{W}_4 \text{ or } \bar{n}_4 & \exp[E(\frac{3}{2})/kT] \end{vmatrix}$$

$$\bar{P} = \begin{vmatrix} 9\tilde{W}_2 & -9\tilde{W}_2 & 0 & 0 \\ -9\tilde{W}_2 & 9\tilde{W}_1 + 16\tilde{W}_3 & -16\tilde{W}_3 & 0 \\ 0 & -16\tilde{W}_2 & 16\tilde{W}_2 + 9\tilde{W}_4 & -9\tilde{W}_4 \\ 0 & 0 & -9\tilde{W}_3 & 9\tilde{W}_3 \end{vmatrix}$$

$$S = \begin{vmatrix} -3/2 & 0 & 0 & 0 \\ 0 & -1/2 & 0 & 0 \\ 0 & 0 & 1/2 & 0 \\ 0 & 0 & 0 & 3/2 \end{vmatrix}$$

where E(i) is the energy of the ith state, S has the four values of the spin S(t) along the diagonal of the spin matrix, and zero elsewhere, and $\bar{P}$ gives the transition rate between the possible values of S(t).

5. Blume and Tjon method:

Armed with the required Hamiltonian (6.5) and equation (6.4), Blume and Tjon [15] used algebraic manipulation to determine the spectral intensity which explicitly appeared in their work. Using their notations, the intensity is given here as

$$I(w) = (2\Gamma)^{-1}\mathrm{Re} \sum_{\substack{m_0 \\ m_1}} \left|\langle I_0 m_0 \left| \mathcal{H}_{int}^{(+)} \right| I_1 m_1 \rangle\right|^2 \times \sum_{ij} p_i$$

$$\langle j \left| \tilde{A}(p) \left[\tilde{E} + 3Q^2 n^2 \tilde{B}(p)\tilde{A}(p)\right]^{-1} \right| i \rangle \quad . \qquad (6.13)$$

The various parameters are explicitly defined as follows:

(i) $p = -i(\omega-\omega_0) + \frac{\Gamma}{2}$,

(ii) $\tilde{A}(p)$ is the Laplace transform of $A(t)$

$= [p\tilde{E} - \tilde{W} - i(C_1-C_0)\tilde{F} + i\beta\tilde{E}]^{-1}$,

(iii) $\tilde{B}(p)$ is the Laplace transform of $B(t)$

$= [p\tilde{E} - \tilde{W} - i(C_1' - C_0)\tilde{F} - i\beta\tilde{E}]^{-1}$,

(iv) $\tilde{E}$ is the unit 4 X 4 matrix ,

$\tilde{F}$ is the 4 X 4 diagonal matrix with $(F_{ii}) = M_s(i) = S_{ii}$,

$C_1 = g_1\beta_N M_1 H_m$,

$C' = g_1(M_1 \pm 2)\beta_N H_m$,

$C = g_0 \beta_N M_0 H_m$,

$B = Q(3M_i^2 - 15/4)$,

$Q = eqQ/12h$,

$\tilde{W} = \bar{P}$ is the matrix of transition probabilities with indices i,j, corresponding to the electronic M state: $i = 1 \rightarrow M_s = -3/2$ etc.; $(P)_{ij}$ are given by equation (6.12) for $i = j$ and $P_{ii} = -\sum_j P_{ij}$; finally P is not a probability matrix for $\sum_j P_{ij} = 0$ (see eq. 6.6).

6. Clebsch-Gordan Coefficient:

So far, the discussion only takes care of the second part of equation (6.13). The first part, the matrix elements $\langle I_0 m_0 | \hat{H}_{int}^{(+)} | I_1 m_1 \rangle$ deal with the absorption of the gamma rays and

also depend on time. The transition probability of this gamma radiation with wave vector $\vec{k}$ and polarization $\vec{e}$ must be calculated. The results give the number of transitions and their intensities in terms of the Clebsch-Gordan (CG) coefficients.

Rose and Brink [59] discussed two ways to approach this absorption problem, namely the semi-classical and the quantum field theory. From their conclusion, the interaction Hamiltonian can be written in terms of the irreducible tensor T_{LM}. By using the Wigner-Eckart theorem for T_{LM}, we obtain the CG coefficients as shown:

$$\langle I_1 m_1 \left| T_{LM}^{<\pi>} \right| I_0 m_0 \rangle = (-1)^{2L} (I_0 L m \cdot M \left| I_1 m_1 \right\rangle \langle I_1 \| T_2 \| I_0 \rangle \quad .$$

The reduced matrix elements can be set to unity. The CG coefficoefficients give the relative values for $\langle I_0 m_0 \left| \hat{\mathcal{H}}_{int}^{(+)} \right| I_1 m_1 \rangle$. The square of the CG coefficients provides the relative intensities of the transitions. For ^{57}Fe, where the transition matrix elements of $\mathcal{H}_{int}^{(+)}$ are of the magnetic dipole (M1) character, there are eight possible transitions between levels. The +3/2→-1/2 and -3/2→+1/2 transitions have zero probability as $\Delta m = \pm 2$, thus only six transitions are allowed. These allowed transitions and their corresponding CG coefficients are listed below [60]:

Transitions	Δm	CG	Relative intensity $(CG)^2$
$-\frac{3}{2} \rightarrow -\frac{1}{2}$	1	$\frac{1}{2\sqrt{3}}$	3
$-\frac{1}{2} \rightarrow \frac{1}{2}$	1	$-\frac{1}{6}$	1
$\frac{1}{2} \rightarrow -\frac{1}{2}$	-1	$-\frac{1}{6}$	1
$\frac{3}{2} \rightarrow \frac{1}{2}$	-1	$\frac{1}{2\sqrt{3}}$	3
$-\frac{1}{2} \rightarrow -\frac{1}{2}$	0	$\frac{1}{\sqrt{2}\ 3}$	2
$\frac{1}{2} \rightarrow \frac{1}{2}$	0	$\frac{1}{\sqrt{2}\ 3}$	2

7. Fitting Procedure

With the parameters defined in the preceding sections, a computer program was written to simulate relaxation spectra for an $S = 3/2$, ^{57}Fe atom. To compute lineshapes, it is only necessary to define matrixes appearing in equation (6.13) and manipulate matrix subroutines.

In the systems studied here $S = 3/2$, $I = 3/2$ and $I = 1/2$, this would require a 128 x 128 matrix $(2I_1 + 1)(2I_2 + 1)(2S + 1)^2$ in Liouville space for a complete calculation. In BT's work, the classical field is assumed fluctuating along the Z-axis of the EFC tensor system. Because of this, the Liouville matrix is diagonal in Mz quantum numbers. Thus we only have to deal with a number of 4 X 4 complex matrixes, which depend on the quantum numbers M_0 and

M_1. However, a coordination transformation is necessary to bring the orientation of H_m as specified above be compatible to equation (1.1). The relations can be found in reference [4].

The inversion of matrixes is furnished under 'invert a matrix' and 'final matrix algebra' in the program. The final matrix is denoted by 'SCR'. The sum of each column of SCR is weighted by the appropriate Boltzmann factors, PB and the square of the Clebsch-Gordan coefficients, since the latter is proportional to the relative intensities of the nuclear transitions. In practice, only six coefficients are necessary [60].

The fitting procedure is straightforward but tedious. This is due to the fact that the crystal field D and E parameters are not known in advance. In addition, one needs the internal field H_{eff} around the nucleus and the spin-spin coupling constant C. The non-trivial time involved in the calculation by using the PDP-11 prevents a least square fitting of the data. Since E is assumed to be zero, a perfect fit is not to be expected.

To begin with, one starts from the lowest temperature by inputting a set of parameters (D, H_{eff}, C, ΔE_Q and η) to generate the theoretical data. ΔE_Q can be obtained from 4.2 K experiment. η is assumed to be the same as the other dtcs with known structure information. After a reasonable plot is obtained, C and D are kept constant and empirically adjust H_{eff} at different temperatures to achieve agreement with the remaining experimental Mossbauer curves.

The analysis of the data depends on (i) whether D is positive or negative and (ii) whether exchange and/or external fields are present. For the sake of completeness, the four cases will be surveyed here, but only the last case will be discussed in detail.

Case(a): D > 0 and no magnetic or exchange fields

A typical example is $Fe(diethyldtc)_2Br$ recrystallized from dichloro-methane [11]. Relaxation was quite fast and no paramagnetic hyperfine structure was observed.

Case(b): D > 0 and magnetic or exchange fields present

Several examples fulfill these conditions. $Fe(Morpholyldtc)_2$ halides [58], $Fe(diethyldtc)_2Br$ precipitated in excess benzene [48] and $Fe(diethyldtc)_2I$ [6]. However, there were no relaxation studies on the last two examples.

Case(c): D < 0 and magnetic or exchange fields present

These conditions can be found in $Fe(diethyldtc)_2Cl$ [4] and $Fe(diethyldsc)_2Cl$ [13-14].

Case(d): D < 0 and no magnetic or exchange fields present

The first example is $Fe(diisopropyl)_2Cl$ [4] and three of the bis-chloro-dtcs described in this thesis. The derived effective spin-spin couplings are listed in Table 6. The physical significance of this parameter will be considered in the discussion.

B. Experimental and Theoretical Results

a. $Fe[S_2CN(Et)(Me)]_2Cl$

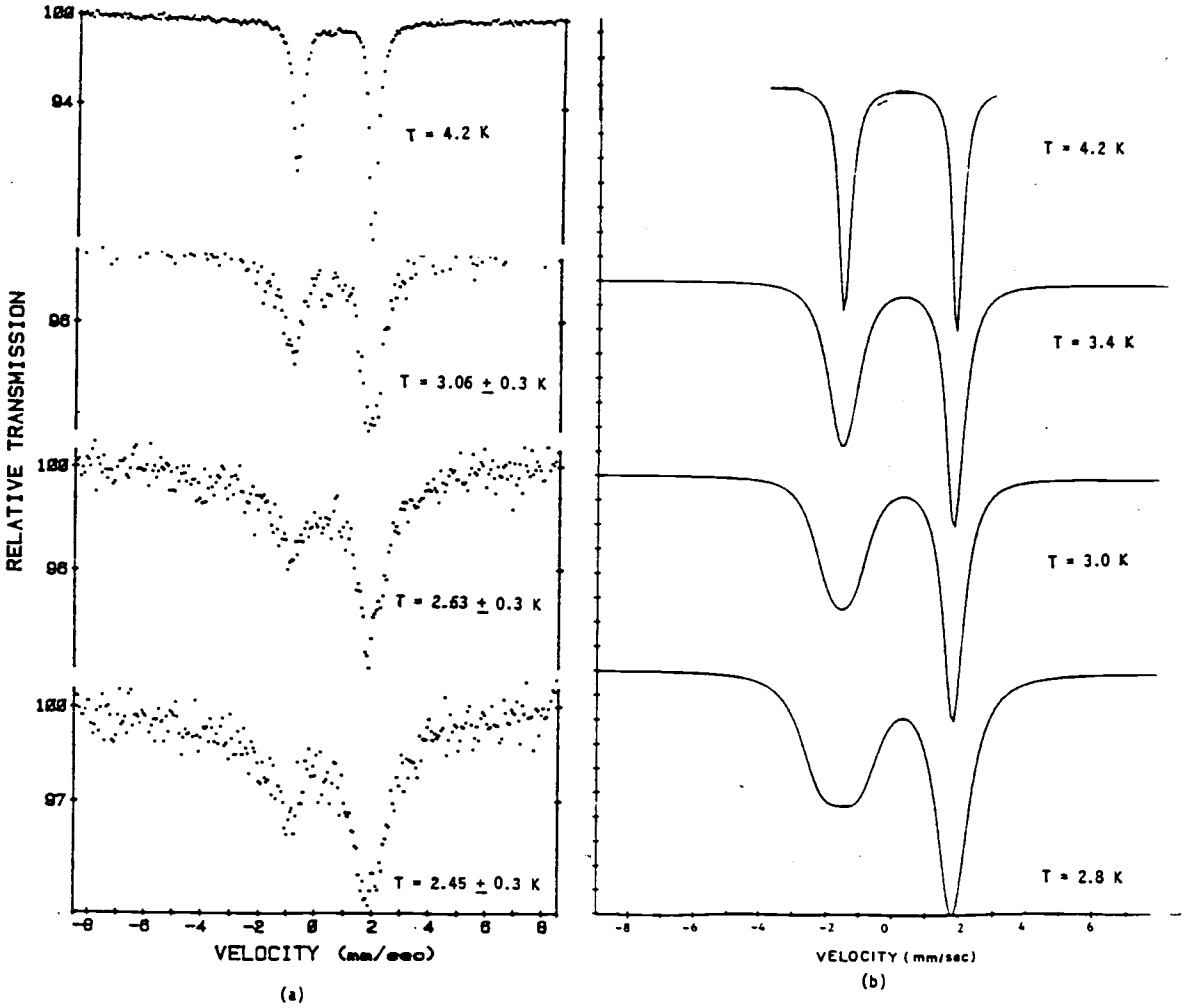

Fig. 16. (a) Mossbauer spectra between 2.45 and 4.2 K.
(b) Computer simulated Mossbauer spectra.

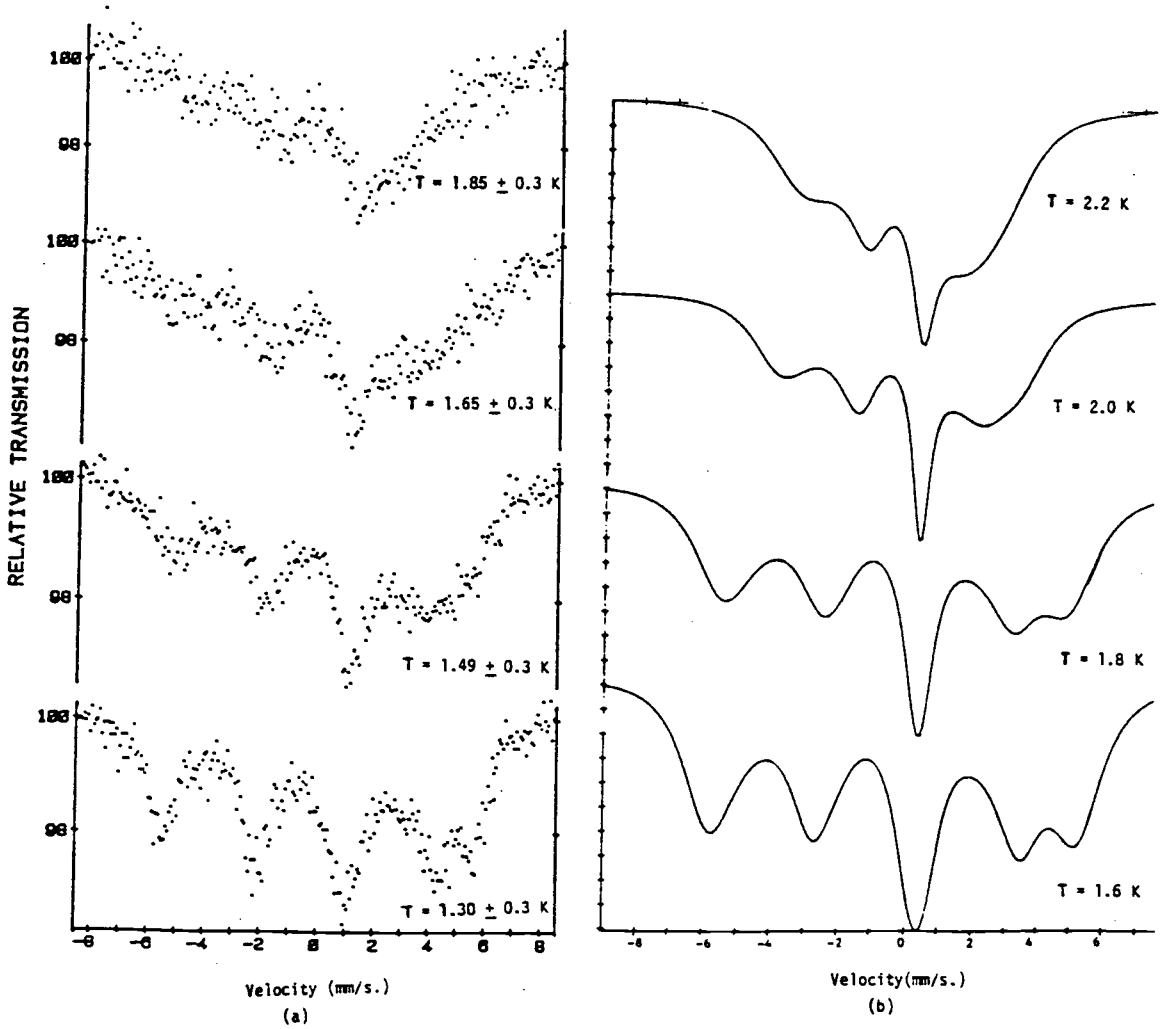

Fig. 17 (a) Mossbauer spectra between 1.30 and 1.85 K.
(b) Computer simulated Mossbauer spectra.

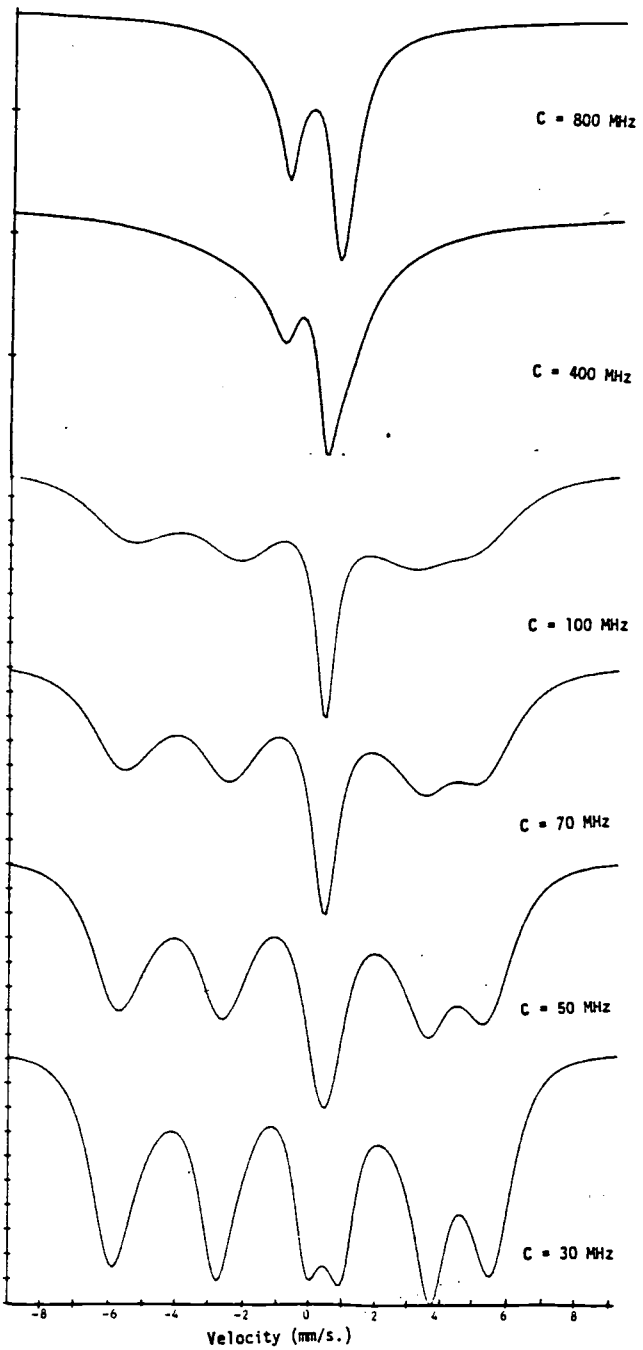

Fig. 18. Computer simulated Mossbauer spectra showing effect of changing spin-spin coupling constant (H_{eff} and D are constants).

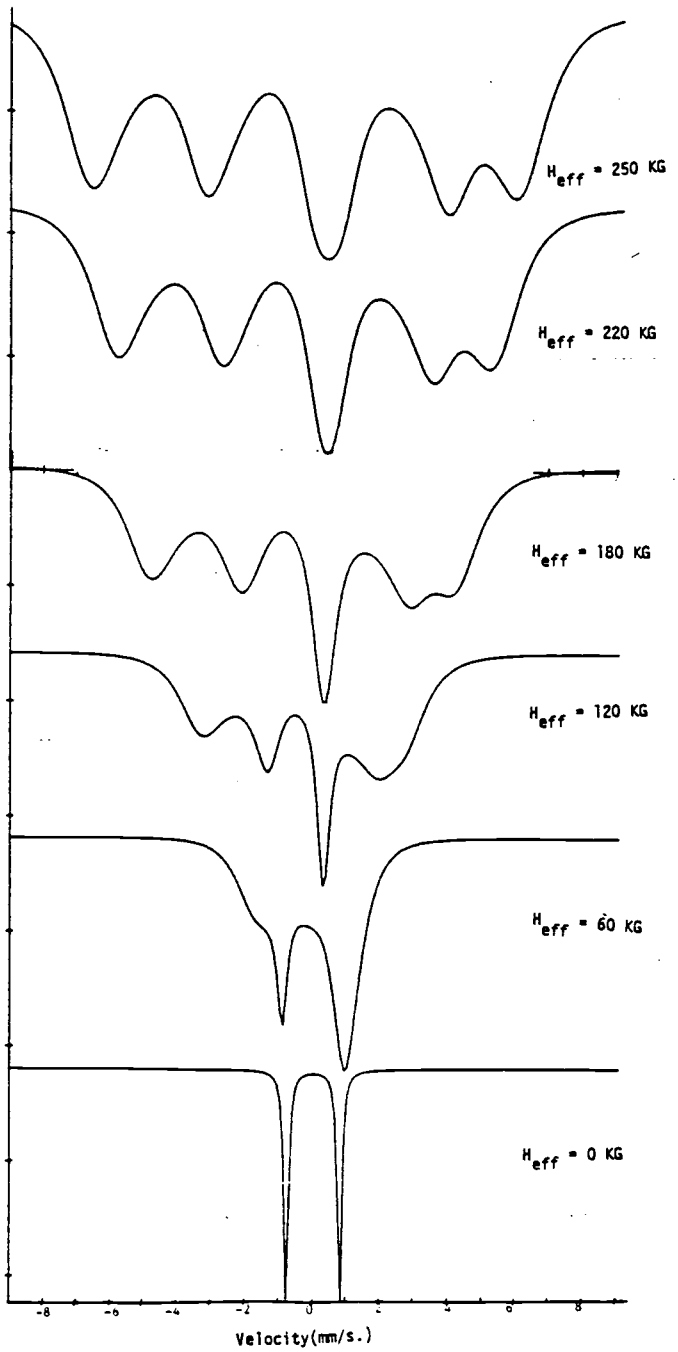

Fig. 19. Computer simulated Mossbauer spectra showing effect of changing the effective magnetic field (D and C are constants).

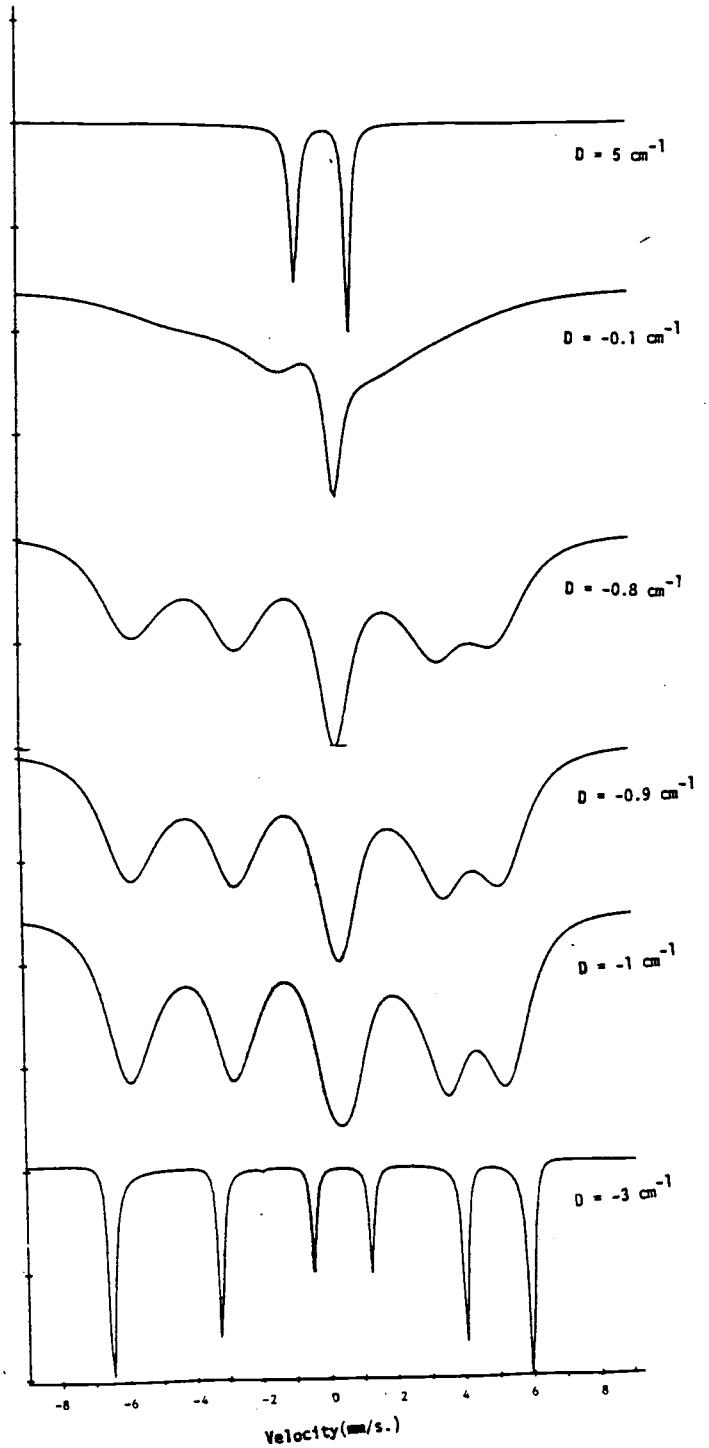

Fig. 20. Computer simulated Mossbauer spectra showing effect of changing the crystal field D parameter(H_{eff} and C are constants).

Table 6. Parameters employed in relaxation spectra calculations

Complex	Crystal field term D (K)	Spin-spin coupling constant C (MHz)	Effective magnetic field H_{eff} (KG)
(a) $Fe[S_2CN(Et)(Me)]_2Cl$	-1.3 ± 0.1	50 ± 2	330 ± 5
(b) $Fe[S_2CN(Et)(Pr)]_2Cl$	-1.4 ± 0.1	53 ± 2	327 ± 5
(c) $Fe[S_2CN(n\text{-}pr)_2]_2Cl$	-0.14	120 ± 10	-------

B. Experimental and Theoretical Results

b. $Fe[S_2CN(Et)(Pr)]_2Cl$

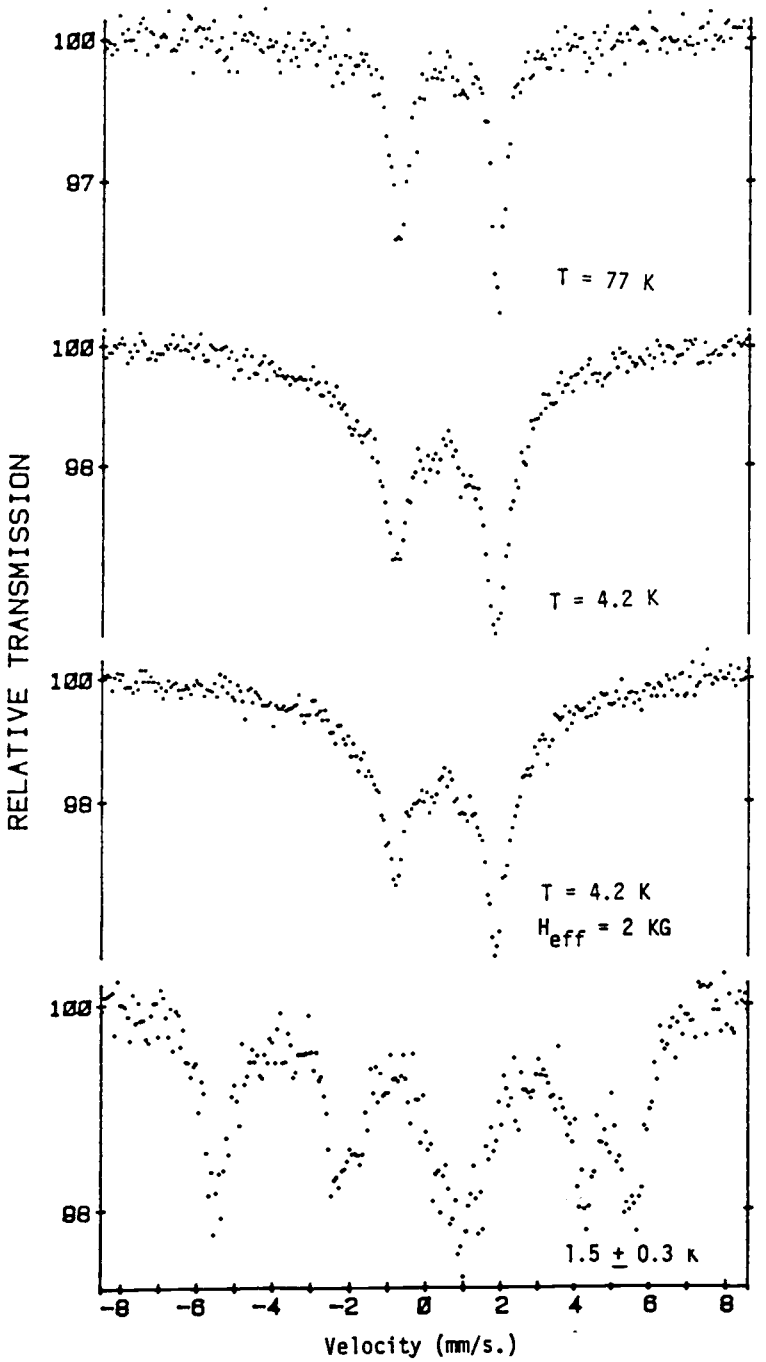

Fig. 21. Mossbauer spectra between 1.5 and 77 K.

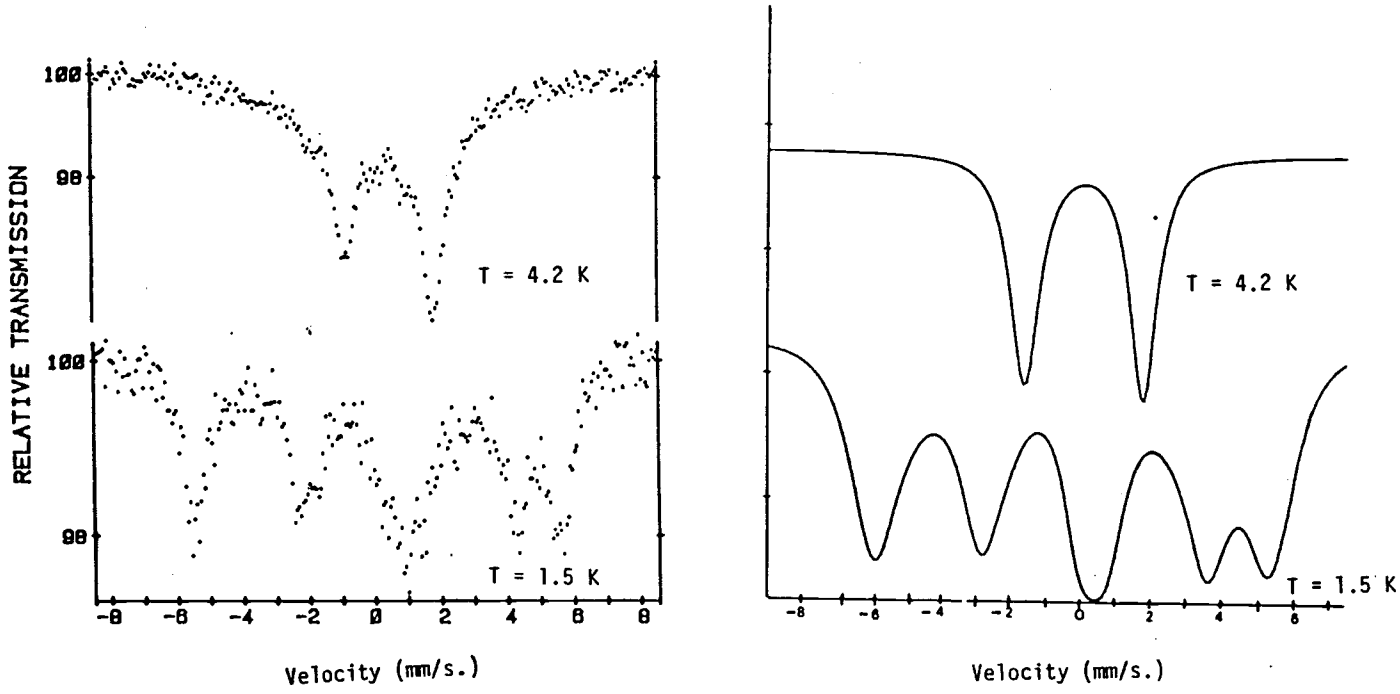

Fig. 22 . (a). Mossbauer spectra between 1.5 and 4.2 K.
(b). Theoretical Mossbauer spectra between 1.5 and 4.2 K.

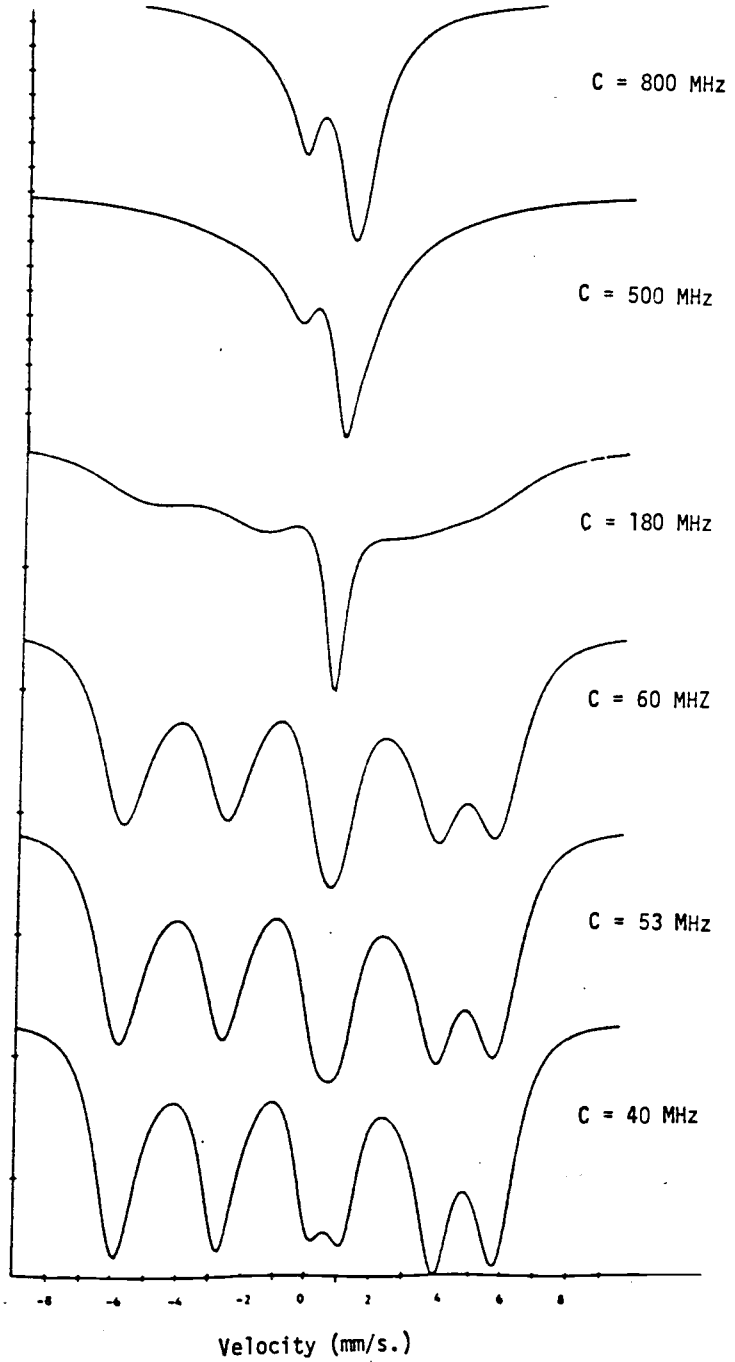

Fig. 23. Computer simulated Mossbauer spectra showing effect of changing spin-spin coupling constant(H_{eff} and D are constants).

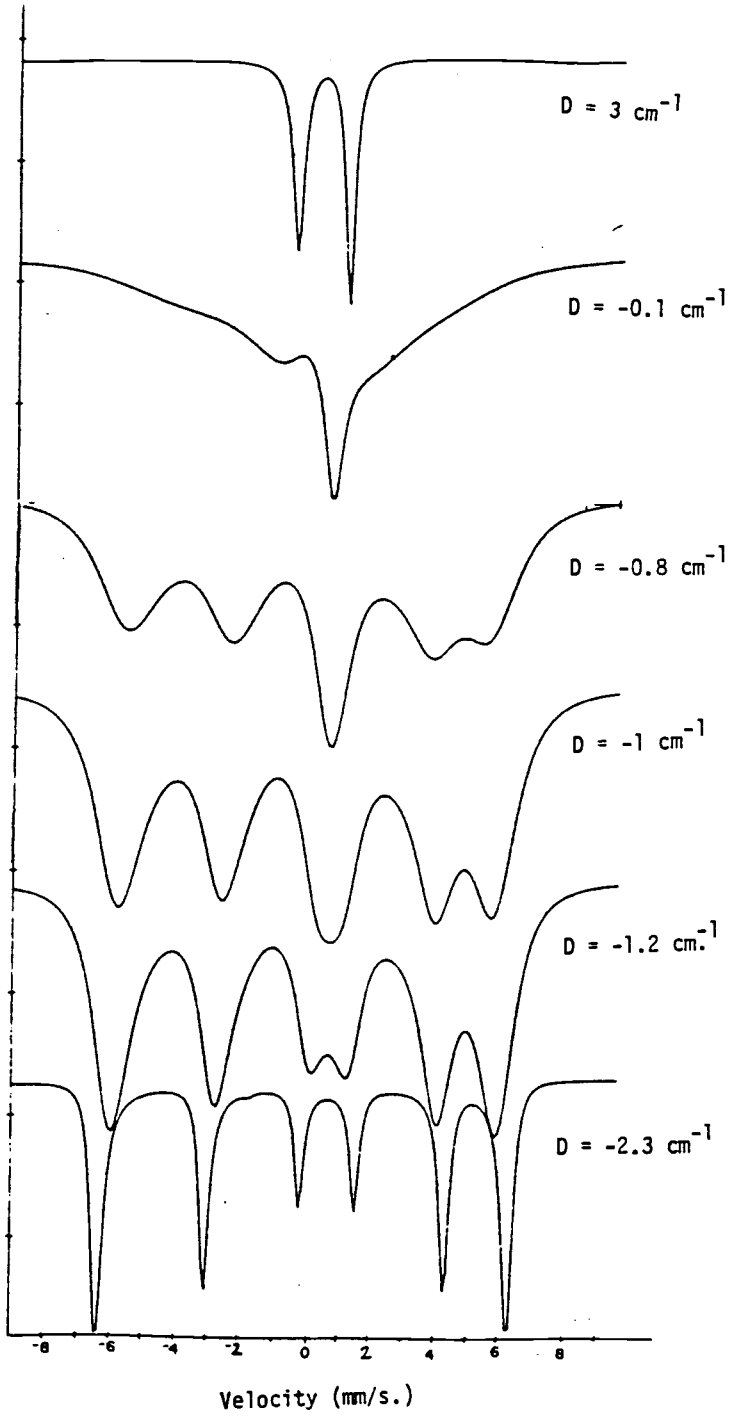

Fig. 24. Computer simulated Mossbauer spectra showing effect of changing the crystal field D parameter (H_{eff} and C are constants).

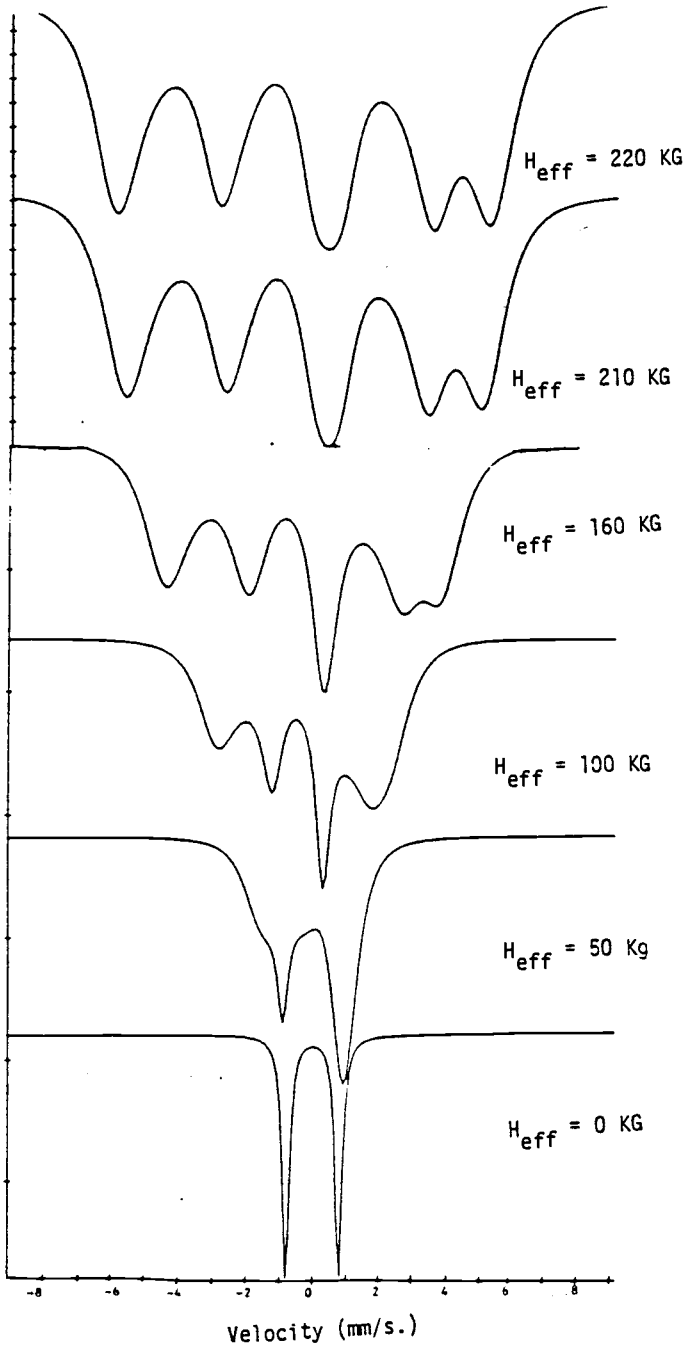

Fig. 25. Computer simulated Mossbauer spectra showing effect of changing the effective magnetic field (C and D are constants).

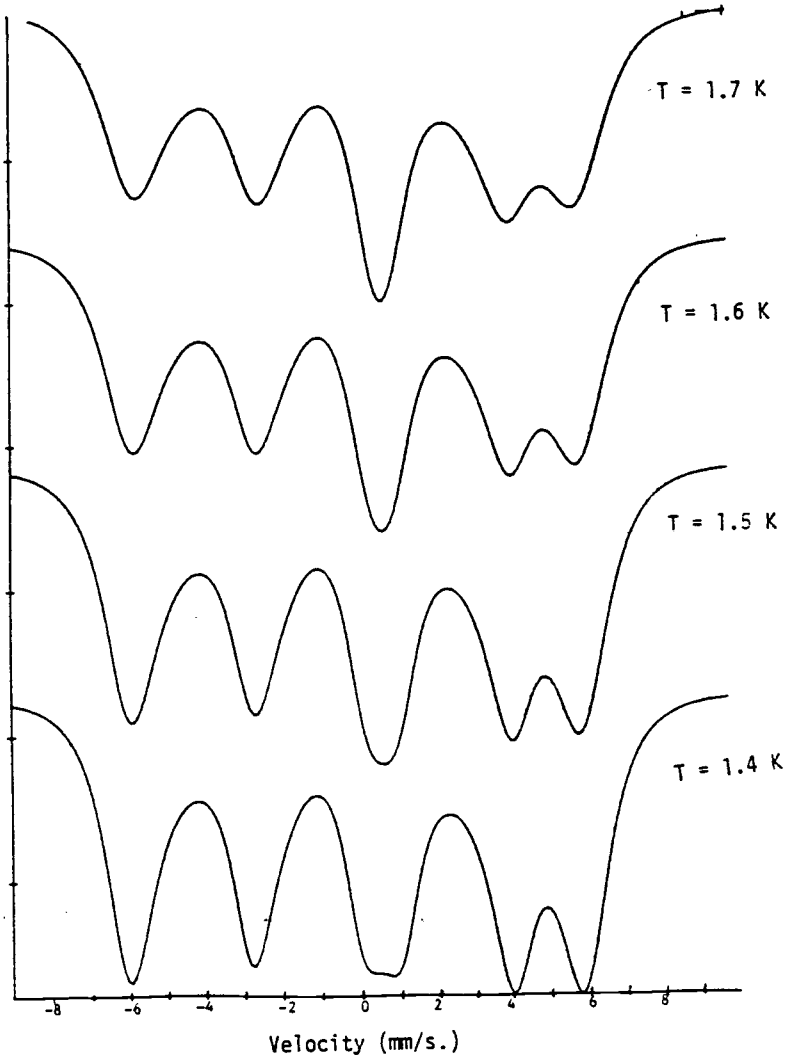

Fig. 26. Computer simulated Mossbauer spectra showing the sensitivity of temperature (C, D and H_{eff} are constants).

B. Experimental and Theoretical Results

c. $Fe[S_2CN(n\text{-}pr)_2]_2Cl$

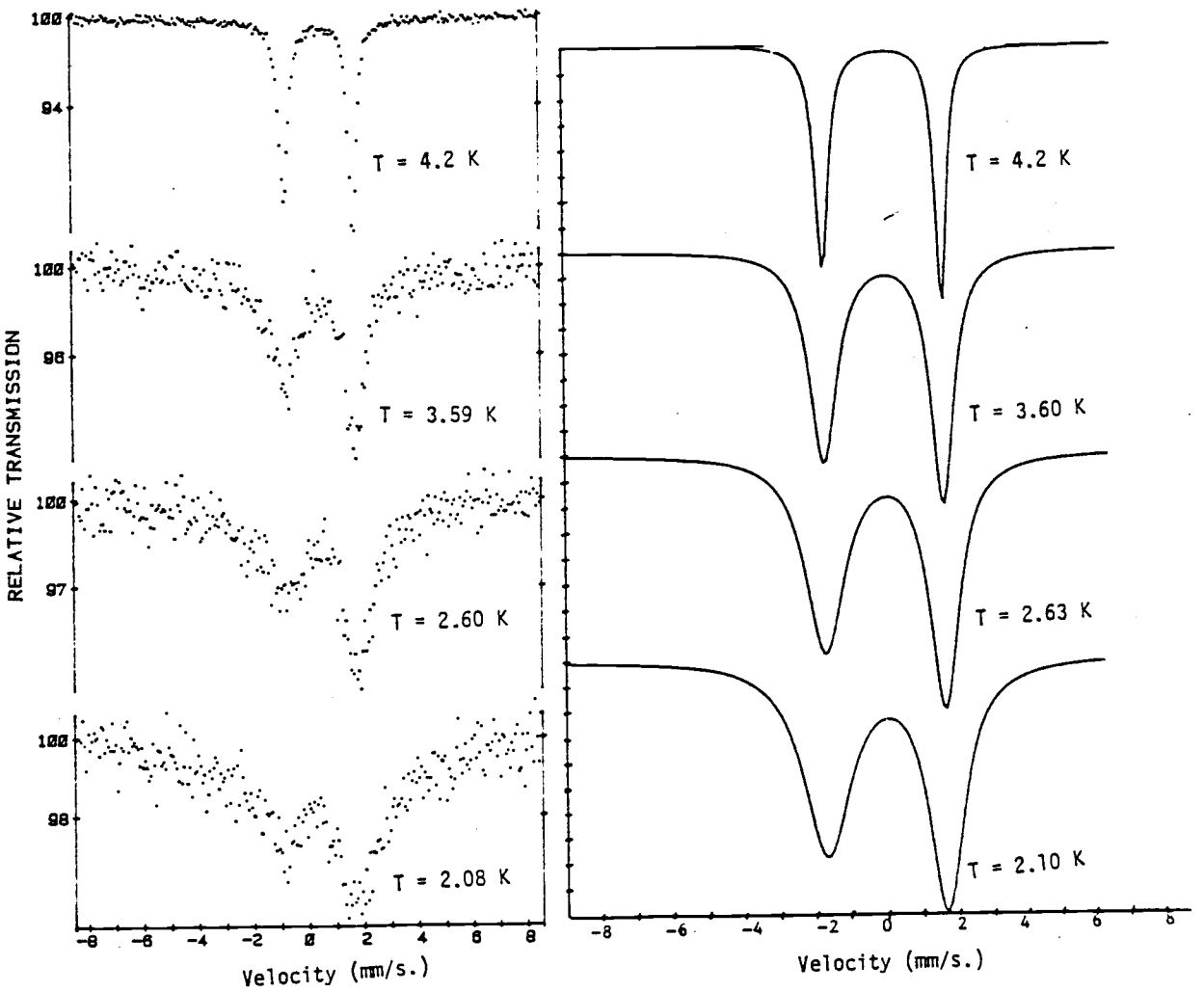

Fig. 27. (a) Mossbauer spectra between 2.08 and 4.20 K.
(b) Theoretical spectra between 2.10 and 4.2 K.

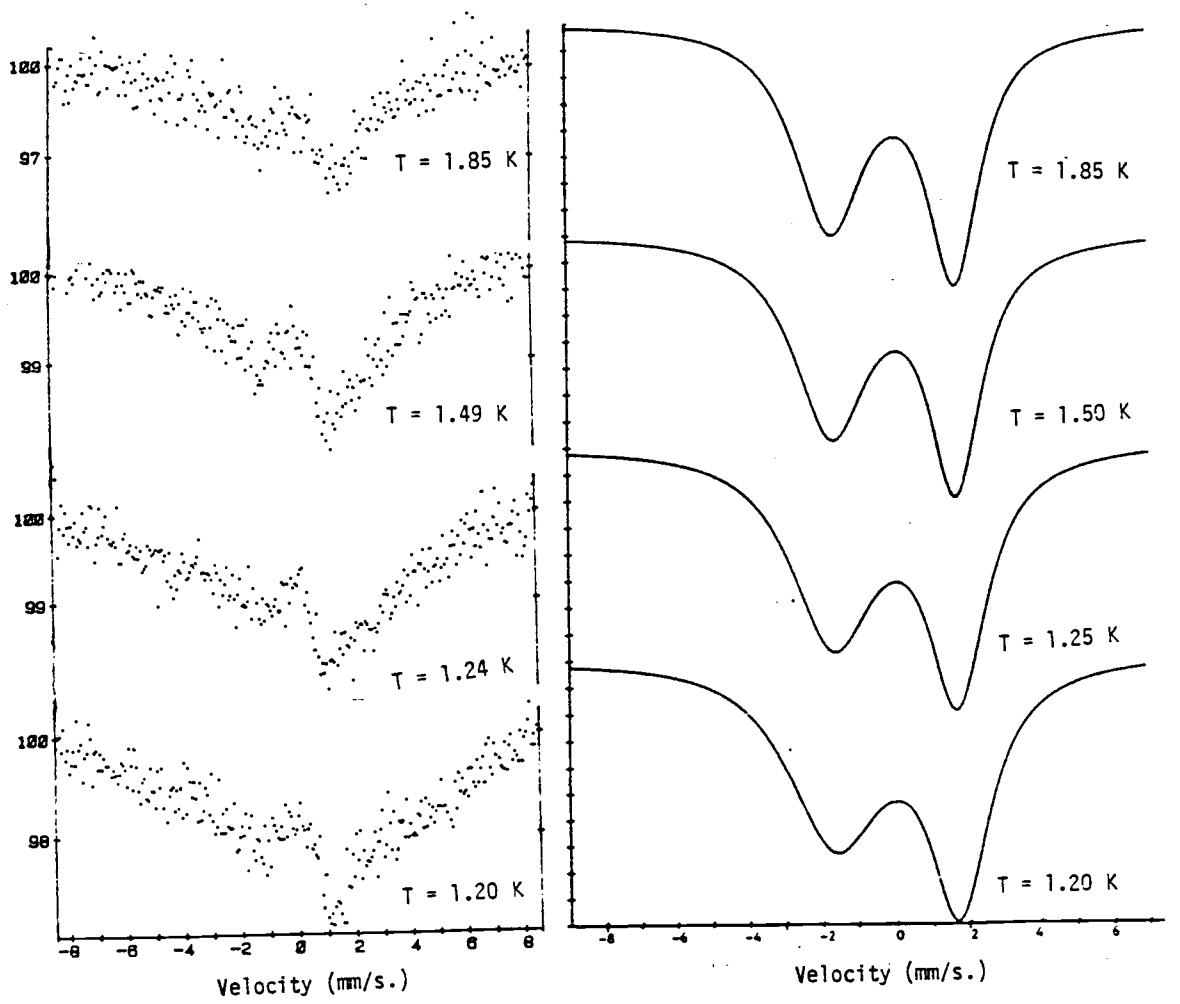

Fig. 28. (a) Mossbauer spectra between 1.09 and 1.85 K.
(b) Theoretical spectra between 1.20 and 1.85 K.

C. Discussion:

Mossbauer experiments were performed on absorbers of $Fe[S_2CN(Et)(Mt)]_2Cl$, $Fe[S_2CN(Et)(Pr)]_2Cl$, and $Fe[S_2CN(n\text{-}pr)_2]_2Cl$. A series of spectra were taken in the temperature range 1.2 - 4.2 K. Before analyzing the relaxation spectra in detail, a discussion of the orientation of electric and magnetic interactions for the iron ion within the molecular axes system must be presented.

From equation (5.5), the internal field is specified in the EFG coordinate system. Concurrently, from equation (1.1), it indicates that the crystal field D and E parameters are not necessarily collinear with the EFG (E is assumed zero in this work).

Previous experiments had reported the following situations:

Case(a): $D(\theta = 90, \varphi = 0)$ is perpendicular to the EFG principle while the internal field lies along the X-axis (a general relation of electric and magnetic hyperfine tensors to the molecular geometry is shown in Fig. 29). D and the quadrupole interaction (e^2qQ) are positive. The nuclear levels $|\pm 1/2\rangle$ are lowest lying and correspond to the left-hand peak of the quadrupolar lines. These levels may be described by the effective nuclear g factors with the magnetic character of the lower energy peak characterized by $g_X = g_Y = 2g_1$, $g_Z = g_1$; while $g_X = g_Y = 0$, and $g_Z = 3g_1$ are assigned to the right-hand peak. Hence the $|\pm 1/2\rangle$ will respond more readily to transverse fluctuations of a

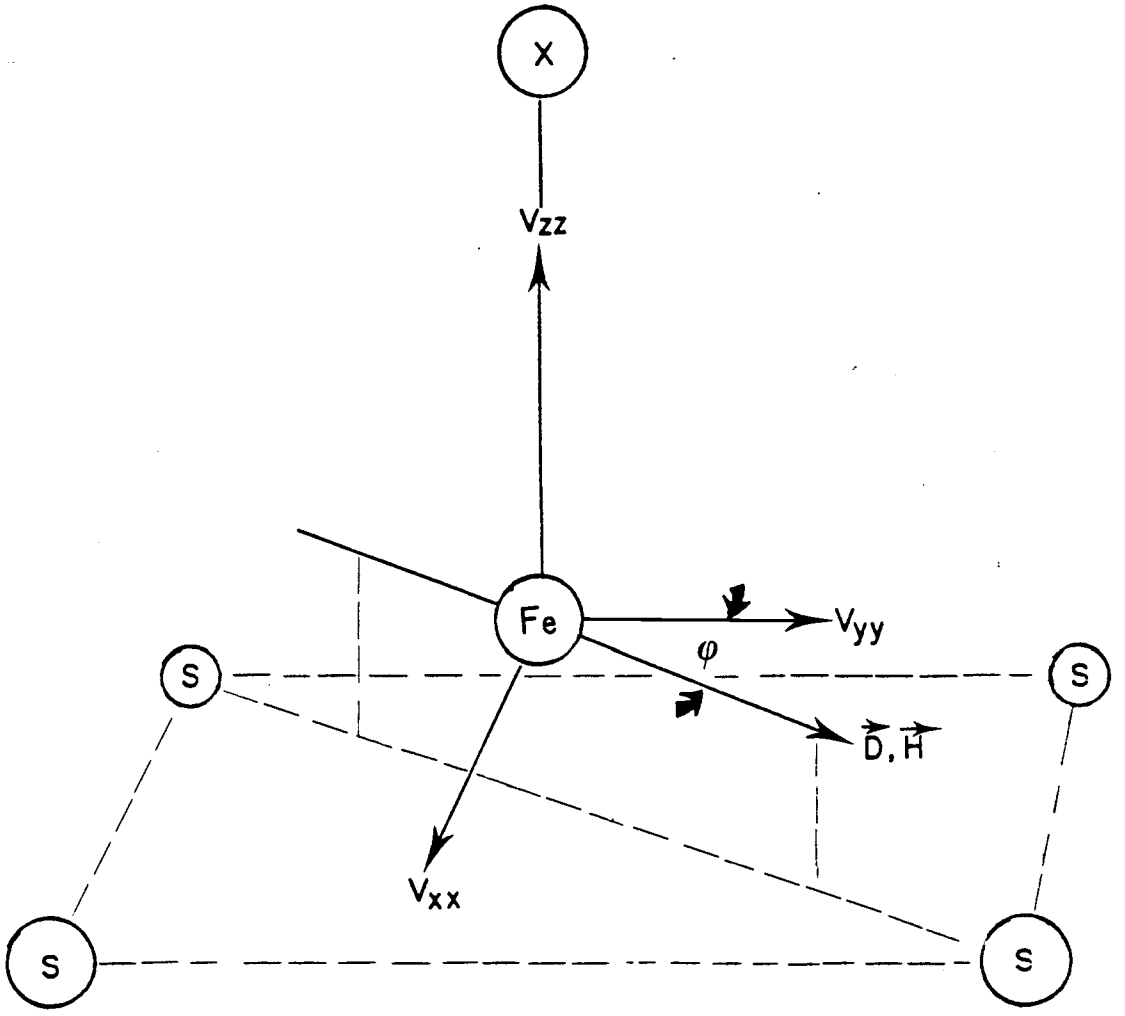

Fig. 29. Relation of electric and magnetic hyperfine tensors to molecular geometry.

magnetic field, i.e. the left peak broadens first. An example is Fe(pyrrolidyldtc)$_2$I [6].

Case(b): Same conditions as case (a) except the internal field is parallel to the EFG principle axis: The $|\pm 3/2>$ will respond to the parallel magnetic field first. Thus the right-hand peak broadens. This case was discussed at length by Blume. [61]. Possible candidates may be Fe[S_2CN(Et)(Pr)]$_2$I and Fe[S_2CN(Et)(Pr)]$_2$ Br reported in this work.

Case(c): Same conditions as case(a) except the molecular field lies along nearly along a diagonal of the rectangle formed by the four sulfur atoms in the iron bisdtc as suggested in Ref.[6].

Case(d): D and the internal field (θ = 90, φ = 0) are both perpendicular to the EFG principle axis. The quadrupole interaction and D are positive. In this situation, the left-hand peak broadens. One example is Fe[S_2CN(Et)$_2$]$_2$ Br crystallized from saturated benzene [48].

Case(e): Same conditions as (d) except D is negative. The left peak will be affected first. This situation received the most attention because of the numerous examples that can be found [4,11,55,62].

This situation is extended as a starting point to discuss the relaxation spectra obtained from the three iron chloro-bis-dtcs.

1. $Fe[S_2CN(Et)(Mt)]_2Cl$:

a. Experimental Mossbauer data:

This sample was prepared according to the method given in the synthesis section (Chapter IIIA). Dichloro-methane was chosen as the solvent. The Mossbauer spectra in the temperature range 1.3 - 4.2 K are given in Figs. 16a and 17a. The quadrupole doublet predominated down to 2.5 K. It can be seen that there was a general broadening down to 1.9 K. The left-hand peak broadened more than the right-hand peak as discussed in case (e). At 1.85 K, the doublet character of the spectrum was poorly defined. Below 1.85 K, paramagnetic hyperfine structure began to appear. At 1.3 K, a fairly well-defined pattern was observed. Comparison with similar paramagnetic compound $Fe[S_2CN(Me)_2]_2Cl$ [55] indicated that the 1.3 K spectrum arises from electronic relaxation among the electronic levels. Furthermore, the temperature range over which relaxation occurs is long in this case. In a ferromagnet, it is only ~~ 2 K.

Three interesting features of the spectrum at 1.3 K are noted compared with the similar paramagnetic compounds $Fe[S_2CN(i\text{-}pr)_2Cl$ and $Fe[S_2CN(Mt)_2]_2Cl$ [55]: First, the relative intensity of the first and second peaks of the lower energy were reversed. Second, the third peak had the strongest intensity. Finally, the relative intensity of the fourth and fifth peaks were also reversed. A likely explanation is that the symmetry of this complex was distorted due to the presence of the mixed alkyl groups at the terminal end of the complex. This may complicate the orientations of

the electric and magnetic hyperfine tensors in the molecular geometry as proposed earlier (see the conclusion also). A single crystal Mossbauer experiment and X-ray structure determination may be able to shed light on this problem.

b. Calculated Mossbauer Spectra:

The fitting procedures to generate the theoretical data were given in Chapter V1A.7. Results are shown in Figs. 16 and 17. Ground term crystal field D parameter, spin-spin coupling constant and effective magnetic field from the three iron dithiocarbamates are summarized in Table 6.

The spin-spin coupling constant determines the strength of the spin-spin interaction, which induces a transition rate as given in equation (6.1). The relaxation constant C found here was in close range in comparison of the previous investigation on the negative D system [4]. In fact, with the consideration of $Fe[S_2CN(Et)(Pr)]_2Cl$, it may be valid to infer here that all paramagnetic $Fe(dtc)_2$ X may have the compatible magnitude of C (less than 200 MHz).

There are other sample calculations given also. They were included to show the effect of changing various parameters. Other variables are listed with the figures. They are intuitively clear so a detailed explanation will not be given at this stage.

2. $Fe[S_2CN(Et)(Pr)]_2Cl$:

a. Experimental Mossbauer data:

There is only one spectrum below 4.2 K given in Fig. 21 due to the shortage of liquid helium to continue the experiment. The quad-

rupole doublet predominated at 77 K. At 4.2 K, broadening started to appear, typical of a negative D system discussed before. A small external field f 2 KG is applied transversed with respect to the γ-ray directions at this temperature also. The effect of the field was to decrease relaxation times. Unfortunately, no striking features developed in the spectrum at 4.2 K. At 1.5 K, a reasonably well-defined hyperfine structure was observed, which indicated clearly this complex is a paramagnet. The hyperfine pattern looked more similar to $Fe[S_2CN(Me)_2]_2Cl$ [55] except the fourth and fifth peaks were almost of equal intensity.

b. Calculated Mossbauer Spectra:

No comparisons of theoretical and experimental data will be given here except at 1.5 K. Theoretical parameters are given in Tables 5 and 6. Additional spectra with various parameters are also included to show the sensitivity of their effects.

3. $Fe[S_2CN(n\text{-}pr)_2]_2Cl$:

a. Experimental Mossbauer data:

The Mossbauer spectra in the temperature range 1.2 - 4.2 K are given in Figs. 27a and 28a. The quadrupole doublet was well-defined at 4.2 K. Relaxation effect started below this temperature. There was a general broadening until 1.85 K, where the doublet became unimportant. However, the magnetic split pattern still could not gain enough strength to appear even at 1.2 K, the lowest temperature our apparatus can reach.

We are postulating that in this complex, the length of the alkyl chain decreased the crystal field splitting $|\ 2D\ |$ (Fig. 15) between the two Kramers doublets, $|\ m_s \pm 3/2\ >$ and $|\ m_s = \pm 1/2\ >$ such that the observed resulting spectrum at 1.2 K was the sum of significant Boltzmann population of these levels.

b. Calculated Mossbauer Spectra:

Theoretical results are summarized in Tables 5 and 6 also. Comparisons between experimental and theoretical data were quite satisfactory. No further comments will be made at this point.

CHAPTER VII. CONCLUSIONS

It is evident from this work that only a small portion of magnetism work was reported due to the scope of this thesis. It is appropriate here to summarize what has been accomplished and indicate directions for future work.

Ten new $Fe(dtc)_2X$ complexes have been discussed in this work. Table 7 summarizes this class of complexes. This table also shows additional complexes which have been synthesized but incompletely characterized, either chemically or magnetically. They are of interest for further research.

The relative importance of the various mechanisms determining the electron density at the Mossbauer nucleus is often an area of controversy because of the wide variety of interpretations based on different assumptions. Experimental data are of considerable use in such circumstances. The data reported here are potentially able to settle some of the unsolved problems because our laboratory has provided extensive and systematic measurements on the isomer shift of $Fe(dtc)_2X$ complexes. It was concluded that in this unusual orbital singlet and spin quartet ground state (S=3/2) for the iron(III) ion, the observed isomer shift for the various complexes is insensitive to the variation of the apical ligand or the N-alkyl groups attached to the nitrogen of the dithiocarbamates. The reasons for this constancy are only partially understood as outlined in Chapter III.C. A detailed calculation like that described for iron oxides [38] is

Table 7. Materials being studied after 1980.

Di-me-dtc-Cl	Di-me-dtc-Br	Di-me-dtc-I	--------
Et-me-dtc-Cl*	Et-me-dtc-Br*	Et-me-dtc-I*	Et-me-dtc-SCN*
Di-et-dtc-Cl	Di-et-dtc-Br	Di-et-dtc-I	Di-et-dtc-SCN
Et-n-pr-dtc-Cl*	Et-n-pr-dtc-Br*	Et-n-pr-dtc-I*	--------
Di-n-pr-dtc-Cl*	Di-n-pr-dtc-Br*	Di-n-pr-dtc-I*	--------
Di-i-pr-dtc-Cl	--------	--------	--------
Di-n-bu-dtc-Cl**	Di-n-bu-dtc-Br**	Di-n-bu-dtc-I**	--------

* Reported in this thesis.

**Unpublished results.

required. The quantity δn_{3d}, which is a function of $B_{\ell d}$ and $S_{\ell d}$ is of special interest (Eq. 3.13). These quantitative results provide direct answers to the relative strength of the covalency effects and overlap distortion acting in these complexes.

Interestingly enough, the same constancy in isomer shift was also observed in several corresponding $Fe(dsc)_2X$ complexes [14]. Combination of these results certainly provides a stimulus for additional theoretical calculations at this time.

The molecular orbital calculations available in the literature provided a basis for the interpretation of 'isomer shift' and 'quadrupole splitting'. More calculations could be done by adding the appropriate basis set of orbitals representing the different alkyl groups at the terminal end of the complexes. The other aspect of Huckel molecular orbital calculations involves the interpretation of ligand hyperfine splitting (hfs) by diluting the paramagnetic iron in a diamagnetic host of similar structure. The ESR data can provide the molecular orbital coefficients if the relative orientations of the molecular and magnetic axes are known [63]. The experiment done by Decurtins [8] intended to serve this purpose. The major difficulty is to look for a host crystal which will accept the guest molecule without distorting the latter. Due to the acquisition of the Vax-750 system at the Chemistry Department of Oregon State University, it may be feasible to carry out the theoretical calculations locally.

The simple model proposed by Epstein et al. [22] gives a qualitative interpretation of the origin of the EFG. The MO approach provided the quantitative results, which are in agreement with the data presented in this work.

A simpler program was used to analyze electronic relaxation due to the computation ability in this laboratory by using the Dec 11/23. The methodology was discussed in length in Chapter VI. Briefly, the paramagnetic hyperfine structure was qualitatively interpretated using a semi-classical model, in which the dipole-dipole interaction randomly modulated the four electronic states. This gives rise to the time dependence fluctuating magnetic field around the Mossbauer nucleus. The analysis neglected the rhombic E term in the spin Hamiltonian and orientation effects in the calculations. Nevertheless, the theoretical spectra were generally compatible with the experimental Mossbauer spectra. It must be kept in mind that the method is only an approximation. In addition, the computation time is not trivial for each execution prior to the installation of VAX-750. The major disagreement is the temperature difference between the experimental and theoretical analysis ($\pm$ 0.3 K) in $Fe[S_2CN(Me)(Et)]_2Cl$. Surprisingly, this difference was the same for the whole temperature range. This material has potentially the most distorted structure and consequently a more rhombic crystal field interaction. The other complexity is the possibility of the formation of two forms of crystals in the sample

replaced by (see Fig. 30). With the new computer system as stated above, a more complete program which allows a general orientation of the molecular field with respect to the crystal field system was activated [58]. This also includes a complete electronic spin-spin interaction Hamiltonian (eq. 6.10), the E term, and nonadiabatic relaxation ($[\hat{\underline{H}}_m, \hat{H}_Q] \neq 0$) in the calculations. Unfortunately, preliminary results were not completed at the conclusion of this writing.

Although this work reports almost a dozen new materials (Table 7), it is impractical to survey the relaxation phenomena or magnetic transition in one thesis for all these complexes owning to the limited human and financial resources. Bis-chloro-dtcs were studied elaborately because of the wealth of information obtained from previous investigations. In the future work, a systematic relaxation study can concentrate on the other bid-dtcs especially those with iodo ligand at the apical position. From past experience, they are likely an antiferromagnet with the crystal field D parameter positive [6,58]. Another experiment is to develop methods for producing solvate and nonsolvate lattices. This was one of the active research areas in this laboratory in the past. The objective is to draw a correlation of magnetic properties with relative orientations of the molecules [48,58]. There are no bulk susceptibility measurements by the Faraday Balance reported here. This method is the direct way to characterize the qualitative nature of cooperative phenomena.

ESR experiments in polycrystals at room temperature and 77 K were performed on these complexes. A single broad line was observed as before showing the paramagnetic character of these materials [10]. The results were not reported here. A complete analysis of crystal field D and E parameters requires in addition, study of the angular and temperature dependence of single crystal spectra at helium temperatures. The temperature variation of the absorption intensity due to the depopulation of the excited Kramers doublet can yield directly crystal field spacing [65]. This experiment is not feasible due to the lack of manpower.

It is somewhat surprising that no new magnetically ordered complexes were observed. $Fe[S_2CN(Et)(Me)]_2Cl$ and $Fe[S_2CN(Et)(Pr)]_2Cl$ are both paramagnetic. But, these examples provide an additional information about spin-spin coupling constants in this class of paramagnetic materials (see Chapter VIC). Furthermore, information was gained concerning the influence of the alkyl groups on the ground state electronic and magnetic behavior of these complexes. One novel result was the finding of a very small zero field splitting in $Fe[S_2CN(n\text{-}pr)_2]_2Cl$ ($D = -0.1\ cm^{-1}$.). This suggests other long chain materials would have similar property. In order to confirm this finding, it would be nice if new chloro-bis-dtcs could be synthesized. Two possible candidates are $Fe[S_2CN(n\text{-}bu)_2]_2Cl$ [64] and $Fe[S_2CN(s\text{-}bu)_2]_2Cl$ [3]. This author believes that it is impossible to recrystallize any bis complexes in highly crystalline form that

atom in the dtc.

Most of these complexes (X = Cl, Br) are good quality crystals. The growth habits of the dtcs with methyl and ethyl groups will likely provide good size crystals for X-ray structure determinations. The structure information will help answering some of the relaxation phenomena (Chapter VIIC). Single crystal Mossbauer experiment can sort out the orientations of electric and magnetic tensors in the molecular systems [62].

Throughout this thesis, the new materials are assumed to have the same structure as depicted in Fig. 1. A question immediately arises. How many isomers are possible for the $Fe(dtc)_2X$ complexes with inequivalent alkyl groups at the terminal ends? Take $Fe[S_2CN(Me)(Et)]_2Cl$ as an example. It can be seen from Fig. 30 that there exist two possible stable forms for this complex. The cis-type is the one with identical alkyl groups in juxtaposition. The other type is designated as the trans-form with equivalent alkyl groups on the opposite sides. The next question is the relative stability or occurrence in crystalline form, or is it possible to have a mixture of both forms in a batch of polycrystals? To address this problem, one can use a simple electrostatic repulsion approach. Nitrogen is the third most electronegative atom, thus a partial positive charge can be assigned to both carbon atoms from the two different alkyl groups attached to the nitrogen atom.

Clearly, the carbon atom in the methyl group will have a larger charge. In order to minimize the electrostatic repulsion between like groups, a maximum separation is preferred. Based on this simple argument, the trans-configuration is favored. The confirmation from X-ray structure determination is in progress.

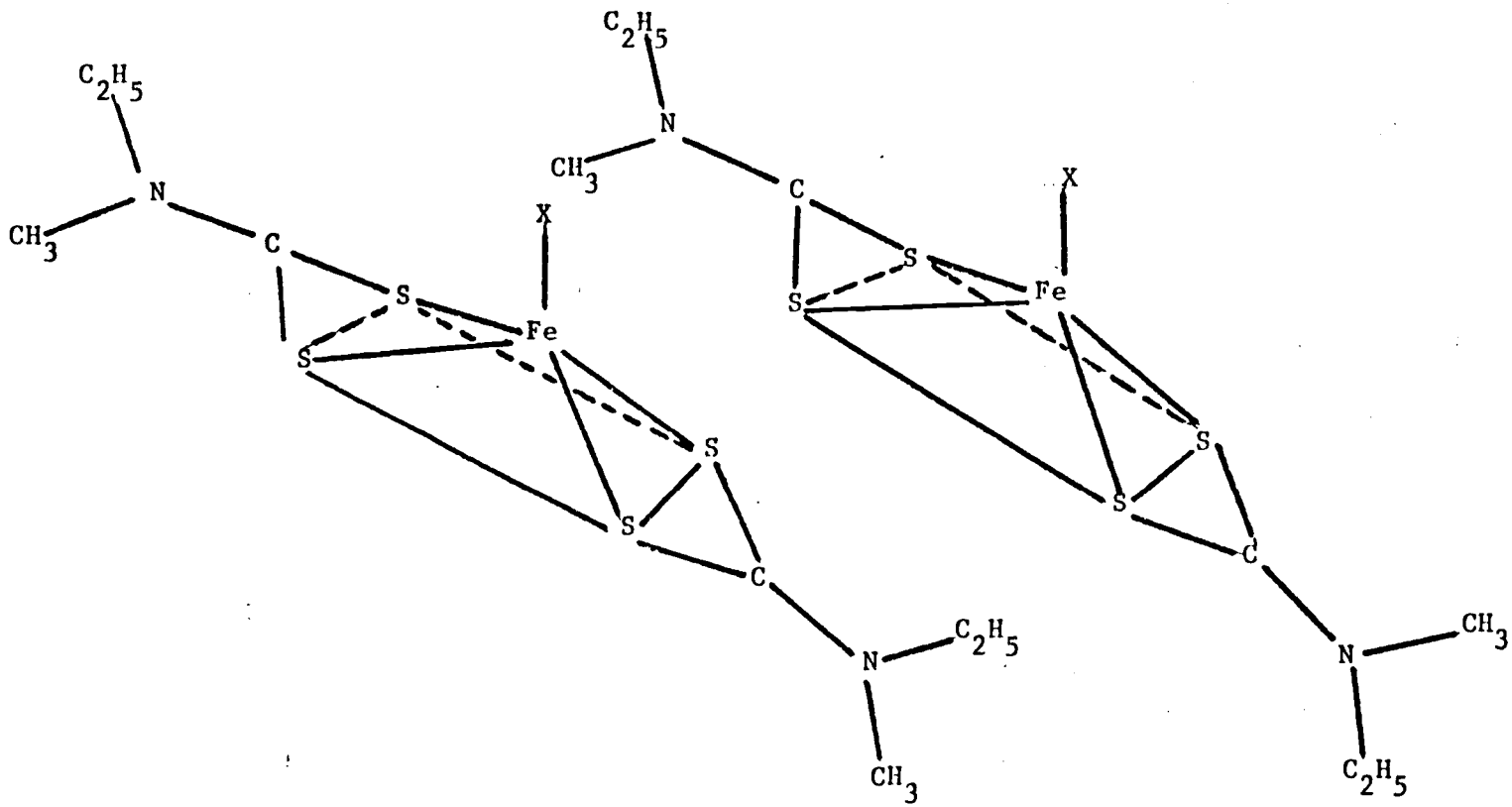

Fig. 30. Two possible configurations of $Fe(dtc)_2X$ with inequivalent alkyl groups: (a) cis-type and (b) trans-type.

BIBLIOGRAPHY

1. H.H. Wickman and A.M. Trozzolo, Phys. Rev. Let., 4, 156 (1965); erratum 16, 162 (1966).

2. R.L. Martin and A.H. White, Inorg. Chem., 6, 712 (1967).

3. B.F. Hoskins, R.L. Martin, and A.H. White, Nature (London), 211 (1966).

4. H.H. Wickman and C.F. Wagner, J. Chem. Phys., 51, 435 (1969).

5. G.C. Brackett, P.L. Richards, and W.S. Caughey, J. Chem. Phys., 54, 4383 (1971).

6. D. Petridis, A. Simopoulos, A. Kostikas, and M. Pasternak, J. Chem. Phys., 65, 3139 (1976).

7. M. Yoshikawa, M. Sorai, H. Suga and S. Seki, J. Phys. Chem. Solids, 41, 1295 (1980).

8. S. Decurtins and H.H. Wickman, J. Chem. Phys., 81, 4251 (1984).

9. H.H. Wickman and F.R. Merritt, Chem. Phys. Lett., 1, 117 (1967).

10. G.E. Chapps, S.W. McCann, H.H. Wickman and R.C. Sherwood, J. Chem. Phys., 60, 990 (1974).

11. H.H. Wickman and A.M. Trozzolo, Inorg. Chem., 7, 63 (1968).

12. H.H. Wickman, A.M. Trozzolo, H.J. Williams, G.W. Hull and F.R. Merritt, Phys. Rev., 155, 563 (1967).

13. F.V. Wells, Ph.D. Dissertation (Oregon State University, 1984; unpublished).

14. G.C. Defotis, B.K. Failon, F.V. Wells and H.H. Wickman, Phys. Rev. B29, 3795 (1984).

15. M. Blume and J.A. Tjon, Phys. Rev., 165, 446 (1968).

16. S. Dattagupta, in Advances in Mossbauer Spectroscopy, ed. B.V. Thesar, P.K. Iyengar, J.K. Srivastava and S.C. Bhargava (Elsevier Scientific), New York, 1983. Chapter 11.

17. S.C. Bhargava, ibid., Chapter 12.

18. F.A. Cotton, Chemical Applications of Group Theory, p. 266, (Wiley-Interscience), New York, 1971.

19. V.R. Marathe, A. Trautwein. A. Kostikas, J. des Phys. (Paris) Colloq., 41, C1-315 (1980).

20. A.H. White, R. Copper, E. Kohot, H. Waterman, and R.L. Martin, Australian J. Chem., 17, 294 (1964).

21. M. Yoshikawa, M. Sorai. H. Suga and S. Seki. Chem. Phys. Letters, 77, 54 (1981).

22. L.M. Epstein and D.K. Straub, Inorg. Chem., 8, 784 (1969).

23. G.K. Wertheim, Mossbauer Effect: Principles and Applications (Academic Press), New York, 1964.

24. V.I. Gol'sanski'i and R.H. Herber, Chemical Applications of Mossbauer Spectroscopy (Academic Press), New York, 1968.

25. J.K. Syrivastava and S.C. Bhargava, in Advances in Mossbauer Spectroscopy, ed. B.V. Thesar, P.K. Iyengar, J.K. Srivasatava and S.C. Bhargava (Elsevier Scientific), New York, 1983, Chapter 1.

26. A.J. Freeman and D.E. Ellis, in Mossbauer Somer Shifts, ed. G.K. Shenoy and F.E. Wagner (North-Holland), New York, 1978, Chapter 4.

27. M.J. Clauser and R.L. Mossbauer in Hyperfine Interactions. ed. R.B. Frankel and A.J. Freeman (Academic Press), New York, 1967, pp. 497-551.

28. D.J. Griffiths, Introduction to Electrodynamics (Prentice-Hall), New Jersey, 1981.

29. G.M. Kalvius and G.K. Shenoy, Atomic Data Nucl. Data Tables, 14, 639 (1974).

30. L.R. Walker, G.K. Wertheim, and V. Jaccarino, Phys. Rev. Letters 6, 98 (1961).

31. W.C. Nieuport, D. Post and P.Th. Van Duijnen, Phys. Rev. B, 17, 91 (1978).

32. J.P. Sanchez, J.M. Friedt, A. Trautwein and R. Reschke, Phys. Rev. B, 19, 365 (1979).

33. R.C. Axtmann, Y. Hazony and J.W. Hurley, Chem. Phys. Lett., 2, 673 (1968).

34. A. Trautwein, F.E. Harris, Theoret. Chim. Acta., 30. 45 (1973).

35. V.R. Marathe and A. Trautwein, in Advances in Mossbauer Spectroscopy, ed. B.V. Thesar, P.K. Iyengar, J.K. Scrivastava and S.C. Bhargava (Elsevier Scientific), New York. 1983. Chapter 7.

36. V.R. Marathe, A. Trautwein, A. Kostikas. unpublished results.

37. G.A. Sawatzky and F. Van Der Woude, J. Phys. (Paris) Colloq., 35, C6-47 (1974).

38. R. Ingalls, F. Van Der Woude, and G.A. Sawatzky, in Mossbauer Isomer Shifts. ed. C.K. Shenoy and F.E. Wagner (North-Holland), New York, 1978, Chapter 7.

39. J.M. Friedt and J. Danon, in Modern Physics in Chemistry, ed. E. Fluck and V.I. Gol'danski'i (Academic Press) London, 1979, Vol. 2, pp. 195-320.

40. P. Ganguli and K.M. Hasselbach, J. des Phys. (Paris) Collog., 41, C1-317 (1980).

41. R.I. Ake and C.M. Harris-Loew, J. Chem. Phys., 52. 1098 (1970).

42. J.L.K.F. deVries, C.P. Keijzers and E. deBoer. Inorg. Chem., 11, 1343 (1972).

43. R. Reschke and A. Trautwein, Theoret. Chim. Acta (Berl.), 47, 85 (1978).

44. S.V. Karyagin, Proc. Acad. Sci., USSR, Phys. Chem. Sect. (English Transl.) 148, 110 (1963).

45. M. Blume, Phys. Rev. Lett., 14, 96 (1965).

46. R.E. Watson and A.J. Freeman, Phys. Rev. 123, 2027 (1961).

47. H.H. Wickman and G.K. Wertheim, in Chemical Applications of Mossbauer Spectroscopy. ed. V.I. Gol'danski'i and R.H. Herber (Academic Press), New York, 1968, pp. 548.

48. S. Decurtins, F.V. Wells, K.C.-P. Sun and H.H. Wickman, Chem. Phys. Lett., 89, 79 (1982).

49. M. Blume, Phys. Rev. Lett., 18, 305 (1967).

50. J.A. Tjon and M. Blume, Phys. Rev., 165, 456 (1968).

51. M. Blume, Phys. Rev., 174, 351 (1968).

52. S. Dattagupta, Phys. Rev. B, 12, 3584 (1975).

53. F. Hartmann-Boutron, Ann. Phys. (Paris), 9, 285 (1975).

54. F. Hartmann-Boutron, J. des Phys. (Paris) Colloq., 41, 01-223 (1980).

55. H. H. Wickman and A.M. Trozzolo, Symposium of the Faraday Society, No. 1, 1967.

56. A. Carrington and A.D. McLachlan, Introduction to Magnetic Resonance (John Wiley & Sons), New York, 1979.

57. A. Abragram, Principles of Nuclear Magnetism (Oxford), London, 1983, Chapter IV.

58. Thesis by J. Grow, Oregon State University, Ph.D. (1978).

59. H.J. Rose and D.M. Brinks, Rev. Mod. Phys., 39, 306 (1967).

60. N.N. Greenwood and T.C. Gibb, Mossbauer Spectroscopy (Chapman and Hall), London, 1971.

61. M. Blume, Phys. Rev. Lett., 14, 96 (1965).

62. H.H. Wickman, J. Chem. Phys., 56, 976 (1972).

63. A.M. Maki and B.R. McGarvey, J. Chem. Phys., 43, 1404 (1965).

64. Unpublished results.

65. J.W. Orton, Electron Paramagnetic Resonance, (Iliffe Books Ltd.), London, 1968.

Appendix I

Abbreviations Used in Thesis

Me	= Methyl	$-CH_3$
Et	= Ethyl	$-C_2H_5$
Pr	= Propyl	$-C_3H_7$
Bu	= Butyl	$-C_4H_9$
R_2dtc	= Dithiocarbamate	$-R_2NCS$
i	= Iso	

Appendix II

General Relaxation Program

```
C     ****************************************************************
      *                                                              *
      *              GENERAL RELAXATION PROGRAM                      *
      *                                                              *
C     *                                                              *
C     *                                                              *
C     *  KEN SUN                                                     *
C     *  TED LAPAGE                                                  *
C     *  HOLLIS H. WICKMAN                                           *
C     *  DEPARTMENT OF CHEMISTRY, OREGON STATE UNIVERSITY            *
C     *                                                              *
C     ****************************************************************
C     *                                                              *
C     *     THIS IS A PROGRAM TO COMPUTE RELAXATION SPECTRA          *
C     *   FOR AN S=3/2, FE57 ATOM. THE LINESHAPE EXPRESSION IS       *
C     *   FROM BLUME AND TJON(BT), PHYS.REV.165,446-456(JAN,1968).   *
C     *   IT UTILIZES AN EXPRESSION FOR A CLASSICAL MAGNETIC FIELD   *
C     *   FLUCTUATION ALONG THE Z-AXIS OF A EFG TENSOR SYSTEM.THIS   *
C     *   PROGRAM GENERALIZES TO 4 FIELDS. TO COMPUTE LINESHAPES     *
C     *   IT IS NECESSARY ONLY TO DEFINE MATRICES APPEARING IN EQ.   *
C     *   B1 OF BT. BT DO A NUMBER OF ALGEBRAIC MANIPULATIONS TO     *
C     *   SIMPLIFY THE LIOUVILLE MATRIX THAT IS IMPLICIT IN THEIR    *
C     *   WORK AND WHICH EXPLICITLY APPEARS IN BLUME, PHYS.REV.174   *
C     *   ,351-358(OCT,1968).BECAUSE THE LIOUVILLE MATRIX  IS        *
C     *   DIAGONAL IN MZ QUANTUM NUMBERS AND IS ONLY 4X4 INSTEAD     *
C     *   OF A 32X32 MATRIX. A NUMBER OF 4X4 MATRICES,               *
C     *   DEPENDING ON M0 AND M1, APPEAR. EACH OF THESE MUST BE      *
C     *   INVERTED. THE NEXT STEP IS TO TAKE MATRIX ELEMENTS OF      *
C     *   THESE INVERTED RELAXATION MATRICES (DENOTED BY UNIV) AND   *
C     *   THEN WEIGHT APPROPRIATE MATRIX ELEMENTS BY WIGNER COEFF-   *
C     *   ICIENTS. IN PRINCIPLE, EACH PAIR OF MI MO INDICES GIVES    *
C     *   RISE TO 4X4 MATRIX TO BE INVERTED. IN PRACTICE ONLY 6 ARE  *
C     *   NOVVANISHING OWING TO THE6 NONVANISHING WIGNER COEFFI-     *
C     *   CIENTS.                                                    *
C     *                                                              *
C     *       EFFECT OF THE CRYSTAL FIELD. AN AXIALLY SYMMETRIC      *
C     *   CRYSTAL FIELD IS ASSUMED PRESENT WITH D PARALLE TO THE     *
C     *   Z-AXIS. THE 4 STOCHASTIC SPIN STATES THUS DEPEND ON THE    *
C     *   CRYSTAL FIELD D TERM IN THE USUAL MANNER;D(MS)=DX(MS**2)   *
C     *   D IS AN IMPUT PARAMETER.                                   *
C     *       EFFECT OF AN EXTERNAL MAGNETIC FIELD. THE PROGRAM      *
C     *   ALLOWS FOR THE PRESENCE OF AN EXTERNAL MAGNETIC FIELD      *
C     *   PARALLEL TO THE Z-AXIS. THE FIELD CAN BE AN EXTERNAL       *
C     *   FIELD OR A MOLECULAR FIELD. THE LATTER IS CALCULATED IN    *
C     *   A SELF-CONSISTENT MANNER WITH A BRILLOUIN FUNCTION         *
C     *   SUBROUTINE. NECESSARY INPUT IS THE CRITICAL TEMPERATURE.   *
C     *                                                              *
C     *   PARAMETERS AND MATRICES APPEARING IN THE PROGRAM:          *
C     *   G0  =0.1378 MHZ/KG. THIS IS 1/(G0=0.18048)                 *
C     *                                X(MUNUC=7.262 KG PER MHZ).    *
C     *        E(MHZ)=G0XA(KG/SPIN)X(MS). THUS THE A TENSOR DATA     *
C     *        IS TAKEN IN UNITS OF KG/SPIN; E.G. 110 KG/SPIN.       *
C     *  THIS INPUT IS DENOTED BY HF IN THE PROGRAM                  *
C     *                                                              *
C     *   HF  = INTERNAL FIELD AROUND THE NUCLEUS IN KG              *
C     *   G1  = GROUND STATE ZEEMAN CONSTANT                         *
C     *   Q   = QUADRUPOLE INTERACTION IN MHZ                        *
C     *   ETA = ASYMMETRY PARAMETER, DIMENSIONLESS                   *
C     *   NT  = NUMBER OF POINTS FOR WHICH A SPECTRUM IS CALC        *
C     *   XL  = LEFT ABSCISSA LIMIT (MHZ)                            *
C     *   XR  = RIGHT ABSCISSA LIMIT(MHZ)                            *
```

```
C     *    C    = RELAXATION RATE (MHZ)                                  *
      *    DT   = CFS PARAMETER (RECIP.CM.)                              *
      *    TT   = TEMPERATURE   (REC. CM.)                               *
C     *    HEX  = EXTERNAL FIELD, IF PRESENT (K.G)                       *
C     *    TC   = CRITICAL TEMPERATURE BELOW WHICH MOLECULAR FIELD       *
C     *           IS PRESENT                                             *
C     * XFIELD= CONTROL PARAMETER TO ACTIVATE MOLECULAR FIELD            *
C     *           CALCULATION                                            *
C     *         = 0 FOR NON-VANISHING TC AND MOLECULAR FIELD CALC.       *
C     *         = 1 FOR EXTERNAL MAGNETIC FIELD, HEX                     *
C     *                                                                  *
C     * NOTE:1. BELOW THE CRITICAL TEMPERATURE, THE MAGNETIC INT-        *
C     *           ERACTION IS GREATER THAN THE NUCLEAR QUADRUPOLE        *
C     *           INTERACTION AND THE HYPERFINE INTERACTION IS ALSO      *
C     *           ASSUMED DIAGONAL IN BT'S WORK. A COORDINATE TRAN-      *
C     *           SFORMATION IS THUS NECESSARY FOR Q AND ETA. THE        *
C     *           RELATION CAN BE OBTAINED FROM HHW AND CFW, THE         *
C     *           JOURNAL OF CHEMICAL PHYSICS, VOLUME 51,#1,435-444      *
C     *           (1JULY69)                                              *
C     *                                                                  *
C     *        2. AFTER A THEORETICAL DATA FILE IS GENERATED, THE        *
C     *           PLOT PROGRAMME FROM THE UTL: AREA CAN BE USED TO       *
C     *           PLOT THE DATA                                          *
C     *                                                                  *
C     *        3. IN ORDER TO HAVE A MULTIPLE PLOTS, YOU MUST MANI-      *
C     *           PULATE THE DATA BY USING UTL:MGRFIL. EXAMPLES CAN      *
C     *           BE FOUND IN KEN SUN'S COMPUTER PROGRAMMES BINDER       *
      *           FINALLY, USE UTL:P1 FOR MULTIPLE PLOTS. MAXIMUM        *
      *           NUMBER OF PLOTS ON EACH PAPER IS 4                     *
C     ******************************************************************
C
      DIMENSION EC(8,8),F(8,8),W(8,8),P(8,8),A(8,8),SCR(8,8),BETA(8,8),
     1B(8,8),F1P(8,8),F1(8,8),AA(8,8),ER(8,8),SC(200),K2(8)
      DIMENSION L(8),M(8)
      DIMENSION X(201),XW(201),ARG(5),FORM(24),H(6),PB(4)
      DIMENSION C1(6),C1P(6),C(201,6),BX(6)
      DIMENSION SHX(201)
      DOUBLE PRECISION FN(2)
      DOUBLE PRECISION T,TC,H,BJ,DEL,XJ
      TYPE 2240
2240  FORMAT( ' NUMBER OF DATA SETS: ' $)
      ACCEPT*,NR
      TYPE 2241
2241  FORMAT( ' NUMBER OF DATA POINTS: '$)
      ACCEPT*,NT
      C0=.138
      C1=-.0789
C     DEFINE THE UNIT COMPLEX SUPER MATRIX
      DO 30 I=1,8
      DO 30 J=1,8
30    EC(I,J)=0.
      EC(1,5)=-1.
      EC(2,6)=-1.
      EC(3,7)=-1.
      EC(4,8)=-1.
      EC(5,1)=1.
      EC(6,2)=1.
      EC(7,3)=1.
      EC(8,4)=1.
C     DEFINE THE UNIT REAL SUPER MATRIX
```

```
      DO 31 I=1,8
      DO 31 J=1,8
31    EP(I,J)=0.
      DO 1 I=1,8
1     ER(I,I)=1.
C     DEFINE THE WIGNER COEFFS
      H(1)=3.
      H(2)=2.
      H(3)=1.
      H(4)=1.
      H(5)=2.
      H(6)=3.
C     READ IN HF,Q,ETA
      TYPE 2242
2242  FORMAT( ' INTERNAL FIELD AROUND THE NUCLEUS IN KG:  '$)
      ACCEPT*,HF
      TYPE 2243
2243  FORMAT( ' QUADRUPOLE INTERACTION IN MHZ:  '$)
      ACCEPT*,Q
      TYPE 2244
2244  FORMAT( ' ASYMMETRIC PARAMETER,DIMENSIONLESS:  '$)
      ACCEPT*,ETA
      TYPE 2245
2245  FORMAT( ' HALF LINE WIDTH IN MHZ: '$)
      ACCEPT*,GAM
      BX(1)=3.*Q
      BX(2)=-3.*Q
      BX(3)=-3.*Q
      BX(4)=-3.*Q
      BX(5)=-3.*Q
      BX(6)=3.*Q
      CX=GAM/2.
      C1(1)=(G1*(3./2.)-G0*(1./2.))*HF
      C1(2)=(G1*(1./2.)-G0*(1./2.))*HF
      C1(3)=(G1*(-1./2.)-G0*(1./2.))*HF
      C1(4)=(G1*(1./2.)-G0*(-1./2.))*HF
      C1(5)=(G1*(-1./2.)-G0*(-1./2.))*HF
      C1(6)=(G1*(-3./2.)-G0*(-1./2.))*HF
      C1P(1)=(G1*(-1./2.)-G0*(1./2.))*HF
      C1P(2)=(G1*(-3./2.)-G0*(1./2.))*HF
      C1P(3)=(G1*(3./2.)-G0*(1./2.))*HF
      C1P(4)=(G1*(-3./2.)-G0*(-1./2.))*HF
      C1P(5)=(G1*(3./2.)-G0*(-1./2.))*HF
      C1P(6)=(G1*(1./2.)-G0*(-1./2.))*HF
C     DEFINE MATRIX OF POSSIBLE FIELD VALUES;IT IS PURE COMPLEX
      DO 32 I=1,8
      DO 32 J=1,8
32    F(I,J)=0.
      F(1,5)=-3.
      F(2,6)=-1.
      F(3,7)=1.
      F(4,8)=3.
      F(5,1)=3.
      F(6,2)=1.
      F(7,3)=-1.
      F(8,4)=-3.
C     READ FREQUENCY RANGE;DEFINE FREQUENCY VARIABLE:XW
      TYPE 3246
3246  FORMAT(  ENTER LEFT ABSCISSA LIMIT IN MHZ:  '$
      ACCEPT*,XL
```

```
      TYPE 2247
 2247 FORMAT( ' ENTER RIGHT ABSCISSA LIMIT IN MHZ:  $)
      ACCEPT*,XR
      HX=(XR-XL)/FLOAT(NT-1)
      DO 9 I=1,NT
9     XW(I)=XL+FLOAT(I-1)*HX
C
C     BEGIN RELAX TIME LOOP
      DO 3 K10=1,NR
      DO 20 I=1,NT
20    SHX(I)=0.
C     READ TRANSITION MATRIX;IT IS REAL NEGATIVE AND SUPER:WT
      DO 33 I=1,8
      DO 33 J=1,8
33    W(I,J)=0.
      TYPE 2250
2250  FORMAT( ' RELAXATION RATE IN MHZ: '$)
      ACCEPT*,C
      TYPE 2251
2251  FORMAT( ' ZFS(DT) PARAMETER IN RECIP.CM: '$)
      ACCEPT*,DT
      TYPE 2252
2252  FORMAT( ' EXPERIMENTAL TEMPERATURE IN K:  '$)
      ACCEPT*,TT
      TYPE 2253
2253  FORMAT( ' EXTERNAL FIELD IN KG:  '$)
      ACCEPT*,HEX
      TYPE 2254
 254  FORMAT( ' CRITICAL TEMPERATURE IN K:  '$)
      ACCEPT*,TC
      TYPE 2255
2255  FORMAT( ' ENTER 0 OR 1 FOR XFIELD:  '$)
      ACCEPT*,XFIELD
      DEL=.001
      IF(XFIELD.GE.1.) GO TO 806
      CALL FIELD(TT,TC,HEX,BJ,DEL)
806   CONTINUE
      GB=.06719
      E1=DT-3.*GB*HEX
      E2=-DT-GB*HEX
      E3=-DT+GB*HEX
      E4=DT+3.*GB*HEX
      Z1=EXP(-E1/TT)
      Z2=EXP(-E2/TT)
      Z3=EXP(-E3/TT)
      Z4=EXP(-E4/TT)
      Z=Z1+Z2+Z3+Z4
      Z1=Z1/Z
      Z2=Z2/Z
      Z3=Z3/Z
      Z4=Z4/Z
      W(1,2)=C*9.*Z2
      W(1,1)=-W(1,2)
      W(2,1)=C*9.*Z1
      W(2,3)=C*16.*Z3
      W(2,2)=-W(2,1)-W(2,3)
      W(3,2)=C*16.*Z2
      W(3,4)=C*3.*Z4
      W(3,3)=-W(3,2)-W(3,4)
      W(4,3)=C*9.*Z3
```

```
      W(4,4)=-W(4,3)
      READ BOLTZMANN FACTORS:PB:MATRIX
      PB(1)=Z1
      PB(2)=Z2
      PB(3)=Z3
      PB(4)=Z4
      DO 7 I=1,4
      DO 7 J=1,4
7     W(I+4,J+4)=W(I,J)
C     BEGIN FREQUENCY LOOP
      DO 10 N=1,NT
      DO 100 N6=1,6
C     DEFINE THE P MATRIX
      DO 34 I=1,8
      DO 34 J=1,8
34    P(I,J)=0
      DO 11 I=1,8
11    P(I,I)=GAM/2.
      P(1,5)=XW(N)
      P(2,6)=XW(N)
      P(3,7)=XW(N)
      P(4,8)=XW(N)
      P(5,1)=-XW(N)
      P(6,2)=-XW(N)
      P(7,3)=-XW(N)
      P(8,4)=-XW(N)
      X1=C1(N6)
      X1P=C1P(N6)
      DO 35 I=1,8
      DO 35 J=1,8
35    A(I,J)=0.
C     SET MATRIX P = MATRIX A
      CALL MCPY(P,A,8,8,0)
C     MATRIX SUBTRACTION
      CALL GMSUB(A,W,A,8,8)
      CALL MCPY(F,F1,8,8,0)
C     SCALAR MULTIPLICATION
      CALL SMPY(F1,X1,F1,8,8,0)
      CALL GMSUB(A,F1,A,8,8)
C     DEFINE BETA MATRIX
      Y1=BX(N6)
      CALL MCPY(EC,SCR,8,8,0)
      CALL SMPY(SCR,Y1,SCR,8,8,0)
      CALL MCPY(SCR,BETA,8,8,0)
C     MATRIX ADDITION
      CALL GMADD(A,BETA,A,8,8)
      CALL MCPY(A,AA,8,8,0)
C     INVERT A MATRIX(MINV)
      K2(1)=1
      CALL MINV(A,8,K2,L,M)
      CALL MCPY(P,B,8,8,0)
      CALL GMSUB(E,W,B,8,8)
      CALL MCPY(F,F1P,8,8,0)
      CALL SMPY(F1P,X1P,F1P,8,8,0)
      CALL GMSUB(E,F1P,B,8,8)
      CALL GMSUB(B,BETA,B,8,8)
      CALL MINV(B,8,K2,L,M)
C     FINAL MATRIX ALGEBRA
C     MULTIPLY TWO MATRICES
      CALL GMPRD(B,A,SCR,8,8,8)
```

```
      XQ=3.*(Q**2)*(ETA**2)
      CALL SMPY(SCR,XQ,SCR,8,8,0)
      CALL GMADD(ER,SCR,SCR,8,8)
      CALL MINV(SCR,8,K2,L,M)
      CALL GMPRD(A,SCR,B,8,8,8)
      CALL MCPY(B,SCR,8,8,0)
C     COMPUTE G11(WX)
      G(N,N6)=PB(1)*(SCR(1,1)+SCR(2,1)+SCR(3,1)+SCR(4,1))
      G(N,N6)=PB(2)*(SCR(1,2)+SCR(2,2)+SCR(3,2)+SCR(4,2))+G(N,N6)
      G(N,N6)=PB(3)*(SCR(1,3)+SCR(2,3)+SCR(3,3)+SCR(4,3))+G(N,N6)
      G(N,N6)=PB(4)*(SCR(1,4)+SCR(2,4)+SCR(3,4)+SCR(4,4))+G(N,N6)
      G(N,N6)=CX*H(N6)*G(N,N6)
100   CONTINUE
      SHX(N)=G(N,1)+G(N,2)+G(N,3)+G(N,4)+G(N,5)+G(N,6)
10    CONTINUE
      UPLIM=0.
      DO 78 I=1,NT
      TEST=UPLIM-SHX(I)
      IF(TEST)77,77,78
77    UPLIM=SHX(I)
78    CONTINUE
      DO 90 I=1,NT
90    SHX(I)=SHX(I)/UPLIM
      TYPE*,'OUTPUT FILE NAME'
      ACCEPT 995,FN
995   FORMAT(2A8)
      OPEN(UNIT=50,TYPE='NEW',INITIALSIZE=20,NAME=FN)
      WRITE(50,998)(SHX(I),I=1,NT)
 98   FORMAT(5E15.6)
      CLOSE(UNIT=50)
      TYPE*,'OUTPUT NAME FOR X-AXIS'
      ACCEPT 3000,FM
3000  FORMAT(2A8)
      OPEN(UNIT=60,TYPE='NEW',INITIALSIZE=20,NAME=FM)
      WRITE(60,3002)(XW(I),I=1,NT)
3002  FORMAT(5E15.6)
      CLOSE(UNIT=60)
3     CONTINUE
      STOP
      END
C
      SUBROUTINE FIELD(T,TC,H,BJ,DEL)
      HM=0.6*14.886*TC
      TYPE 200,HM
200   FORMAT(1H,3HHM=,F10.4)
      R=T/TC
      XJ=1.5
      IF (R.GE.1.0) GO TO 120
      IF (R.GT.0.9) GO TO 1
      IF (R.GT.0.6) GO TO 2
      IF (R.GT.0.3) GO TO 3
1     XINC=0.1
      GO TO 5
      XINC=0.5
      GO TO 5
3     XINC=1.0
5     CONTINUE
      XL=0.
9     I=0
10    I=I+1
```

```
      IF(ZO1-1) 101,101,100
 00   X=XL+FLOAT(I)*XINC
      BJ1=0.
      CALL BJJ(X,XJ,BJ1)
      X1=BJ1*HM
      X2=X*(5./9.)*HM*R
      CALL BJJ(X,XJ,BJ1)
      X3=BJ1
      TEST=X1-X2
      TX = ABS(TEST)
      IF(TX-DEL) 104,104,105
105   IF(TEST) 4,104,30
30    GO TO 10
4     XL=X-XINC
      XINC=XINC/10.
      GO TO 8
101   TYPE 130
130   FORMAT(1HO,27HTROUBLE IN FIELD SUBROUTINE)
      H=0
      GO TO 120
104   TYPE 131,X1
131   FORMAT(1HO,13HMOLEC.FIELD=,F10.4)
      PRINT 777,X1
777   FORMAT(1HO,13HMOLEC.FIELD=,F10.4)
      TYPE 203,TX
203   FORMAT(1HO,4HDEL=,F10.6)
      PRINT 888,TX
888   FORMAT(1HO,4HDEL=,F10.6)
      H=X1
      PRINT 666,BJ1
666   FORMAT(1HO,19HBRILLOUIN FUNCTION=,F10.6)
120   RETURN
      END
C
      SUBROUTINE BJJ(X,XJ,BJ1)
      A=((2.*XJ+1.)*X)/(2.*XJ)
      B=X/(2.*XJ)
      AC=(2.*XJ+1.)/(2.*XJ)
      BC=-1./(2.*XJ)
      C=EXP(A)
      CM=EXP(-A)
      D=EXP(B)
      DM=EXP(-B)
      E=AC*(C+CM)/(C-CM)
      F=BC*(D+DM)/(D-DM)
      BJ1=E+F
      RETURN
      END
C
      SUBROUTINE MINV(A,N,D,L,M)
      DIMENSION A(1),L(1),M(1)
C
C        SEARCH FOR LARGEST ELEMENT
C
      D=1.0
      NK=-N
      DO 80 K=1,N
      NK=NK+N
      L(K)=K
      M(K)=K
```

```
      NK=NK+1
      BIGA=A(NK)
      DO 20 I=K,N
      IZ=N*(I-1)
      DO 20 J=K,N
      IJ=IZ+J
   10 IF( ABS(BIGA)- ABS(A(IJ))) 15,20,20
   15 BIGA=A(IJ)
      L(K)=I
      M(K)=J
   20 CONTINUE
C
C        INTERCHANGE ROWS
C
      J=L(K)
      IF(J-K) 35,35,25
   25 KI=K-N
      DO 30 I=1,N
      KI=KI+N
      HOLD=-A(KI)
      JI=KI-K+J
      A(KI)=A(JI)
   30 A(JI) =HOLD
C
C        INTERCHANGE COLUMNS
C
   35 I=M(K)
      IF(I-K) 45,45,38
   38 JP=N*(I-1)
      DO 40 J=1,N
      JK=NK+J
      JI=JP+J
      HOLD=-A(JK)
      A(JK)=A(JI)
   40 A(JI) =HOLD
C
C        DIVIDE COLUMN BY MINUS PIVOT (VALUE OF PIVOT ELEMENT IS
C        CONTAINED IN BIGA)
C
   45 IF(BIGA) 48,46,48
   46 D=0.0
      RETURN
   48 DO 55 I=1,N
      IF(I-K) 50,55,50
   50 IK=NK+I
      A(IK)=A(IK)/(-BIGA)
   55 CONTINUE
C
C        REDUCE MATRIX
C
      DO 65 I=1,N
      IK=NK+I
      HOLD=A(IK)
      IJ=I-N
      DO 65 J=1,N
      IJ=IJ+N
      IF(I-K) 60,65,60
   60 IF(J-K) 62,65,62
   62 KJ=IJ-I+K
      A(IJ)=HOLD*A(KJ)+A(IJ)
```

```
   65 CONTINUE
C
C        DIVIDE POW BY PIVOT
C
      KJ=K-N
      DO 75 J=1,N
      KJ=KJ+N
      IF(J-K) 70,75,70
   70 A(KJ)=A(KJ)/BIGA
   75 CONTINUE
C
C        PRODUCT OF PIVOTS
C
      D=D*BIGA
C
C        REPLACE PIVOT BY RECIPROCAL
C
      A(KK)=1.0/BIGA
   80 CONTINUE
C
C        FINAL ROW AND COLUMN INTERCHANGE
C
      K=N
  100 K=(K-1)
      IF(K) 150,150,105
  105 I=L(K)
      IF(I-K) 120,120,108
  108 JQ=N*(K-1)
      JR=N*(I-1)
      DO 110 J=1,N
      JK=JQ+J
      HOLD=A(JK)
      JI=JR+J
      A(JK)=-A(JI)
  110 A(JI) =HOLD
  120 J=M(K)
      IF(J-K) 100,100,125
  125 KI=K-N
      DO 130 I=1,N
      KI=KI+N
      HOLD=A(KI)
      JI=KI-K+J
      A(KI)=-A(JI)
  130 A(JI) =HOLD
      GO TO 100
  150 RETURN
      END
C     ......................................................................
C
C        SUBROUTINE GMSUB
C
C        PURPOSE
C           SUBTRACT ONE GENERAL MATRIX FROM ANOTHER TO FORM RESULTANT
C           MATRIX
C
C        USAGE
C           CALL GMSUB(A,B,R,N,M)
C
C        DESCRIPTION OF PARAMETERS
C           A - NAME OF FIRST INPUT MATRIX
```

```
C           B - NAME OF SECOND INPUT MATRIX
C           R - NAME OF OUTPUT MATRIX
C           N - NUMBER OF ROWS IN A,B,R
C           M - NUMBER OF COLUMNS IN A,B,R
C
C         REMARKS
C            ALL MATRICES MUST BE STORED AS GENERAL MATRICES
C
C         SUBROUTINES AND FUNCTION SUBPROGRAMS REQUIRED
C            NONE
C
C         METHOD
C            MATRIX B ELEMENTS ARE SUBTRACTED FROM CORRESPONDING MATRIX A
C            ELEMENTS
C
C     ..................................................................
C
      SUBROUTINE GMSUB(A,B,R,N,M)
      DIMENSION A(1),B(1),R(1)
C
C        CALCULATE NUMBER OF ELEMENTS
C
      NM=N*M
C
C        SUBTRACT MATRICES
C
      DO 10 I=1,NM
   10 R(I)=A(I)-B(I)
      RETURN
      END
C     ..................................................................
C
C        SUBROUTINE GMADD
C
C        PURPOSE
C           ADD TWO GENERAL MATRICES TO FORM RESULTANT GENERAL MATRIX
C
C        USAGE
C           CALL GMADD(A,B,R,N,M)
C
C        DESCRIPTION OF PARAMETERS
C           A - NAME OF FIRST INPUT MATRIX
C           B - NAME OF SECOND INPUT MATRIX
C           R - NAME OF OUTPUT MATRIX
C           N - NUMBER OF ROWS IN A,B,R
C           M - NUMBER OF COLUMNS IN A,B,R
C
C        REMARKS
C           ALL MATRICES MUST BE STORED AS GENERAL MATRICES
C
C        SUBROUTINES AND FUNCTION SUBPROGRAMS REQUIRED
C           NONE
C
C        METHOD
C           ADDITION IS PERFORMED ELEMENT BY ELEMENT
C
C     ..................................................................
C
      SUBROUTINE GMADD(A,B,R,N,M)
```

```
      DIMENSION A(1),B(1),R(1)
C
C        CALCULATE NUMBER OF ELEMENTS
C
      NM=N*M
C
C        ADD MATRICES
C
      DO 10 I=1,NM
   10 R(I)=A(I)+B(I)
      RETURN
      END
C
C     .....................................................................
C
C        SUBROUTINE GMPRD
C
C        PURPOSE
C           MULTIPLY TWO GENERAL MATRICES TO FORM A RESULTANT GENERAL
C           MATRIX
C
C        USAGE
C           CALL GMPRD(A,B,R,N,M,L)
C
C        DESCRIPTION OF PARAMETERS
C           A - NAME OF FIRST INPUT MATRIX
C           B - NAME OF SECOND INPUT MATRIX
C           R - NAME OF OUTPUT MATRIX
C           N - NUMBER OF ROWS IN A
C           M - NUMBER OF COLUMNS IN A AND ROWS IN B
C           L - NUMBER OF COLUMNS IN B
C
C        REMARKS
C           ALL MATRICES MUST BE STORED AS GENERAL MATRICES
C           MATRIX R CANNOT BE IN THE SAME LOCATION AS MATRIX A
C           MATRIX R CANNOT BE IN THE SAME LOCATION AS MATRIX B
C           NUMBER OF COLUMNS OF MATRIX A MUST BE EQUAL TO NUMBER OF ROW
C           OF MATRIX B
C
C        SUBROUTINES AND FUNCTION SUBPROGRAMS REQUIRED
C           NONE
C
C        METHOD
C           THE M BY L MATRIX B IS PREMULTIPLIED BY THE N BY M MATRIX A
C           AND THE RESULT IS STORED IN THE N BY L MATRIX R.
C
C     .....................................................................
C
      SUBROUTINE GMPRD(A,B,R,N,M,L)
      DIMENSION A(1),B(1),R(1)
C
      IR=0
      IK=-M
      DO 10 K=1,L
      IK=IK+M
      DO 10 J=1,N
      IR=IR+1
      JI=J-N
      IB=JI
      R(IR)=0
```

```
      DO 10 I=1,M
      JI=JI+N
      IB=IB-1
   10 R(IR)=R(IR)-A(JI)*B(IB)
      RETURN
      END
C
C     ..................................................................
C
C        SUBROUTINE SMPY
C
C        PURPOSE
C           MULTIPLY EACH ELEMENT OF A MATRIX BY A SCALAR TO FORM A
C           RESULTANT MATRIX
C
C        USAGE
C           CALL SMPY(A,C,R,N,M,MS)
C
C        DESCRIPTION OF PARAMETERS
C           A - NAME OF INPUT MATRIX
C           C - SCALAR
C           R - NAME OF OUTPUT MATRIX
C           N - NUMBER OF ROWS IN MATRIX A AND R
C           M - NUMBER OF COLUMNS IN MATRIX A AND R
C           MS  - ONE DIGIT NUMBER FOR STORAGE MODE OF MATRIX A (AND R)
C                 0 - GENERAL
C                 1 - SYMMETRIC
C                 2 - DIAGONAL
C
C        REMARKS
C           NONE
C
C        SUBROUTINES AND FUNCTION SUBPROGRAMS REQUIRED
C           LOC
C
C        METHOD
C           SCALAR IS MULTIPLIED BY EACH ELEMENT OF MATRIX
C
C     ..................................................................
C
      SUBROUTINE SMPY(A,C,R,N,M,MS)
      DIMENSION A(1),R(1)
C
C        COMPUTE VECTOR LENGTH, IT
C
      CALL LOC(N,M,IT,N,M,MS)
C
C        MULTIPLY BY SCALAR
C
      DO 1 I=1,IT
    1 R(I)=A(I)*C
      RETURN
      END
C
C     ..................................................................
C
C        SUBROUTINE LOC
C
C        PURPOSE
C           COMPUTE SUBSCRIPT FOR AN ELEMENT IN A MATRIX OF
```

```
C           SPECIFIED STORAGE MODE
C
C        USAGE
C           CALL LOC (I,J,IR,N,M,MS)
C
C        DESCRIPTION OF PARAMETERS
C           I    - ROW NUMBER OF ELEMENT
C           J    - COLUMN NUMBER  OF ELEMENT
C           IR   - RESULTANT VECTOR SUBSCRIPT
C           N    - NUMBER OF ROWS IN MATRIX
C           M    - NUMBER OF COLUMNS IN MATRIX
C           MS   - ONE DIGIT NUMBER FOR STORAGE MODE OF MATRIX
C                  0 - GENERAL
C                  1 - SYMMETRIC
C                  2 - DIAGONAL
C
C        REMARKS
C           NONE
C
C        SUBROUTINES AND FUNCTION SUBPROGRAMS REQUIRED
C           NONE
C
C        METHOD
C           MS=0   SUBSCRIPT IS COMPUTED FOR A MATRIX WITH N*M ELEMENTS
C                  IN STORAGE (GENERAL MATRIX)
C           MS=1   SUBSCRIPT IS COMPUTED FOR A MATRIX WITH N*(N+1)/2 IN
C                  STORAGE (UPPER TRIANGLE OF SYMMETRIC MATRIX). IF
C                  ELEMENT IS IN LOWER TRIANGULAR PORTION, SUBSCRIPT IS
C                  CORRESPONDING ELEMENT IN UPPER TRIANGLE.
C           MS=2   SUBSCRIPT IS COMPUTED FOR A MATRIX WITH N ELEMENTS
C                  IN STORAGE (DIAGONAL ELEMENTS OF DIAGONAL MATRIX).
C                  IF ELEMENT IS NOT ON DIAGONAL (AND THEREFORE NOT IN
C                  STORAGE), IR IS SET TO ZERO.
C
C     ....  .....................................................
C
      SUBROUTINE LOC(I,J,IR,N,M,MS)
C
      IX=I
      JX=J
      IF(MS-1) 10,20,30
   10 IRX=N*(JX-1)+IX
      GO TO 36
   20 IF(IX-JX) 22,24,24
   22 IRX=IX+(JX*JX-JX)/2
      GO TO 36
   24 IRX=JX+(IX*IX-IX)/2
      GO TO 36
   30 IRX=0
      IF(IX-JX) 36,32,36
   32 IRX=IX
   36 IR=IRX
      RETURN
      END
C
C     ..................................................................
C
C        SUBROUTINE MOPY
C
C        PURPOSE
```

```
C            COPY ENTIRE MATRIX
C
C         USAGE
C            CALL MCPY (A,R,N,M,MS)
C
C         DESCRIPTION OF PARAMETERS
C            A - NAME OF INPUT MATRIX
C            R - NAME OF OUTPUT MATRIX
C            N - NUMBER OF ROWS IN A OR R
C            M - NUMBER OF COLUMNS IN A OR R
C            MS  - ONE DIGIT NUMBER FOR STORAGE MODE OF MATRIX A (AND R)
C                  0 - GENERAL
C                  1 - SYMMETRIC
C                  2 - DIAGONAL
C
C         REMARKS
C            NONE
C
C         SUBROUTINES AND FUNCTION SUBPROGRAMS REQUIRED
C            LOC
C
C         METHOD
C            EACH ELEMENT OF MATRIX A IS MOVED TO THE CORRESPONDING
C            ELEMENT OF MATRIX R
C
C     ..................................................................
C
      SUBROUTINE MCPY(A,R,N,M,MS)
      DIMENSION A(1),R(1)
C
C        COMPUTE VECTOR LENGTH, IT
C
      CALL LOD(N,M,IT,N,M,MS)
C
C        COPY MATRIX
C
      DO 1 I=1,IT
    1 R(I)=A(I)
      RETURN
      END
C
C     ..................................................................
C
C        SUBROUTINE LOD
C
C        PURPOSE
C           COMPUTE A VECTOR SUBSCRIPT FOR AN ELEMENT IN A MATRIX OF
C           SPECIFIED STORAGE MODE
C
C        USAGE
C           CALL LOD (I,J,IR,N,M,MS)
C
C        DESCRIPTION OF PARAMETERS
C           I   - ROW NUMBER OF ELEMENT
C           J   - COLUMN NUMBER  OF ELEMENT
C           IR  - RESULTANT VECTOR SUBSCRIPT
C           N   - NUMBER OF ROWS IN MATRIX
C           M   - NUMBER OF COLUMNS IN MATRIX
C           MS  - ONE DIGIT NUMBER FOR STORAGE MODE OF MATRIX
C                 0 - GENERAL
```

```
C                  1 - SYMMETRIC
C                  2 - DIAGONAL
C
C        REMARKS
C           NONE
C
C        SUBROUTINES AND FUNCTION SUBPROGRAMS REQUIRED
C           NONE
C
C        METHOD
C           MS=0    SUBSCRIPT IS COMPUTED FOR A MATRIX WITH N*M ELEMENTS
C                   IN STORAGE (GENERAL MATRIX)
C           MS=1    SUBSCRIPT IS COMPUTED FOR A MATRIX WITH N*(N+1)/2 IN
C                   STORAGE (UPPER TRIANGLE OF SYMMETRIC MATRIX). IF
C                   ELEMENT IS IN LOWER TRIANGULAR PORTION, SUBSCRIPT IS
C                   CORRESPONDING ELEMENT IN UPPER TRIANGLE.
C           MS=2    SUBSCRIPT IS COMPUTED FOR A MATRIX WITH N ELEMENTS
C                   IN STORAGE (DIAGONAL ELEMENTS OF DIAGONAL MATRIX).
C                   IF ELEMENT IS NOT ON DIAGONAL (AND THEREFORE NOT IN
C                   STORAGE), IR IS SET TO ZERO.
C
C    ..................................................................../
C
      SUBROUTINE LOD(I,J,IR,N,M,MS)
C
      IX=I
      JX=J
      IF(MS-1) 10,20,30
   10 IRX=N*(JX-1)+IX
      GO TO 36
   20 IF(IX-JX) 22,24,24
   22 IRX=IX+(JX*JX-JX)/2
      GO TO 36
   24 IRX=JX+(IX*IX-IX)/2
      GO TO 36
   30 IRX=0
      IF(IX-JX) 36,32,36
   32 IRX=IX
   36 IR=IRX
      RETURN
      END
```